AN ABSTRACT OF THE THESIS OF

Kuang-Jen Wang for the degree of Doctor of Philosophy in Mechanical Engineering presented on August 30, 1996. Title: Drilling Process Evaluation by Predicting Drilled Hole Quality and Drill Bit Wear With On-Line Acoustic Emission Signals.

Redacted for privacy

Abstract approved: _____
Robert K. Paasch

Improvement of manufacturing productivity is dependent on the successful automation of manufacturing processes, the success of which is based in turn upon the availability of information which describes the state of manufacturing operations. Acoustic Emission (AE) signals related to the cutting process and tool wear have been recently applied to monitor manufacturing processes, and various AE parameters can be used to provide process information. For example, when cutting tools become worn, AE energy generated at the interface of tool flank and work piece increases. This study is thus an experimental investigation of the AE spectrums representing AE signals energy distribution to determine the possibility of extracting useful parameters to provide on-line information about drilled-hole quality and drill-bit wear.

An experiment conducted using a radial-arm drilling machine was employed to collect on-line AE drilling process spectrums, yielding eight indicator parameters. Drill wear states were measured using a machine vision system. Assessment of the drilled hole quality was based on tolerances established in Geometric Dimensioning

and Tolerancing (GD&T). Correlations among drill wear, drilled-hole quality measurements, and the AE spectrum indicator parameters were examined by regression analysis. A forward-stepwise variable selection procedure was used to select the best-fit regression model for each drilled hole quality measurement associated with the set of one AE parameter raised to different powers. According to quality measurements, drilled holes were categorized as either "acceptable" or "unacceptable" holes, using cluster analysis with a group-averaging method. The usage of AE parameters to decide to which group a drilled hole belonged was also examined.

From the experimental evidence, it was observed that there are strong relationships between AE parameters and drill-wear state and the quality measurements of drilled holes. AE parameters could be useful predictor variables to provide information to controller/operators to evaluate current drilling processes. Based on the status information of drill wear and the quality measurements, drilling processes can be adjusted accordingly.

Drilling Process Evaluation by Predicitng Drilled Hole Quality and Drill Bit Wear With On-Line Acoustic Emission Signals

by

Kuang-Jen Wang

A THESIS

submitted to

Oregon State University

in partial fulfillment of
the requirements for the
degree of

Doctor of Philosophy

Completed August 30, 1996
Commencement June 1997

Doctor of Philosophy thesis of Kuang-Jen Wang presented on August 30, 1996

APPROVED:

Redacted for privacy

Major Professor, representing Mechanical Engineering

Redacted for privacy

Head of Department of Mechanical Engineering

Redacted for privacy

Dean of Graduate School

I understand that my thesis will become part of the permanent collection of Oregon State University libraries. My signature below authorizes release of my thesis to any reader upon request

Redacted for privacy

Kuang-Jen Wang, Author

ACKNOWLEDGMENTS

Gratitude is expressed toward my thesis major advisor, Professor Robert K. Paasch, for his guidance and assistance during my graduate study at Oregon State University.

Appreciation is also given to other members of my committee, including Professors William F. Reiter, Charles E. Smith, Timothy C. Kennedy, and Michael R. Milota, for their interest and support.

Thanks are also extended to the staff, faculty and my fellow students in the Mechanical Engineering program at Oregon State University.

I would like to express my deepest gratitude toward my God for His faithfulness and blessings, to my father Shieh-Mien Wang for his continuous support, and to my dearest mother Tsai-Lien Yeh Wang for her love and patience.

TABLE OF CONTENTS

TABLE OF CONTENTS (Continued)

TABLE OF CONTENTS (Continued)

TABLE OF CONTENTS (Continued)

LIST OF FIGURES

LIST OF FIGURES (Continued)

LIST OF FIGURES (Continued)

LIST OF FIGURES (Continued)

LIST OF TABLES

Drilling Process Evaluation by Predicting Drilled Hole Quality and Drill Bit Wear With On-Line Acoustic Emission Signals

CHAPTER 1. INTRODUCTION

1.1 Motivation

Quality assurance, material saving, and cycle-time reduction are the three main objectives of the improvement of manufacturing productivity. The way to achieve these goals is highly dependent on the successful automation of these manufacturing processes. The success of the automation of these processes relies on the availability of data which describes the state of the operation. An attempt to build up a process monitor which can provide information about tool condition and quality of work is necessary [1]. Out of all metal-cutting processes, the hole-making process is the most widely used. It is estimated to be more than 30% of the total metal-cutting business [2]. It is therefore desirable to monitor drill wear and hole quality changes during the hole-drilling process.

One aspect of controlling the drilling process is monitoring drill-wear status. The cutting edge of a drill is the weakest element influencing the capacity of a hole-drilling system. It affects the ability of the cutting operation to satisfy specified performance characteristics. A drill-wear inspection system provides information about drill status. With this information, optimum planning for tool change is possible.

Quality inspection of finished holes is another key to controlling the drilling process. It helps in deciding when to initiate adaptive changes to control the drilling process and prevents the production of substandard hole qualities even before the failure point of the drill bit. In most cases, more than one hole must be drilled on a component or work piece and the drilling process continues on each piece until all of the holes have been finished. In the past, the quality of a drilled hole could only be inspected after the entire process was finished, or by stopping the process after each hole was drilled. The main disadvantage to inspecting after all holes on a piece have been drilled is that there may be defects in holes manufactured before the last. If we cannot detect the defects at the moment the hole is finished, the work expended on drilling the rest of the holes on the same part might be wasted. If we do stop the process and detect the defects at the moment the hole is finished, we might either adjust the hole drilling process to assure the following drilled hole has good quality or just stop the process and scrap the work piece. The advantage to adjusting the current hole drilling process is that we can minimize the number of defects in the part. This saves the time and cost of reworking the parts. The advantage for scrapping the work piece and going back to the beginning with a new work piece saves the time and cost saving of having worked on an unsatisfactory part. This kind of quality control by stopping to inspect and make adjustments is usually called off-line process control. An off-line drilling process inspection which needs to stop the manufacturing process in order to inspect the drill bit and the quality of hole which has just been made is shown in Figure 1.1.

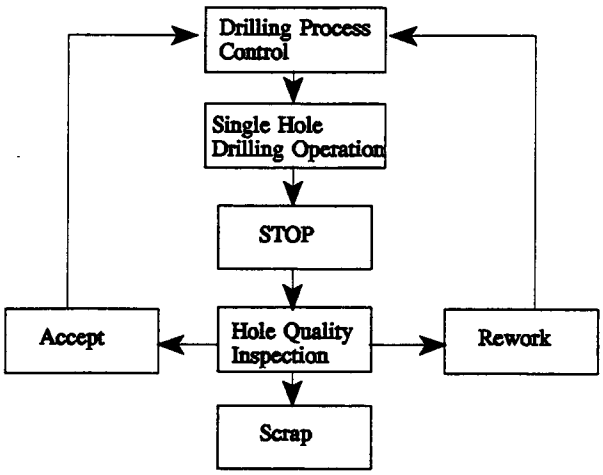

Figure 1.1. Off-line hole quality inspection and process control for multiple-hole drilling operation on same work piece; the process needs to be interrupted to inspect work quality.

The drawback of off-line control is that if there is no defect on the hole and the drill is still in good shape, the process was stopped unnecessarily, breaking the rhythm of the manufacturing process, which is both time consuming and costly. Therefore, an on-line hole quality and drill bit wear monitoring system, as shown in Figure 1.2, is needed to evaluate the drilled hole quality and the wear of drill bit on line. An on-line monitoring system does not need to stop the process to inspect both hole quality and drill wear. Based on non-stop hole quality and drill wear inspection, the controller can adjust the process as needed to ensure quality without stopping production. Through an on-line hole quality and drill wear monitoring system, a higher degree of adaptive control for a drilling process can be accomplished. The schematic diagram of this kind of hole drilling process control is shown in Figure 1.3.

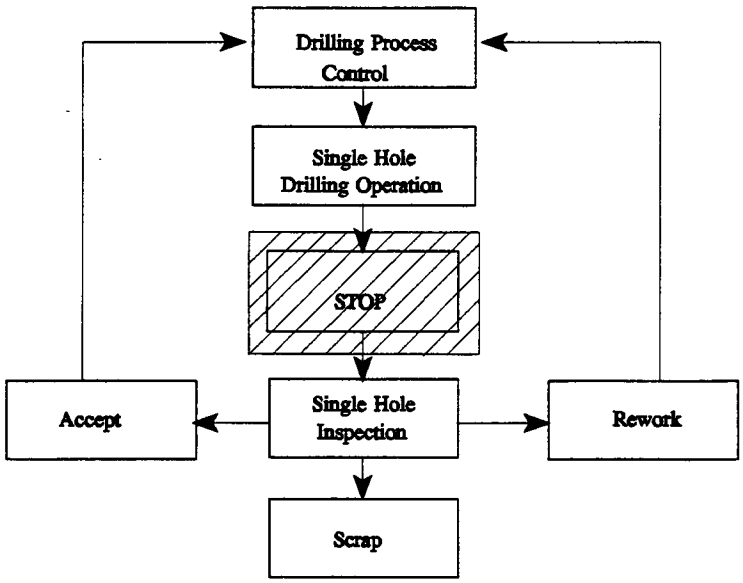

Figure 1.2. On-line hole quality inspection and process control for the multiple-hole drilling operation on same work piece; stop step is removed from the process and process is not interrupted.

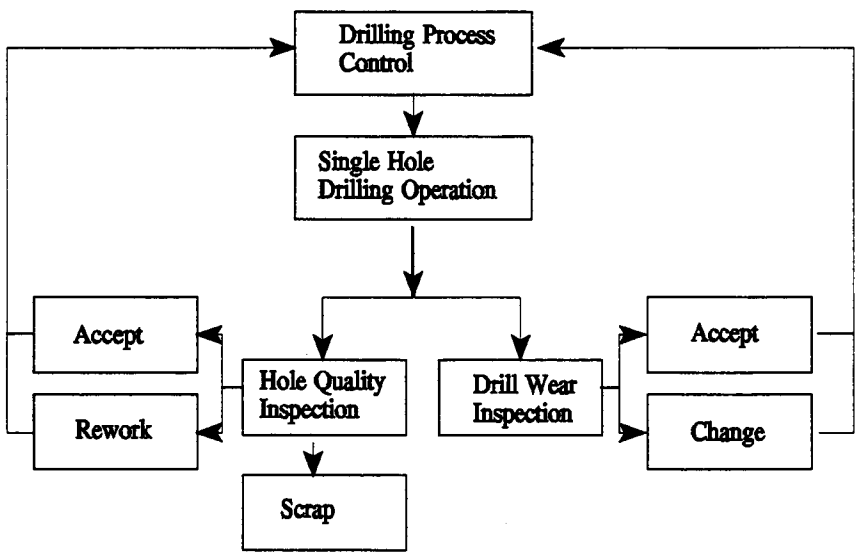

Figure 1.3. Hole drilling process with on-line hole quality prediction and drill-wear monitoring system.

After all, if we could get more information about hole quality and the cutting edge condition of the drill bit in the current process, we can adjust the process on-line to lengthen drill-bit life and to drill better quality holes. On one hand, these advantages depend on whether or not there are systems for measuring drilled hole quality and for detecting drill wear. On the other hand, directly inspecting hole quality and drill bit wear on-line is impractical.

Therefore, an on-line system to predict hole qualities and tool wear measurement has been investigated by several researchers using modeling methodology. These researchers have given most of their attention to the study of tool wear monitoring systems. Although their research showed credible results on tool wear monitoring, the data collection procedures are not effectual or practical. The main purpose of the current research is to improve the efficiency of data collection procedures by developing a drill-wear prediction methology which overcomes the deficiencies of earlier data collection procedures and to investigate the possibility of predicting the quality of drilled holes.

For application consideration, these monitors must be reliable, relatively easy to apply, and yield output closely correlated to the characteristics of the operation under control. Acoustic emission (AE) generated during the manufacturing process has been chosen to carry out on-line automatic monitoring of machining process in recent studies. Acoustic emission is a non-destructive inspecting technique used in monitoring manufacturing processes. Acoustic emission is the transient elastic energy released in materials undergoing deformation. Since the frequency content of the AE signal is well beyond the range of frequencies generally associated with the

dynamic behavior of machine tools, then the signal should relate to the cutting process only. Besides, the acoustic transducer is usually small, cheap, and can be installed such that it does not disturb the normal machining process. This transducer provides a relatively easy way to apply a sensor to monitoring a machining process for a practical industrial application without disturbing the normal machining operation [3]. Moreover, recent studies indicate that the output signal detected by the AE transducer is reliable and closely correlated to the characteristics of the cutting process under control [1][3]. These advantages in the usage of AE for monitoring make the AE transducer the best candidate for the present study.

1.2 Objective

In the current investigation, we focus on the possibility of building an on-line hole quality prediction system. But, the ideas considered to develop this quality prediction system are still concerned with the requirements for the drill wear prediction methodology. This involves the major objective of the present study, establishing some performance indices which may describe the state of the quality of drilled holes, together with the study of the initial relationship between the current AE measurement and the drill-bit flank wear. In addition, the relationship between hole quality and drill-bit flank wear will be learned.

1.3 Research Outline

For the purpose of this investigation, a literature review in chapter 2 provides a good background of accomplished work and methodology of past research on tool wear monitoring. The cutting force and cutting energy in a drilling process extended from the cutting force and cutting energy of the classical metal cutting theoretical model are discussed in the theory study in chapter 3. In addition to the drilling process modeling, the different AE signal processing methods are presented in chapter 4. The quality definitions and measurements of a drilled hole from the view of geometric dimensioning and tolerancing as well as the potential causes of hole quality divergence are also given in the theory study in chapter 5. With respect to the application, a technique for measuring and detecting the appropriate AE signal for a drilling process on a radial arm drilling machine will be developed in chapter 6. The machine vision system and the coordinate measuring machine (CMM) used to measure flank wear of the drill bit and the hole qualities respectively are also discussed in chapter 6. The result of experiments on a radial arm drilling machine is collected. To gain an experimental understanding of the relationships among the quality measurements of drilled holes, drill flank wear, and AE of the drilling process, statistical analyses conveyed in the collected data are presented in chapter 7. Finally, the conclusions and recommendations for further work are reported in chapter 8.

CHAPTER 2. LITERATURE REVIEW

Producing high quality products with a fully automated machine tool system has been investigated in industry and academia for four decades. The current study focuses on the on-line evaluation and control of drilling processes, based on a thorough review of earlier research to investigate feasible methods for improving the quality of the drilled hole manufactured. The subject is reviewed here in five parts: causes of hole quality variation, whirling and chatter vibrations, drill-wear monitoring, modeling of cutting forces and hole-quality evaluation. Since both drill-bit geometry and machine alignment can change the behavior of a drill bit and the drill bit's behavior change influences hole quality, studying the causes of hole quality variation and whirling and chatter vibrations can provide a fundamental understanding of the relationships among drill bit geometry, machine alignment, vibration and whirling and hole quality variation. Reviewing the modeling of cutting forces, drill-wear monitoring and hole-quality evaluation, some information about feasible methods is provided. The feasible methods developed in past work can be stepping stones to the prediction method used in the current study.

2.1 Causes of Hole-Quality Variation

In order to evaluate the drilling process based on drilled-hole quality, the causes of drilled-hole quality variations must be reviewed. From this information, the confounding factors in the experimental work of the current study can be

selected and controlled and, consequently, the evaluation methods for the drilling process can be developed.

Drill geometry and drilling-machine alignment were proposed to be the causes of hole-quality variations by Galloway [4] and Kahng and Ham [2]. The influence of the geometrical parameters of the drill point on hole qualities was investigated by Galloway in 1957 [4]. He pointed out that hole accuracy is markedly dependent on the symmetry of drill-point geometry. The asymmetry resulting from relative lip height causes the axis of rotation of the drill point to be displaced from the nominal rotation axis. The mean hole oversize increases linearly with the relative lip height. Moreover, the relative lip height could also seriously affect hole straightness, roundness, and alignment.

In 1975, an experimental study by Kahng investigating the relationship between initial hole qualities and quality improvement by the sequential processes such as reaming and boring [2]. Three errors, including displacement of hole axis, roundness, and parallelism, were observed in the initial hole making process by using a twist drill. There are two main convictions to the hole quality variations. One is the initial deflection of the drilling path contributed by the deflection of the arm of the machine tool. The other is the variation in either relative lip height or point centrality of chisel edge produced when the drill was ground. It was also shown that the contact conditions at initial penetration affect primarily the errors in hole quality. Moreover, a center hole prior to drilling operation leads to improvement of the hole quality.

Furthermore, drill-bit behaviors, such as whirling and chatter vibration caused by both drill geometry and drilling-machine alignment, which consequently affect hole quality, are introduced in the following section.

2.2 Whirling and Chatter Vibrations

The vibration behavior of a drill bit can change the shape of the hole profile. When the profile of the hole becomes some kind of polygon, a roundness error is produced for the drilled hole. Extended from the understanding of the relationship among the drill bit geometry, drill spindle alignment and drill vibration behavior, some initial information is provided on how roundness errors of drilled holes occurs in a drilling process.

Two vibrational phenomena, i.e. whirling and chatter vibrations, occur during a drilling process. These vibrational phenomena were discussed by Fujii et al. [5-8] and Lee et al. [9]. In these studies, analytical models were developed to investigate the drill whirling and chatter vibrations qualitatively and quantitatively. In Fujii's work [5-7], it was shown that whirling vibration occurs at the beginning of a drilling process. Whirling vibration, following an elliptical orbit, is a self-excited vibration accompanied by a phase lag with respect to the revolution of the work piece. The vibration energy is induced by the regenerative effect at the main cutting edges. Oppositely, the flank surface of the main cutting edges was found to function qualitatively as a damper of the vibration. A flank collision index, θ_C, was developed to show the degree of difficulty of the drill flank in contacting the work-

piece surface [6]. The index was estimated in such a way that effects of the point angle, relief angle, and chisel-edge length of drill bit were taken into account. The flank collision index increases with an increase in either point angle or relief angle or with a decrease in chisel-edge length. The degree of difficulty of the drill flank in contacting the work piece surface is based on the spatial relationship between the drill-flank surface and work-piece surface in a cutting condition. The approaching direction of work-piece material to the major-cutting direction is defined as the angle, θ_P , between the relative cutting velocity vector and the major cutting edge [5][6]. Once a vibration is initiated, θ_P will change according to the vibration behavior of the drill bit. If θ_P happens to be larger than the angle, θ_C , the drill-flank surface will collide with the bottom surface of the hole just machined. Therefore, θ_C shows the ease or difficulty of the drill flank in contacting the work piece surface and hence will be called the flank collision index. The larger the flank-collision index, the more difficult it is for the flank surface to contact the work-piece face. In other words, the resulting damping effect on drill whirling vibration from the collision between the flank face and work piece surface decreased as the flank-collision index increased. That is, the drills with large point angles, large relief angles and small chisel edge length will rarely cause the collision of the flank surface against the work piece during drilling. That means the whirling vibration will start at shallower hole depth and the vibration amplitude will increase as the flank-collision index increases.

The initial skidding motions of the drill, resulting from the eccentricity between the spindle rotation axis and the drill axis, affect hole positional accuracy.

The wandering motions of the drill influence the shape of the hole profile, i.e. the roundness of the hole. In 1987, Lee et al. [9] developed a mathematical model to investigate the drill-wandering motion. It showed that during the initial penetration, an odd-sided polygonal hole was formed. With increasing hole depth, the number of sides of the polygon increases and the profile of the hole gradually becomes round. The wandering motion simulated by the analytical models agreed closely with the experimental results for the initial penetration process. The corresponding experimental results in his work also showed that the multifaced point drills generate less skidding and wandering motions during drill entry than conventional drill points do, which agrees with the results of Fujii's work [5-7]. This is due to the fact that multifaced drills have a considerably smaller chisel-edge length which leads to a quicker stabilization of the motion.

In 1988, Ema et al. [8] investigated the behavior of chatter vibration. Chatter vibration is regenerative vibration motion and undulation on a machined work-piece surface produced by the inclination of the drill point. In a drilling process whirling vibration starts in the beginning of the drilling operation and is damped after the main cutting edges have penetrated the work piece at certain hole depth. However, when the drill penetrates deeper, chatter vibration starts and its amplitude increases first and then gradually decreases. The study showed that chatter frequency remained a constant value during chatter vibration and coincided with the bending natural frequency of the drill when the drill point was supported in a machined hole. Further studies on the effect of the spindle speed indicated that the amplitude of chatter vibration was significantly affected by the spindle speed.

2.3 Drill-Wear Monitoring Methods

Drill-wear monitoring methods used in past research was reviewed in order to develop an algorithm for evaluating drilling processes on-line in the current study. Among those monitoring methods, most attention was paid to the wear of the weakest elements, such as cutting tool edges, which influence the system's capacity via tool-wear monitoring systems. In wear monitoring systems, process parameters such as temperature, vibration amplitude, power, torque, forces, and AE have been used as indicators of tool wear and failure. Methodology to predict drill wear in order to replace the drill bit prior to significant damage had been demonstrated [10-18].

The wear on the outer corner of the drill margin was used as the drill wear measurement [10]. By using a quartz dynamometer, a relationship between the drill wear and one minor drilling force, called radial force, was found by Lenz and Mayer [10]. This method was dependent on the asymmetry of the two cutting lips. At the beginning of a drilling process, wear is only produced at one cutting lip. As soon as the height of both cutting lips is equal, the second lip, which is now sharper, starts cutting the work piece. Before the second lip starts cutting, the RMS of the radial force increases as the wear on the first lip progresses. As soon as the second lip starts cutting, the RMS of the radial force drops to a minimum point. He concluded that the tool life criterion is identified when the RMS of the radial force achieves a minimum close to that of the sharp drill.

Yee and Bloomquist [11] have used vibration analysis techniques to predict drill breakage for small drill bits. An accelerometer was mounted on the work piece

to detect the increasing vibration patterns due to the contact between the drill and walls of the hole being drilled. Successful breakage predictions of 1 mm diameter drills by this method were demonstrated.

Thangaraj and Wright [12] studied the use of rate of change of the thrust force for predicting drill failure. The wear on the outer corner of the drill margin was used as the wear measurement and sharp spikes in the thrust force were observed under failure condition. The work piece was mounted on a Kistler piezo-electric platform-type Dynamometer, and the downward thrust forces exerted by the drill were thus recorded. A sharp increase in the rate of change of the thrust force had been found for several seconds before serious failure. The proposed method had shown effectiveness in predicting drill failure before excessive damage occurred under a wide range of cutting conditions.

Liu and Wu [13] developed an on-line system to detect flank wear area by using a sensor fusion strategy with both acceleration and thrust force signals [13]. This method depends on the changes in vibrational signals and the thrust force increases due to drill wear during drilling processes. Therefore, the percent increase of the peak-to-peak amplitude of vertical acceleration and the percent increase of drilling thrust were chosen to be indices of drill wear. A two-category linear classifier was used with the two signals. The drill wear-area was also classified into two groups: usable and worn-out. The success rate of the proposed model was claimed to be over 90%.

Recently, neural networks have attracted the attention of many researchers. Neural networks are highly parallel computing systems, used to perform pattern

recall, classification, and prediction tasks. They have a great degree of robustness and can be applied to modeling nonlinear mapping as well as to recognition of characteristic features with the data possibly corrupted by noise. Because of this robustness, neural networks have recently received considerable attention from researchers in manipulating the incomplete sensory data in the automatic monitoring of machining processes [14-16].

In a recent work by Govekar and Grabec [16], a self-organizing neural network was applied to classify the drill flank-wear state from both cutting momentum and thrust force signals. During a drilling process, the successive cutting momentum and thrust-force signals were digitized, transformed, and averaged into a 128-component vector. The corresponding experiment showed that the change of drill wear was reflected both in the change of the norm of the averaged power spectra vector of momentum as well as in the change of both the norm and structure of the averaged power spectra vector of thrust force. According to the observations, 30 feature components extracted from the two spectra vectors, and three drill-wear status vectors, were used as input to the neural network to form prototypes in the adaptation stage. After adaptation, in the classification stage, an incomplete vector with only the 30 components from the two signals was supplied to the neural network, and the three drill-wear status vectors could be estimated.

The sensors used in the above investigations are either dynamometers or accelerometers. A dynamometer is used to detect such cutting force signals as thrust force, radial force and torque. One disadvantage in using a dynamometer is that the force measurement is not sufficiently sensitive to the progression of tool wear, but

is too sensitive to the prevailing cutting conditions. Another major difficulty is that the work piece must be mounted on the dynamometer, and thus the machining process is disturbed and discontinuous. These disadvantages make dynamometers impractical for industrial applications.

As for the accelerometer, the problem of mounting the sensor on the cutting tool or work piece is the same as that encountered when using a dynamometer. Another difficulty associated with accelerometers is in isolating the frequency information when trying to correlate the vibrational signal of the cutting tool with the progress of tool wear. It is difficult to separate frequency information with respect to tool wear from frequency information due to the machine dynamics.

Acoustic emissions (AE) signals, generated during the manufacturing process, have been used in recent research to automatic on-line monitor machining processes. AE, or the transient elastic energy released in materials undergoing deformation, is a non-destructive inspection technique. Since the frequency content of the AE signal is well beyond the range of frequencies generally associated with the dynamic behavior of machine tools, the signal should relate to the cutting process only. Acoustic transducers are usually small, cheap, and do not disturb the normal machining process, and provide a relatively easy way to monitor a machining process for an industrial application without disturbing the normal machining operation [3]. Moreover, the output signal detected by the AE transducer is reliable and closely correlated to the characteristics of the cutting process under control. Chandrashekhar et al. [17] have tried to predict drill wear by using the RMS value of the AE signal as a measurement parameter [17]. This method was based on a

mathematical experiment model developed by the Kannatey-Asibu and Dornfeld [18]. The model expressed that the RMS value of AE signal is proportional to the power expended in the cutting process. The experimental AE_{rms} values indicate that as the drill becomes dull, the RMS value of the AE signal increases sharply. This sharp increase can be used effectively to monitor the wear of the drills. This initial success in the usage of AE for the monitoring of drill wear provides the confidence in the use of AE for the current study.

2.4 Modeling of Cutting Forces and Acoustic Emission Energy

Since the drilling force and the AE signals were used by most past research work, a review of the modeling cutting forces and acoustic energy in the metal-cutting process is helpful, providing theoretical background to those monitoring methods based on cutting forces or AE.

Analytical models of cutting forces based on classical, thin-shear zone cutting models have been developed to predict the thrust and torque in the drilling process [19-24]. A two-dimensional orthogonal metal-cutting model was chosen by several researchers, including Pal et al. [19] and Williams [20, 21], to apply to drilling process analyses. The work of Williams in 1974 [21] was to simulate the drilling action of a two-flute twist drill with an orthogonal cutting model. The whole drilling process was divided into three models corresponding to the effect of the feed velocity on the cutting rake angle at the main cutting edge, chisel edge, and drill center. Empirical equations were derived for predicting total torque and thrust

forces provided with cutting conditions, drill geometry, and an empirical factor which is related to the work material. The computed results of torque and thrust forces were shown favorably in the experiment test results.

In addition to the correlation between predicted results and experimental results of thrust and torque forces indicated by the two-dimensional model, a few attempts to apply the three-dimensional oblique-cutting model at the main cutting lips also showed promising results [22-24]. In Wiriyacosol and Armarego [24], the main cutting lip was represented by a classical oblique cutting model and the lip was divided into numerous single oblique cutting elements. The total thrust and the total torque at the main lip were found by summing up those elements' thrust and torque. A similar approach was considered for the chisel edge region. The chisel edge was considered as a number of single orthogonal cutting elements with highly negative rake angles. Again, the total thrust and the total torque at the chisel edge were found by summing their thrust and torque. The force contributed from the indentation process region where the clearance angle changes to negative was ignored in this model. The total drilling thrust and torque for the whole drill was found by adding up the values for the two drill regions.

Kannatey-Asibu and Dornfeld proposed the first model to present the AE energy from an orthogonal cutting process [18]. Three deformation zones were defined in their work, i.e. primary deformation zone, secondary deformation zone, and tertiary zone. The AE powers generated from the first two deformation zones were determined. A further model was proposed by Lan and Dornfeld [25]. In this work, the AE power generated from the tertiary zone was added to the model of

Kannatey-Asibu and Dornfeld. This power was added to account for the power generated from the flank land wear. More detailed descriptions of these models will be given in chapter 3.

2.5 Hole-Quality Evaluation

The purpose of drill-wear monitoring is to provide a method for automatically controlling a drilling process and ensuring that acceptable holes are drilled. The process would allow adequate time to replace the drill bit. However, in addition to the time determination in terms of drill wear, monitoring on-line changes in quality measurements of drilled holes can provide more useful information for controlling the drilling process. The reason behind this is that, since unacceptable hole qualities may be produced even before the failure point of the drill bit, an on-line hole quality monitor might be needed to decide when to initiate an adaptive change to control the drilling process.

A drilling force which can be measured on-line was used in an experimental investigation by Radhakrishnan and Wu in 1981 [26] for prediction of hole surface quality for composite materials. The lamination frequency associated with the laminated fiber of the composite material was used to present the waviness of the hole surface. This lamination frequency was given by the ratio of number of laminations per inch of material to the time taken by the drill to penetrate an inch of material. The correlation between the change in this frequency and drilling forces was investigated. The experimental result showed that the static nature of the

cutting force such as the mean or peak thrust/torque did not provide a reliable indication of changes in hole surface quality. Comparatively, the dynamic characteristics of the drilling thrust force using the Dynamic Data System developed by Wu in 1977 [27] showed a very strong correlation between the hole surface and the changes in the standard deviation of the lamination-frequency content of the drilling-thrust force.

2.6 Summary

As has been introduced in the previous section, besides drill-wear monitoring, which can provide drill wear information, additional information about drilled hole quality will be useful and can be provided by monitoring on-line changes in the quality measurements of drilled holes. Therefore, the current study includes an effort to develop an on-line drilled-hole quality prediction method. Although the objectives of Radhakrishnan's research are very similar to this work, there are three restrictions in Radhakrishnan and Wu's work [26]. First, the use of cutting force as the indicator is not sufficiently sensitive to the progression of tool wear, but is too sensitive to the prevailing cutting conditions. In comparison with the force signal, the AE signal has more isolating ability which relates the signal to the cutting process only. Secondly, when cutting force is used as the indicator, a dynamometer is needed to detect the force signals and the work piece must be mounted on the sensor. This layout makes the machining process disturbed and discontinuous. Hence, the dynamometer is impractical for industrial applications. Lastly, the

methodology developed by Radhakrishnan is heavily dependent on the variation of different layers in the composite material, i.e., the lamination frequency. The methodology may not be suitable for a hole drilling process with homogeneous material. Considering these restrictions in Radhakrishnan's work, a method which provides predicted on-line information about drilled hole quality for hole-drilling process evaluation with homogeneous steel material is the objective of current study. Also, the AE signal is used as the indicator parameter in the current study in order to preserve signal sensibility and to develop a practical method for industrial applications. Also, on-line drill-wear monitoring is investigated in the current study.

From this review of past work regarding the subject of on-line drilling process evaluation and control, it seems there is a missing link. The work on drill-wear monitoring seems to be based on an assumption. This assumption is that, if the drill is getting worn, the drilled hole quality may be getting worse. Based on this assumption, being able to detect drill wear and to replace the drill bit before it fails can preserve the drilled hole quality. Unfortunately, past research provides no information on how drill wear affects the change in quality of a drilled hole. Therefore, the correlation between hole quality and drill wear is one item of interest in the current study. After viewing those causes which affect hole quality, the drill bit used in the current study is kept as only one type of the same geometry parameters to eliminate the effect of drill geometries on drilled-hole quality. Then, the correlation between drill wear and quality measurements of drilled hole can be uncovered.

CHAPTER 3. THE MECHANICS AND ENERGY OF METAL CUTTING

The acoustic emission (AE) signal generated in a drilling process is used as the indicator parameter for the current study. The initial relationship between AE measurement and drill-bit flank wear is involved in the objective of this study. Therefore, a theoretical relationship between AE energy generated during the drilling process and drill-flank wear is needed to provide the theoretical foundation for the present study. This equation describes how AE power changes along with flank wear area propagation. However, a drilling process involves orthogonal as well as oblique cutting operations. To make this dissertation self-contained, an introduction to the mechanics of metal cutting is provided in this chapter. The introduction starts with the basic concepts of metal cutting, i.e. an introduction to orthogonal and oblique cutting operations, and the terminology used in metal cutting and to describe tool wear in the metal cutting process. Then, chosen models of cutting forces for orthogonal and oblique metal cutting operations are introduced. Combining the forces in these two cutting operations, the drilling forces in a drilling operation are obtained. Based on these force models, energy in orthogonal cutting, oblique cutting, and drilling operations is introduced, respectively. Finally, a theoretical relationship between AE energy and drill flank wear is derived.

3.1 Introduction to Metal Cutting

Metal cutting operations can be modeled by either the orthogonal cutting process or the oblique cutting process, as shown in Figure 3.1. In the orthogonal cutting process, the cutting edge is perpendicular to the direction of the velocity of the work piece material relative to the cutting tool. It is assumed that the chip flows up

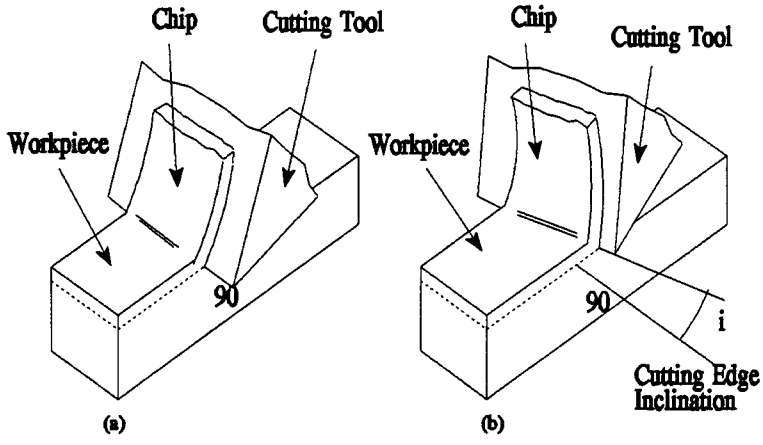

Figure 3.1 Metal cutting process model: (a) orthogonal cutting, (b) oblique cutting.

the surface of the wedge-shaped tool with the chip velocity parallel to the direction of the velocity of the work-piece material. Under this assumption all analyses, based on the plane that contains two velocity vectors, can be done. Therefore, orthogonal cutting represents a two-dimensional cutting case rather than a three-dimensional problem and the cutting action can be analyzed more easily if the edge of the tool is set at right angles to the cutting direction. Metal cutting operations

modeled as orthogonal cutting include: turning a tube, cutoff or parting operations, and some cases of shaping or planning. However, in practice, the cutting edge is rarely at right angles to the cutting direction. Most cutting operations involve an oblique cutting process. In oblique cutting, the cutting edge is inclined at an angle to a line drawn at right angles to the direction of the velocity of the work-piece material. In oblique cutting the assumption of the chip flowing up the surface of the wedge-shaped cutting tool with the chip velocity parallel to the direction of the velocity of the work-piece material is no longer applicable. This makes the oblique cutting process a three-dimensional cutting case rather than a two-dimensional problem like orthogonal cutting, and analysis of the cutting action can be more complicated. The metal cutting operations which can be modeled as oblique cutting include: helical end mills, face mills or many turning cases.

Since orthogonal cutting represents a two-dimensional cutting case and the analysis of the cutting action can be more easily analyzed, most experimental and theoretical research work of the metal cutting process has been limited to this simplified two-dimensional type of cutting. The drilling process includes both orthogonal and oblique cutting. Orthogonal cutting will be described first, followed by a discussion of oblique cutting [28-32].

3.2 General Terms in Metal-Cutting Operations

In metal cutting the interaction between the wedge-shaped cutting tool and the work-piece material is shown in Figure 3.2. The cutting edge is formed by the

intersection of two surfaces of the wedge-shaped cutting tool. The surface which the chip flows on and along is known as the rake face, or more simply as the face. The surface ground back to clear the new or machined work-piece surface is known as

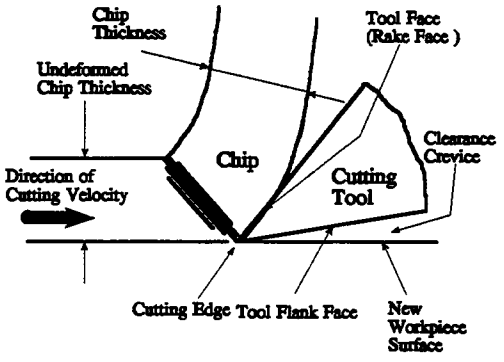

Figure 3.2 Terminology in a metal cutting process.

the flank. Thus, there exists a clearance crevice between the tool flank and the new work-piece surface. The thickness of the surface layer of material removed by the action of the tool is called the undeformed chip thickness. Although in practical cutting operations this thickness often varies as cutting proceeds, for simplicity, it is usually arranged to be constant in analysis [28-32].

One of the most important variables in metal cutting is the rake angle. The rake angle is specified by the angle between the tool face and a line perpendicular to the new work surface as shown in Figure 3.3. This angle significantly affects the cutting force during a cutting operation. The larger the angle is, the smaller the cutting force needed. The convention of sign of the rake angles is defined and illustrated in Figure 3.3.

The tool flank plays no part in the process of chip removal. However, the angle defined as the clearance angle, between the flank and the new work piece surface as shown in Figure 3.3 can significantly affect the rate at which the cutting tool wears [28].

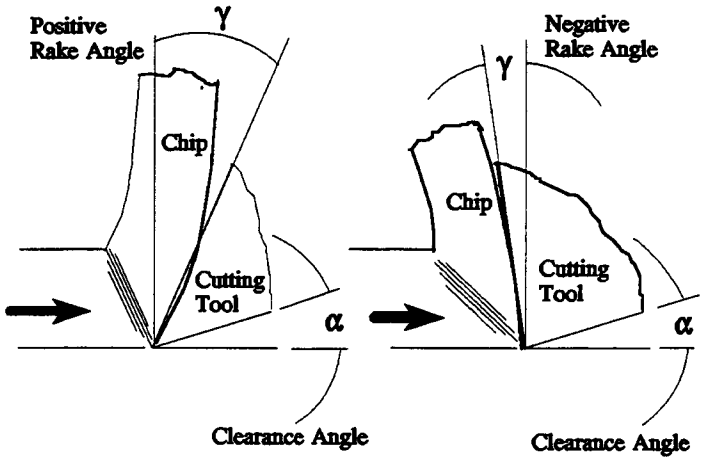

Figure 3.3 Sign definition of the rake angle in metal cutting.

During the cutting process, the surface layer of constant thickness is removed by the relative movement of the tool and work piece. In order for the tool cutting edge to move along the cutting line, the material is compressed between the cutting edge and the uncut material just behind it. The material cut is forced to deform and slide up the tool face. The largest compressive stresses are located farthest from the cutting edge and are balanced by the tensile stresses in the zone nearest the cutting edge, hence the cut material curls outwardly or away from the cut surface. This deformed material sliding over the tool face is called the chip. This deformation process is called shearing action. The region where the shearing or deformation

takes place is illustrated in two basic models, as shown in Figure 3.4. Merchant [29] claims that shearing action takes place along a thin plane specified from the tool point to a point on the free work piece surface [30] and that no action

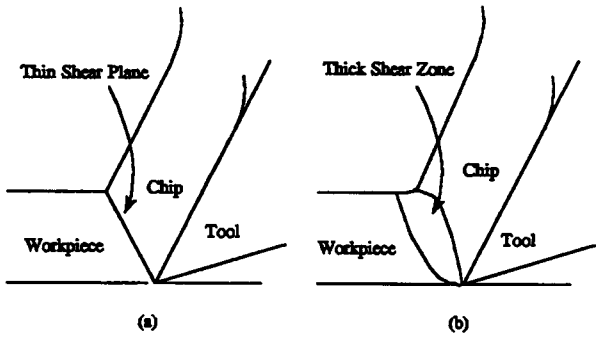

Figure 3.4 Two basic models for deformation zone in metal cutting process.

takes places on either side of this shear plane, as shown in Figure 3.4a. In practice, the shearing action is not confined in a plane but occurs in a zone of finite size, and, accordingly, a model called thick zone model is proposed by Palmer and Oxley [31,32], as illustrated in Figure 3.4b.

3.3 Tool Wear Measurement

Progressive tool wear takes place by a process of attrition on both the rake and flank faces. Wear on the tool face is characterized by the formation of a cavity or a crater which is produced by the attrition of the chip flowing along the tool face. Rubbing action on the surface of a newly generated work-piece causes wear on the flank face extending back from the cutting edge. This flat surface is called a wear

land. When tools are used under normal and economical conditions, the flank wear of a tool is usually the controlling factor. Wear on the flank face of a cutting tool is caused by friction between the newly machined work-piece surface and the contact area on the tool flank face. The worn area, referred to as the wear land, on the flank face is approximately parallel to the new work-piece surface being machined. The width of the wear land is usually taken as a measure of the amount of wear and can be determined by means of a toolmaker's microscope or an optical measuring system.

3.3.1 Flank Wear of Insert Tools in Turning Operations

In turning operations, a single point insert is used. A typical worn single point tool is shown in Figure 3.5a. The wear on the flank face is not uniform along the active cutting edge. Therefore, it is necessary to specify the locations of the wear when deciding on the amount of tool wear. As shown in Figure 3.5a, the wear land is usually fairly uniform in the central position of the active cutting edge, i.e., zone B. The average wear land width in this region is used as the wear measurement of an insert tool used during turning operations.

3.3.2 Relationship Between Flank Wear and Machining Time During Turning Operations

The typical relationship between the progress of flank wear land width and time are shown in Figure 3.5b. The wear curves can be divided into three stages:

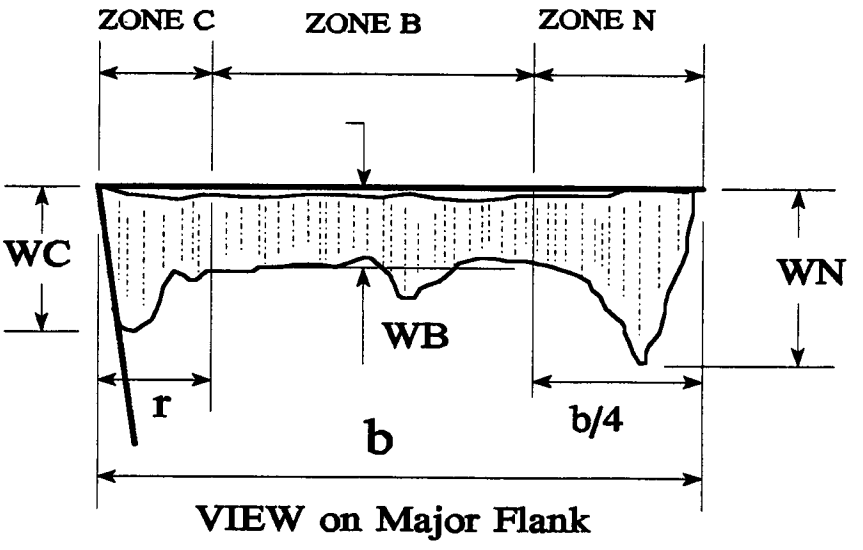

(a)

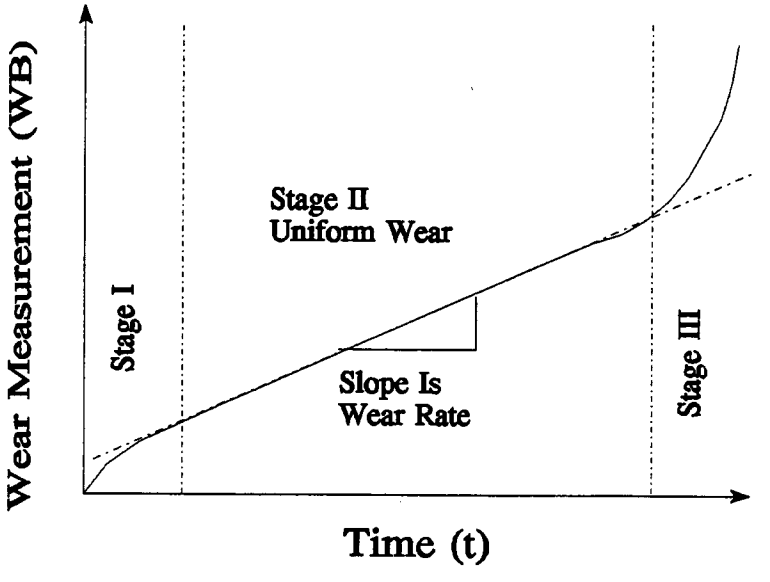

(b)

Figure 3.5 Typical flank wear and wear measurement of an insert tool: (a) flank wear pattern; (b) flank wear curve.

(a) Stage I, the rapid initial wear stage, where the sharp cutting edge is quickly broken down and a finite wear land is established; (b) Stage II, the relatively long period of very gradual wear at a uniform rate; and (c) Stage III, the final period of rapid wear occurring at a gradually increasing rate.

Metal cutting experiments held on a turning machine were conducted by Iwata in 1977 [33] and Kannatey-Asibu and Dornfeld in 1982 [34]. Both of their experimental plots of corresponding flank wear against cutting time were quite in approval with typical wear curves.

3.3.3 Flank Wear on Drills During Drilling Operations

A twist drill is used in most drilling operations. In reviewing the literature, there appears to be no fixed criterion to characterize drill wear conditions. While, in general, flank wear was used in almost all previous research attempting to characterize drill wear conditions [5,10,12,16,17], different measurements were used in the different investigations to define drill-flank wear.

Figure 3.6 shows the different measurements of drill flank wear used in past research. Also, the characteristic pattern of flank-wear development with machining time in turning operations was found and used in a couple of the studies with regard to drill-flank wear monitoring [12,17]. Bandyopadhyay and Wu [35] used the average flank wear, $(va+vb+vc+vd)/4$, as the drill-wear measurement to develop a drill-life monitoring algorithm. Lenz and Mayer [10] used the wear in the outer corner of the drill margin as the drill-life criterion in his research. Thangaraj and

Wright [12] also use the flank wear at the outer corner in his research [12]. A plot of the measured flank wear with respect to the number of holes drilled was obtained

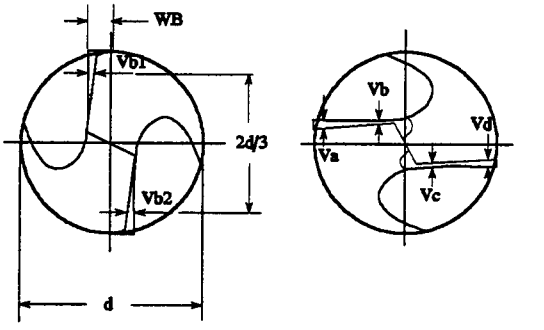

Figure 3.6 Different drill wear measuring definitions.

in his work. Except during the period of initial wear, i.e. wear stage I, the plot showed agreement with the theoretical pattern of the wear-development curve. Govekar and Grabec [16] used $(vb1+vb2)/2$ to represent drill-flank wear. Chandrashekhar et al. [17] used the width of the flank wear land at the outer corner of the main cutting edge as the drill-wear measurement. For this research, an expression based on uniform wear stage, wear stage II, of a theoretical wear-development curve was developed.

3.4 Forces in the Cutting Operation

As discussed previously, there are two models available for describing the shear zone (Figure 3.4). Experimental observations indicate that at a low cutting

speed the thick shear zone model applies. But, as the speed increases, the deformation zone decreases so that it appears that this zone collapses to a single plane, and then the thin shear plane model applies. At low cutting speeds, as defined by Zorev [36], the effects of cutting temperature and cutting speed on the deformation process were considered negligible. However, in practical cutting conditions, cutting speeds are considered high relative to the defined low-cutting speeds [36]. The

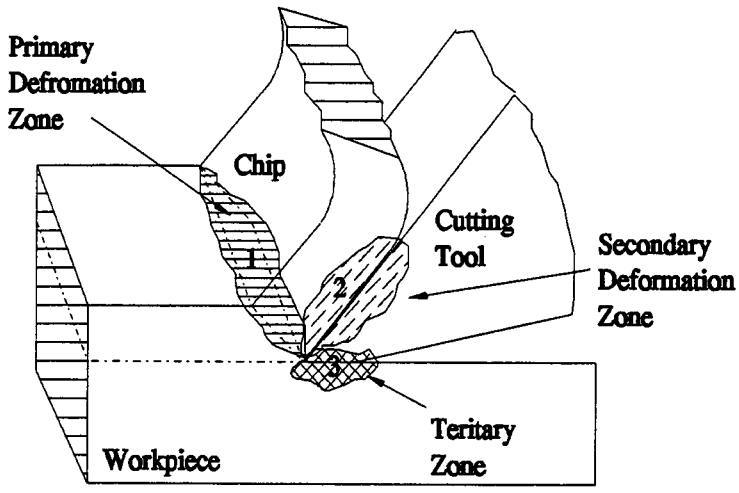

Figure 3.7 Deformation zones in metal cutting model.

thin shear plane model is thus adopted here for its much simpler analysis. Three areas, as shown in Figure 3.7, need to be considered in the analysis of a cutting process: primary, secondary and tertiary [37]. The basic chip formation process occurs here in the primary deformation zone. This zone extends from the tool cutting edge to the junction between the surface of the chip and the work piece. The

chip formed in the primary zone moves along the tool face and is further deformed in the process. This chip-tool interface, where further deformation and sliding takes place, is called as the secondary deformation zone. In the tertiary zone, the newly formed work-piece surface which has resulted from a separation of the cut material from the parent work piece moves off on the flank side of the tool [37].

3.4.1 Mechanics of Orthogonal Cutting

A forces and velocities diagram of the Merchant thin-shear plane model is shown in Figure 3.8. *R* is the resultant force which is applied to the entire cutting process. Since no cutting tool is perfectly sharp, the resultant force *R* is distributed over two areas, i.e. the area where tool contacts the chip and the area where the

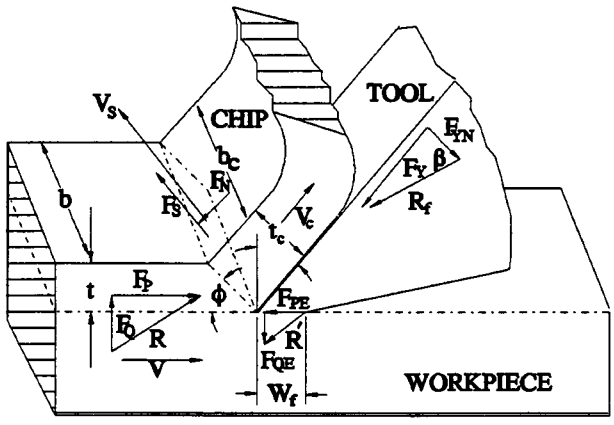

Figure 3.8 Orthogonal metal-cutting model.

cutting edge contacts the work piece. The resultant force R is decomposed into two components, R_f, and R'. R_f is the force applied to the chip at the tool chip interface and R' is the force acting on the contact between the tool and the new work piece surface. The small contact area between the new work-piece surface and the tool flank face is caused by the deformation of the tool material due to the high stresses acting near the tool cutting edge. Because of this contact, a friction force, F_{PE}, arises in this tool flank face that contributes nothing to removal of the chip [28]. In the force analysis of a metal-cutting process, force dynometers are used and the resultant force is determined experimentally from the measurements of the two orthogonal force components, i.e. F_P, in the cutting direction, and F_Q, normal to the cutting direction. Once F_P and F_Q were obtained, other force components could be obtained based on the measurements of F_P and F_Q. The relationship between the resultant force R and its components is shown in Figure 3.8. Based on the forces equations derived by Armarego and Brown [30], the combined forces due to flank wear and the forces used in chip removal are defined and given by the following equations:

a. F_P and F_Q are the total orthogonal force components. F_P is in the direction of the tool motion and F_Q is normal to F_P.

b. F_S and N_S are the shearing force and compressive force, respectively. F_S is the force causing deformation of the material along the shear plane; N_S is normal to F_S.

c. F_Y and F_{YN} are the friction force and normal force on the tool face, respectively. F_Y is the force along the tool face and opposes motion of the chip up the tool.

d. F_{PE} and F_{QE} are the friction force and the normal force on the tool flank face, respectively.

$$F_P = F_P' + F_{PE} \tag{3.1}$$

$$F_Q = F_Q' + F_{QE} \tag{3.2}$$

$$F_S = F_P'\cos\phi - F_Q'\sin\phi \tag{3.3}$$

$$N_S = F_P'\sin\phi + F_Q'\cos\phi \tag{3.4}$$

$$F_Y = F_P'\sin\gamma + F_Q'\cos\gamma \tag{3.5}$$

$$F_{YN} = F_P'\cos\gamma - F_Q'\sin\gamma \tag{3.6}$$

where ϕ is the shear angle and given by

$$\phi = \tan^{-1}\left[\frac{\frac{t}{t_c}\cos(\gamma)}{1-\frac{t}{t_c}\sin(\gamma)}\right] \tag{3.7}$$

with γ the tool rake angle, t_c the chip thickness, and t the undeformed chip thickness. F_P' and F_Q' are the cutting and thrust forces. respectively. They contribute to removal of the chip and are given by

$$F_P' = \frac{tb\tau_\kappa\cos(\beta-\gamma)}{\sin(\phi)\cos(\phi+\beta-\gamma)} \tag{3.8}$$

$$F_Q' = \frac{tb\tau_\kappa\sin(\beta-\gamma)}{\sin(\phi)\cos(\phi+\beta-\gamma)} \tag{3.9}$$

with τ_k the shear stress on the shear plane which is assumed uniform over this plane, b the width of cut, and β the angle between the friction force on the chip-tool interface and the force normal to the rake face. The forces F_{PE} and F_{QE} contributed from flank wear, as derived by Rubenstein and Connolly [38,39], are respectively given as $F_{PE}= \mu\ C\ HbWf$ and $F_{QE}= C\ HbWf$, with μ as dry-sliding friction, H the material hardness parameter, C the constant, b the cutting width, and Wf the flank wear land. With one step further, $W_{area}= bWf$, the theoretical relationship derived by Rubenstein and Connolly can be changed into the forms as

$$F_{PE} = \mu CHW_{area} \tag{3.10}$$

$$F_{QE} = CHW_{area} \tag{3.11}$$

where the W_{area} is tool flank wear area.

In orthogonal metal cutting, as shown in Figure 3.8, three important velocity components are involved in the cutting process. Cutting velocity, V, is the speed with which the work piece moves relative to the tool. Shear velocity, V_S, is the speed with which the chip moves relative to the work piece on the shear plane. Chip velocity, V_C, is the speed with which the chip moves relative to the tool in the direction of the shear plane. The relationship between these velocity components can be derived as [30]:

$$V_C = \frac{\sin\phi}{\cos(\phi-\gamma)}V \tag{3.12}$$

$$V_S = \frac{\cos\gamma}{\cos(\phi-\gamma)}V \tag{3.13}$$

where Φ is the shear angle defined as before and γ is the rake angle [30].

3.4.2 Mechanics of Oblique Cutting

Although many practical machining processes were simplified as orthogonal cutting in many investigations, an oblique cutting model may more closely describe the physics for practical metal cutting operations [28]. In an oblique cutting model the cutting edge is no longer normal to the cutting velocity and indicated by the inclination angle. The inclination angle (i in Figure 3.9) is measured between the cutting edge and the normal to the cutting velocity in the plane of the newly machined surface. Major differences between the orthogonal cutting and oblique cutting are that the chip flow direction is in general no longer normal to the cutting edge and that the process is three dimensional.

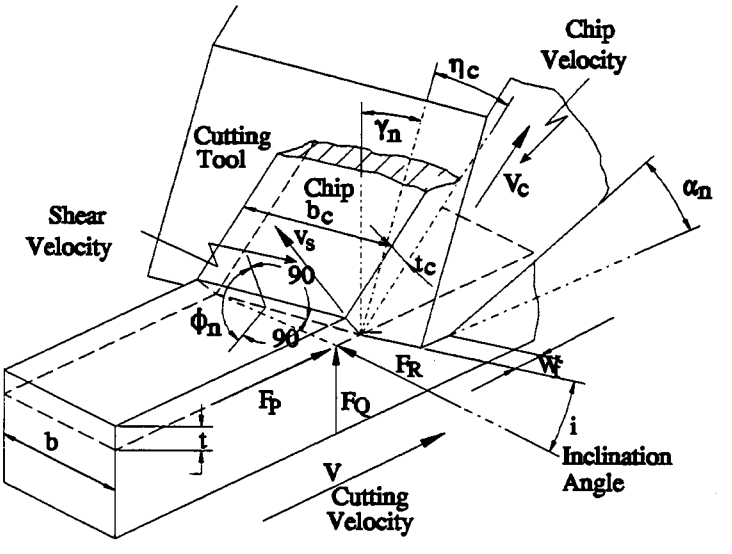

Figure 3.9 Oblique metal-cutting model.

To model the cutting forces in an oblique cutting, corresponding cutting angles need to be redefined. The rake angle is no longer measured from the tool rake face to a line perpendicular to the cutting velocity in the plane containing cutting velocity. There are several alternative planes in which this angle may be measured. In general, normal rake angle is used in cutting force analysis. Normal rake angle is the angle between the rake face and the normal to the cutting velocity measured in the plane normal to the cutting edge as shown in Figure 3.9. As with the rake angle, several alternative definitions of the shear angle are possible. One general definition is the angle measured in a plane normal to the cutting edge. This is called the normal shear angle as shown in Figure 3.9. In addition to deciding which is the most appropriate rake angle and shear angle, it is clear that an essential requirement for predicting cutting forces for oblique cutting is a knowledge of the chip flow angle, as shown in Figure 3.9. A chip flow angle is the angle between the chip flow velocity and the normal to the cutting edge, in the plane of the rake face. The chip flow velocity would be in the plane parallel to the cutting velocity and perpendicular to the newly machined surface [40].

Instead of two force components, three force components need to be considered: F_P, parallel with the cutting velocity, F_Q, perpendicular to the newly machined surface, and F_R, perpendicular to F_P and F_Q (Figure 3.9). Experimentally, the resultant force is computed based on the measurements of these three orthogonal components using force dynometers. Other force components can also be determined accordingly. The relationship between the resultant force R and its components is shown in Figure 3.9. As for orthogonal cutting, based on the forces equations

derived by Armarego and Brown [40], after incorporating with the force contribution from the wear these forces are given as follows:

$$F_P = F_P' + F_{PE} \tag{3.14}$$

$$F_R = F_R' + F_{RE} \tag{3.15}$$

$$F_Q = F_Q' + F_{QE} \tag{3.16}$$

Where F_P' , F_R' , and F_Q' are the three cutting forces, respectively, which contribute to removal of the chip and are given by

$$F_P' = \frac{tb\tau_\kappa}{\sin(\phi_n)} \left\{ \frac{\cos(\beta_n - \gamma_n) + \tan(i)\tan(\eta_c')\sin(\beta_n)}{\sqrt{\cos^2(\phi_n + \beta_n - \gamma_n) + \tan^2(\eta_c')\sin^2(\beta_n)}} \right\} \tag{3.17}$$

$$F_Q' = \frac{tb\tau_\kappa}{\sin(\phi_n)\cos(i)} \left\{ \frac{\sin(\beta_n - \gamma_n)}{\sqrt{\cos^2(\phi_n + \beta_n - \gamma_n) + \tan^2(\eta_c')\sin^2(\beta_n)}} \right\} \tag{3.18}$$

$$F_R' = \frac{tb\tau_\kappa}{\sin(\phi_n)} \left\{ \frac{\cos(\beta_n - \gamma_n)\tan(i) - \tan(\eta_c')\sin(\beta_n)}{\sqrt{\cos^2(\phi_n + \beta_n - \gamma_n) + \tan^2(\eta_c')\sin^2(\beta_n)}} \right\} \tag{3.19}$$

with β_n, the mean friction angle in plane normal to cutting edge; γ_n, the normal rake angle; i, inclination angle; t, undeformed chip thickness; t_c, chip thickness; τ_k, yield shear stress of material; ϕ_n, the normal shear angle; and η_C', the chip flow angle on the tool face. The normal shear angle, Φ_n, is given by

$$\phi_n = \tan^{-1}\left[\frac{\frac{t}{t_c}\cos(\gamma_n)}{1 - \frac{t}{t_c}\sin(\gamma_n)} \right] \tag{3.20}$$

Since the friction force would be expected to be collinear with the chip-flow direction, that is, $\eta_C' = \eta_C$, based on Stabler's experimental results, η_C', friction force direction angle on the rake face, is given as

$$\eta_C = \eta_C' = i \tag{3.21}$$

Again, modified from the forces due to flank wear derived by Rubenstein [38] and Connolly and Rubenstein [39], force contributions from tool wear in an oblique cutting are extended from those in orthogonal cutting and are given as follows:

$$F_{PE} = \mu C H W_{area} \tag{3.22}$$

$$F_{RE} \approx 0 \tag{3.23}$$

$$F_{QE} = C H W_{area} \tag{3.24}$$

with μ, dry sliding friction; H, material hardness parameter; C, constant; and W_{area}, tool flank wear area.

As for orthogonal cutting, the force which contributes to the removal of a chip can be considered to act as two components on the shear plane, F_S and N_S, and two components on the rake face, F_Y and F_{YN}. F_S and N_S are the shear force and compressive force respectively. F_S is the force causing deformation of the material along the shear plane, and N_S is normal to F_S. The shear force ,F_S, is inclined at an angle, η_S', to the normal cutting edge in the shear plane. Similarly, F_Y is the friction force along the tool face and opposes the motion of the chip up the tool. F_{YN}, is the normal force on the tool face. The friction force, F_Y, is at an angle, η_C', to the normal cutting edge in the rake face. In general, chip velocity and friction

force are collinear as are shear velocity and shear force in the shear plane, $\eta_S' = \eta_S$. Thus, the shear flow angle and chip flow angle could be used in their place and the F_S, N_S, F_Y and F_{YN} could be expressed as:

$$F_s = \sqrt{\{[F_P'\cos(i)+F_R'\sin(i)]\cos(\phi_n)-F_Q'\sin(\phi_n)\}^2+[F_P'\sin(i)-F_R'\cos(i)]^2} \tag{3.25}$$

$$N_s = [F_P'\cos(i)+F_R'\sin(i)]\sin(\phi_n)+F_Q'\cos(\phi_n) \tag{3.26}$$

$$F_Y=\sqrt{\{(F_P'\cos(i)+F_R'\sin(i))\sin(\gamma_n)+F_Q'\cos(\gamma_n)\}^2+(F_P'\sin(i)-F_R'\cos(i))^2} \tag{3.27}$$

$$F_{YN} = [F_P'\cos(i)+F_R'\sin(i)]\cos(\gamma_n)-F_Q'\sin(\gamma_n) \tag{3.28}$$

with those variables defined as before [40].

In an oblique metal cutting, as shown in Figure 3.9, there are also three important velocity components involved in the cutting process: the cutting velocity, V; the shear velocity, V_S, in the shear plane; and the chip velocity, V_C, in the plane of the tool rake face. The relationship between these velocity components, V_C, V_S, and V can be derived in terms of the normal shear angle and normal rake angle as follows [40]:

$$V_s = \frac{\cos(\gamma_n)\cos(i)}{\cos(\phi_n-\gamma_n)\cos(\eta_s)}V \tag{3.29}$$

$$V_s = \frac{\sin(\phi_n)\cos(i)}{\cos(\phi_n-\gamma_n)\cos(\eta_s)}V \tag{3.30}$$

with η_s, the shear flow angle on the shear plane, given by

$$\eta_s = \tan^{-1}\left[\frac{\tan(i)\cos(\phi_n-\gamma_n)-\tan(\eta_c)\sin(\phi_n)}{\cos(\gamma_n)}\right] \tag{3.31}$$

3.5 Mechanics of the Drilling Process

Hole-making processes are the most widely used among all the metal-working processes. There are several different types of hole-making processes. The most common operation is drilling with a twist drill to generate an internal cylindrical surface. Unlike the single point cutting tool discussed in the orthogonal or oblique cutting operation, a drill bit is a multi-point cutting tool. Different cutting operations, such as orthogonal cutting or oblique cutting, are carried at different cutting edges in one drill bit. To model cutting forces in a drilling process accurately, an integration of orthogonal cutting and oblique cutting operations is necessary.

In the current investigation a split point twist drill is used. A split twist drill has two positive rake angle cutting edges extending to the center of the drill. One is the primary cutting edge (or main cutting edge) along the intersection of the conical point with the flute, and the other is the secondary cutting edge extending from the end of the primary cutting to the center of the drill produced by a web-thinning process. Since the relationships between the directions of the cutting velocity and the cutting edge are different, the two distinct regions of the drill, namely, the primary cutting lips and the secondary cutting lips, need to be analyzed separately (Figure 3.10). A modeling method developed by Wiriyacosol and Armarego [24] for the standard twist- drilling process is modified for the split-drilling process in

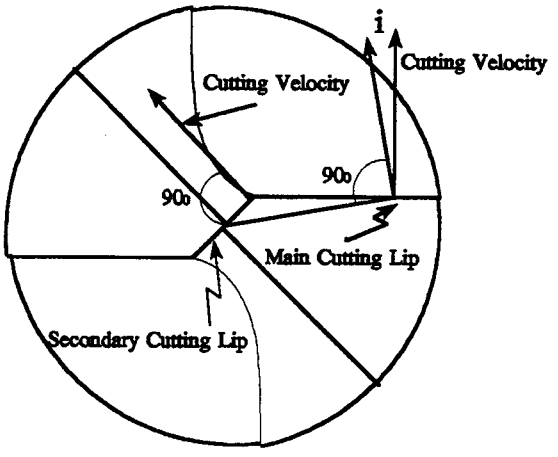

Figure 3.10 Relationship between cutting velocity direction and cutting edge for main and secondary cutting lips.

this investigation. Cutting processes at the primary cutting lips and secondary cutting lips are described by the classical single-edge oblique-cutting model and the orthogonal cutting model, respectively. Each lip is considered to consist of many single-edge cutting elements where the variation in cutting conditions within each element may be ignored and the conditions of that element are represented by the conditions at the mid-point of that elemental cutting edge. The summation of the elemental values provide the total thrust force and torque. The feed velocity at the secondary cutting lips cannot be ignored, and the dynamic cutting velocity of the cutting process needs to be considered.

3.5.1 Mechanics of Primary Cutting Lips

Various drill elements, angles, and dimensions are illustrated in Figure 3.11. In Figure 3.11, D is the diameter of the drill and L_C is the chisel-edge diameter, twice the length of the secondary cutting lip. W is half the chisel-edge width and ψ is the chisel-edge angle. p is the half-point angle of the drill and the L is lead of helix. Cl_0 is the lip clearance angle at the periphery and δ_0 is the helix angle (or rake angle) at the outer corner. For any element, such as the jth element from the outer corner of the drill point, the elemental thrust, $\Delta Thrust_{mj}$, torque, $\Delta Torque_{mj}$, and those intermediate parameters developed by Wiriyacosol and Armarego [24] from oblique cutting analysis are summarized as

$$\Delta Thrust_{mj}=2\{\Delta F_{QM}\cos(\Psi)\sin(p)-\Delta F_{RM}[\cos(i)\cos(p)+\sin(i)\sin(p)\sin(\psi)]\} \quad (3.32)$$

$$\Delta Torque_{mj} = 2\ r\ \Delta F_{PM} \quad (3.33)$$

where chisel-edge angle, ψ, and half point angle of the drill, P, are defined as before. Drill-web angle at any point on the main cutting, ω, and inclination angle, i, are given by

$$\omega = \sin^{-1}\left(\frac{W}{r}\right) \quad (3.34)$$

$$i = \sin^{-1}[\sin(p)\sin(\omega)] \quad (3.35)$$

with r, radius at the mid-point of the jth element of the cutting lip, given by

$$r = \{ [\frac{D\cos(\omega_0)}{2} - (j-\frac{1}{2})\Delta l \sin(p)]^2 + W^2 \}^{\frac{1}{2}} \tag{3.36}$$

where W is half the chisel edge width and j is the jth element. Drill-web angle at the outer corner, ω_0, and elemental cutting edge length, Δl, are given by

$$\omega_0 = \sin^{-1}(\frac{2W}{D}) \tag{3.37}$$

$$\Delta l = \frac{[D\cos(\omega_0) - L_C\cos(\pi - \psi))]}{2M_{main}\sin(p)} \tag{3.38}$$

with D, diameter of the drill; L_C, chisel edge diameter; W, half the chisel edge width; and M_{main}, total number of element of the main cutting lip. Incorporating the cutting forces contributed from drill wear, the components of the resultant force developed by Wiriyacosol and Armarego [24] in an oblique cutting, ΔF_{PM}, ΔF_{QM}, and F_{RM}, are modified and given by

$$\Delta F_{PM} = \frac{tb\tau_\kappa}{\sin(\phi_n)} \{ \frac{\cos(\beta_n - \gamma_n) + \tan(i)\tan(\eta_c)\sin(\beta_n)}{\sqrt{\cos^2(\phi_n + \beta_n - \gamma_n) + \tan^2(\eta_c)\sin^2(\beta_n)}} \} + \mu CHW_{area} \tag{3.39}$$

$$\Delta F_{QM} = \frac{tb\tau_\kappa}{\sin(\phi_n)\cos(i)} \{ \frac{\sin(\beta_n - \gamma_n)}{\sqrt{\cos^2(\phi_n + \beta_n - \gamma_n) + \tan^2(\eta_c)\sin^2(\beta_n)}} \} + CHW_{area} \tag{3.40}$$

$$\Delta F_{RM} = \frac{tb\tau_\kappa}{\sin(\phi_n)} \{ \frac{\cos(\beta_n - \gamma_n)\tan(i) - \tan(\eta_c)\sin(\beta_n)}{\sqrt{\cos^2(\phi_n + \beta_n - \gamma_n) + \tan^2(\eta_c)\sin^2(\beta_n)}} \} \tag{3.41}$$

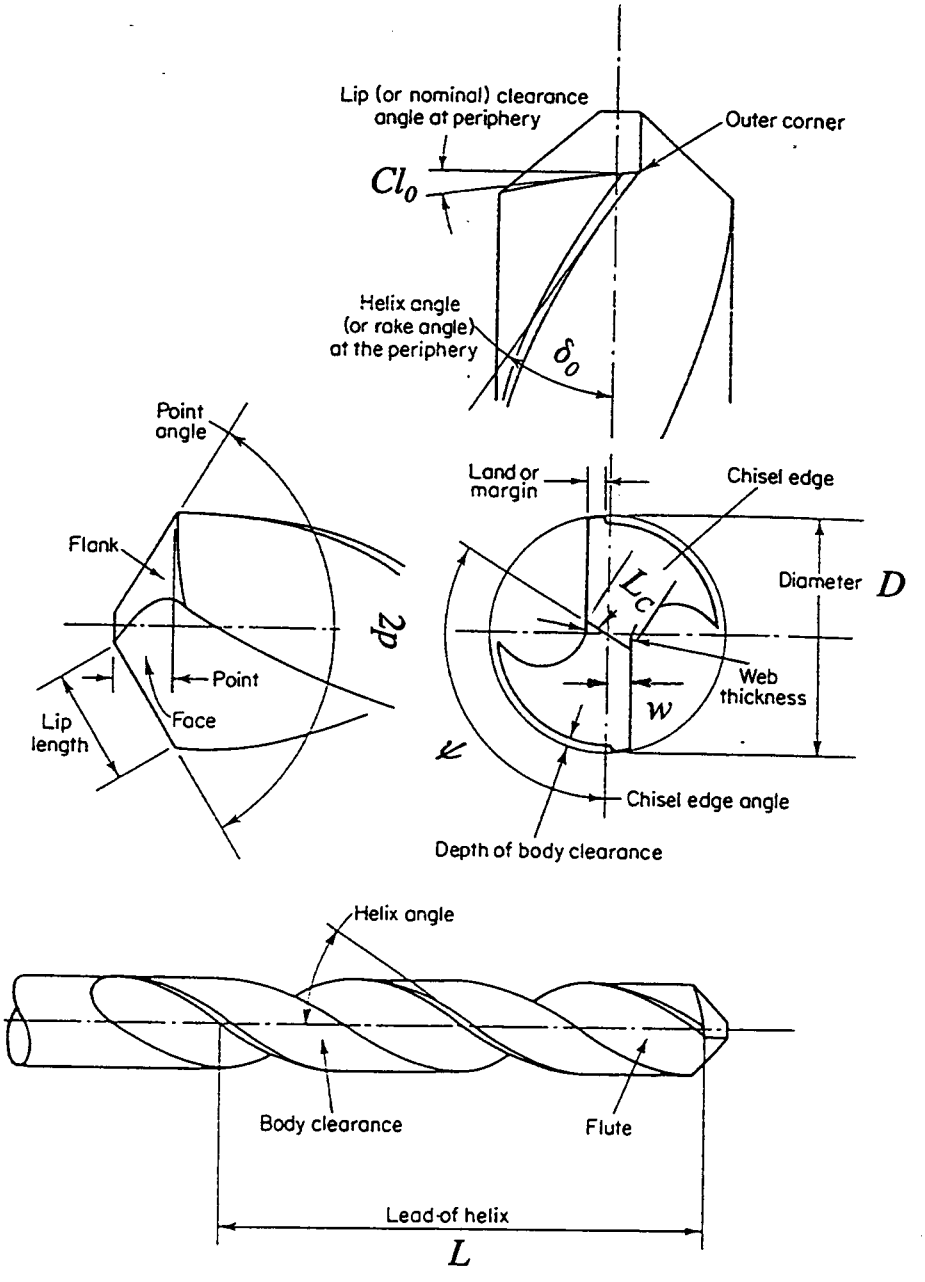

Figure 3.11 Geometric parameters of a standard twist drill.

where Φ_n and η_c are represented in equation (3.20) and (3.21), and β_n is the mean friction angle in the plane normal to the cutting edge. The cutting width of the jth drilling element is denoted by b which is given by

$$b = \Delta l \cos(i) \tag{3.42}$$

t is the undeformed chip thickness of the jth drilling element and is given by

$$t = \frac{f \sin(p)\cos(\xi)}{2} \tag{3.43}$$

with feed rate f. ξ is the reference angle by projecting the cutting velocity in the normal plane and is expressed as

$$\xi = \tan^{-1}[\cos(p)\tan(\omega)] \tag{3.44}$$

τ_k is the yield shear stress of material. Cl_n is the normal clearance angle of the jth drilling element and is given by

$$Cl_n = \xi - \psi \tag{3.45}$$

γ_n is the normal rake angle of the jth drilling element and is given by

$$r_n = r_{ref} - \xi \tag{3.46}$$

Reference rake angle at the main cutting lip, γ_{ref}, is given by

$$r_{ref} = \tan^{-1}\left[\frac{\tan(\delta)\sin(\omega)}{(\sin(p) - \cos(p)\sin(\omega)\tan(\delta)]}\right] \tag{3.47}$$

where δ is the helix angle at any point on the main cutting lip.

The total thrust force and torque for the whole main cutting lip region is:

$$Thrust_{main} = \sum_{j=0}^{j=M_{main}} [\Delta Thrust_{mj}] \tag{3.48}$$

$$Torque_{main} = \sum_{j=0}^{j=M_{main}} [\Delta Torque_{mj}] \tag{3.49}$$

3.5.2 Mechanics of Secondary Cutting Lips

The cutting process at the secondary cutting lips is presented by the classical single-edge orthogonal cutting model. In this region, the feed velocity can not be ignored. As shown in Figure 3.12a, when the feed is increased, the effective rake angles increase and the effective clearance angles decrease. Hence, the dynamic

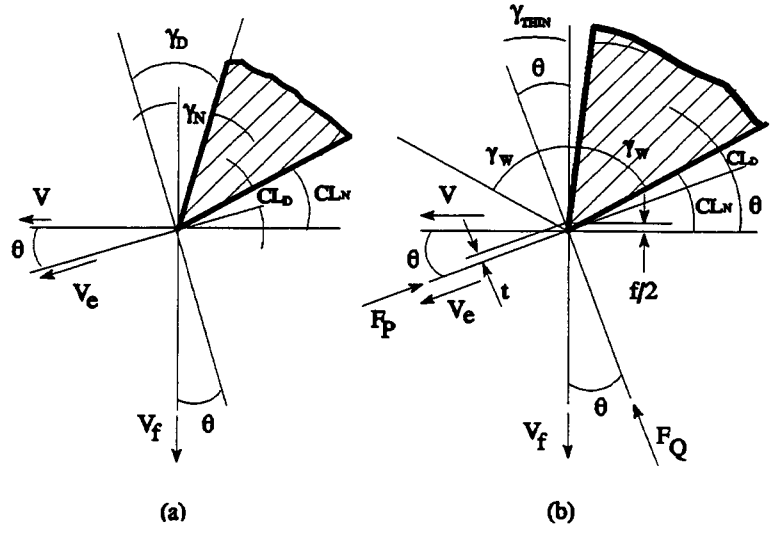

Figure 3.12 Effect of the direction of resultant cutting velocity on (a) normal rake and normal clearance, and (b) on the drilling process.

cutting velocity, rake angle, and clearance angle of the cutting process need to be incorporated into the analysis. The cutting process of the secondary cutting lips is shown in Figure 3.12b. When the cutting operation gets closer to the center of the drill point, the effect of feed velocity is gets larger and the clearance angle becomes smaller. An indentation process may apply when the clearance angle becomes negative. The region in which an orthogonal cutting model can be applied was identified by Wiriyacosol and Armarego [24]. He claimed that when r is equal to r_L, the clearance angle is zero, and that r_L could be expressed as follows:

$$r_L = \frac{f \tan(p) \sin(\pi - \psi)}{2\pi} \tag{3.50}$$

Therefore, for any element in the region where $r_L < r < L_C/2$, an orthogonal cutting model can be applied. For instance, the kth element from the outer corner, the elemental thrust, $\Delta Thrust_{SK}$, and torque, $\Delta Torque_{SK}$, from the orthogonal cutting analysis derived by Wiriyacosol and Armarego [24] are given by

$$\Delta Thrust_{SK} = 2\ [\Delta F_{PS}\sin(\theta)+\Delta F_{QS}\cos(\theta)] \tag{3.51}$$

$$\Delta Torque_{SK} = 2\ r\ [\Delta F_{PS}\cos(\theta)+\Delta F_{QS}\sin(\theta)] \tag{3.52}$$

θ is the feed angle, the angle from the feed velocity to the perpendicular direction of dynamic cutting velocity, and is given by

$$\theta = \tan^{-1}\left(\frac{f}{2\pi r}\right) \tag{3.53}$$

with

$$r = \frac{L_C}{2} - (k - \frac{1}{2})\, b \tag{3.54}$$

b is the cutting width of the kth drilling element at the second cutting lip and is given by

$$b = \frac{[\, L_C - 2r_L \,]}{2M_{second}} \tag{3.55}$$

with r_L given in equation (3.50) and M_{second} as the total number of elements for the second cutting lip. Again, incorporating the cutting forces contributed from drill wear, the components of the resultant force, ΔF_{PS} and ΔF_{QS}, which come from the classical orthogonal cutting model, and those intermediate variables derived by Wiriyacosol and Armarego [24] are summarized and given as follows:

$$F_{PS} = \frac{tb\tau_\kappa \cos(\beta - \gamma_D)}{\sin(\phi)\cos(\phi + \beta - \gamma_D)} + \mu CHW_{area} \tag{3.56}$$

$$F_{QS} = \frac{tb\tau_\kappa \sin(\beta - \gamma_D)}{\sin(\phi)\cos(\phi + \beta - \gamma_D)} + CHW_{area} \tag{3.57}$$

where b and ϕ are given in equation (3.55) and (3.7), respectively. γ_D is the dynamic rake angle at the second cutting lip. With web-thinning angle γ_{thin}, the dynamic rake angle, γ_D, developed by Wiriyacosol and Armarego [24] for standard twist drill is modified and is given by

$$\gamma_D = \theta + \gamma_{thin} \tag{3.58}$$

t is the undeformed chip thickness of the kth drilling element and is given by

$$t = \frac{f\cos(\theta)}{2} \tag{3.59}$$

The total thrust force and torque for the whole secondary cutting lip region are respectively given by

$$Thrust_{2nd} = \sum_{k=0}^{k=M_{SECOND}} [\Delta Thrust_{SK}] \tag{3.60}$$

$$Torque_{2nd} = \sum_{k=0}^{k=M_{SECOND}} [\Delta Torque_{SK}] \tag{3.61}$$

With the addition of the thrust force and torque for the main cutting lip region to the thrust force and torque for the secondary cutting lip region, respectively, the total thrust force and torque for the whole drill bit can be derived as:

$$THRUST_{DRILL} = Thrust_{main} + Thrust_{2nd} \tag{3.62}$$

$$TORQUE_{DRILL} = Torque_{main} + Torque_{2nd} \tag{3.63}$$

3.6 Energy in the Cutting Operation

AE has impressed researchers in machine-tool condition monitoring and process analysis over the last several years. Measured energy content of the AE signals is the most suggestive method to analyze AE. Energy transmitted by the AE signals is sensitive to the changes of energy generated in a cutting process. Moreover, a correlation can be found between the energy generated and changes in a cutting process. Thus, changes in the measured energy of the AE signals indicate changes in the cutting conditions such as tool wear. Several parameters, each one of them

representing one aspect of the AE signal energy, are used in the present study to inspect the changes in both drill wear and hole quality in a drilling process. To make this study self-contained, existing theories and established models for the energy generated in classical metal cutting are summarized in the following sections.

3.6.1 Energy Content of the Orthogonal Cutting Process

The first model proposed to predict AE energy from the orthogonal cutting process is discussed in Kannatey-Asibu's Ph.D. thesis in 1980 [37] and published in 1981 [18]. The model was formulated by calculating the work rate in both the primary and secondary zones. The calculation was carried out based on a simplified Ernst and Merchant model of orthogonal metal cutting. The work rates in the first two deformation zones, i.e. primary and secondary zones developed by Kannatey-Asibu and Dornfeld [18,37] are summarized as follows. The work rate in the primary zone is the product of the shear force and shear velocity and is given by

$$\dot{W}_s = tb\tau_\kappa \left\{ \frac{\cos(\beta-\gamma)\cos\phi}{\sin(\phi)\cos(\phi+\beta-\gamma)} - \frac{\sin(\beta-\gamma)}{\cos(\phi+\beta-\gamma)} \right\} \cdot \frac{\cos\gamma}{\cos(\phi-\gamma)} V \qquad (3.64)$$

where t, b, ϕ, β, γ, τ_k, V are defined as before. The corresponding Merchant's shear-angle relationship is given by

$$\beta = \frac{\pi}{2} + \gamma - 2\phi \qquad (3.65)$$

With Merchant's shear-angle relationship substituted into equation (3.64), the work rate in the primary zone is given by

$$\dot{W}_s = bt\tau_k \frac{\cos\gamma}{\sin\phi\cos(\phi-\gamma)} V \tag{3.66}$$

with b, depth of cut; t, uncut chip thickness; τ_k, average material shear strength; Φ, shear angle; γ, rake angle; and V, cutting velocity.

In the secondary deformation zone, the mean coefficient of friction on the tool-chip interface can be calculated by measured cutting forces, $\mu = [F_Y / F_{YN}]$. An observation showed that the coefficient of friction determined in this way is exceptionally high, which indicates that a more complex process is at work in this zone. It is found that two different processes are at play in this zone, sliding friction and bulk deformation. These two processes separate the interface into two regions, sliding and sticking. Hence, the work rate of the secondary zone calculated as product of friction force, F_Y, and chip velocity, V_C, is no longer applied. The work rate in the sliding region and the sticking region are given respectively as [37]:

$$\dot{W}_{c1} = \frac{1}{3}\tau_k b(l-l_l)V_c \tag{3.67}$$

$$\dot{W}_{c2} = \tau_k b l_l V_c \tag{3.68}$$

with l, contact length between the chip and the tool rake face; l_l, length from the tool edge to the end of the sliding zone on the tool rake face; and V_c, chip velocity.

A further refinement of Kannatey-Asibu's model was proposed by Lan and Dornfeld [24]. In his model, a term, $tb\tau_k W_f V$, was added to encompass the work rate in the tertiary zone. Using W_{area} instead of bW_f, the work rate of the tertiary zone can be presented as:

$$\dot{W}_w = \tau_\kappa W_{area} V \tag{3.69}$$

with W_{area} denoting the average wear area of the tool flank wear and V cutting velocity.

Combining all the expressions, an equation describing the energy generated in the orthogonal cutting process based on the Ernst and Merchant model is given by

$$\dot{W} = \tau_k V[\frac{\cos\gamma}{\sin\phi\cos(\phi-\gamma)} tb + \frac{b}{3}(l+2l_l)\frac{\sin\phi}{\cos(\phi-\gamma)} + W_{area}] \tag{3.70}$$

In practice, not all the energy during cutting can be represented by the acoustic signals. Most of the energy is lost through the heat generated while cutting, the damping in interface between AE source and transducers, and so on. By incorporating some constants which contemplate the energy lost, a relationship between the energy of the acoustic emission signal and the cutting parameters is given as

$$\dot{W} = C_1\{\tau_k V[C_2\frac{\cos\gamma}{\sin\phi\cos(\phi-\gamma)} tb + C_3\frac{t}{3}(l+2l_l)\frac{\sin\phi}{\cos(\phi-\gamma)} + C_4 W_{area}]\}^m \tag{3.71}$$

where C_2, C_3, and C_4 are factors of signal attenuation, and power, m, is material dependent. Signal attenuation factors, C_2, C_3, and C_4, correspond to signal transmission losses between the primary shear zone, secondary deformation zone, and wear zone and transducers on the material vice, respectively. They are determined from experimental measurements.

3.6.2 Energy Content of the Oblique Cutting Process

In the oblique cutting process, based on the same algorithm but different force and velocity formulations, the work rates in different deformation zones which are proposed in this research are discussed as follows. The work rate in the primary zone is given as:

$$\dot{W}_s = \frac{bt\tau_k}{\sin(\phi_n)} \frac{\cos(\gamma_n)}{\cos(\phi_n - \gamma_n)\cos(\eta_s)} V \tag{3.72}$$

The work rate in the secondary deformation zone is also divided into two parts: sliding and sticking. Work rates, $\dot{W}_{c1}$ *and* $\dot{W}_{c2}$, in the sliding and sticking regions are given respectively as:

$$\dot{W}_{c1} = \frac{1}{3}\tau_k b(l - l_l) \frac{\sin(\phi_n)\cos(i)}{\cos(\phi_n - \gamma_n)\cos(\eta_c)} V \tag{3.73}$$

$$\dot{W}_{c2} = \tau_k b l_l \frac{\sin(\phi_n)\cos(i)}{\cos(\phi_n - \gamma_n)\cos(\eta_c)} V \tag{3.74}$$

Work rate, $\dot{W}_w$, in the teritary zone is given by

$$\dot{W}_w = \tau_k W_{area} V \tag{3.75}$$

Combing all three deformation zones, in an oblique cutting process the relationship between the energy content of acoustic emission signals and a cutting process based on the Ernst and Merchant model is given by:

$$\dot{W} = C_1\{\ \tau_k V\ [\ C_2 \frac{tb}{\sin(\phi_n)} \frac{\cos(\gamma_n)}{\cos(\phi_n-\gamma_n)\cos(\eta_s)} + C_3 \frac{t}{3}(l+2l_l) \frac{\sin(\phi_n)\cos(i)}{\cos(\phi_n-\gamma_n)\cos(\eta_c)} + C_4 W_{area}\ ]\ \}^m \tag{3.76}$$

with m = material dependent factor determined from experimental measurement,

C_2 = signal attenuation factor corresponding to signal transmission losses between shear zone and transducers on material vice,

C_3 = signal attenuation factor corresponding to signal transmission losses between chip tool interface zone and transducers on material vice,

C_4 = signal attenuation factor corresponding to signal transmission losses between wear zone and transducers on material vice,

b = depth of cut (width of chip),

t = uncut chip thickness,

τ_k = average material shear strength,

ϕ_n = normal shear plane angle,

γ_n = normal rake angle,

η_c = chip flow angle on tool face,

η_s = shear flow angle on shear plane,

i = inclination angle,

V = cutting velocity,

l = contact length between chip and tool rake face in the direction of cutting velocity,

l_l = length from tool edge to the end of sliding zone on tool rake face in the direction of cutting velocity, and

W_{area} = average wear area of tool flank wear.

3.6.3 Drilling Process Power

Two models are frequently used to describe the power of the AE signal in a drilling process. First, with relationship as, $AE_{power} \propto AE_{rms}^2$, the relationship, $AE_{rms} = c1[P_C]^m$, derived by Kannatey-Asibu [18] and Dornfeld [37] can be modified to illustrate the AE signal power in the drilling process as:

$$AE_{power} = C1[P_{DRILL}]^m \tag{3.77}$$

where P_{DRILL} is the power expended in the drilling process which can be calculated as the summation of the rotational power and feed power. This is expressed as [17]:

$$P_{DRILL} = \frac{2\, N_{rpm}\, \pi\, TORQUE_{DRILL}}{396{,}000} + \frac{THRUST_{DRILL}\, f_{Feed}\, N_{rpm}}{396{,}000} \tag{3.78}$$

where N_{rpm} is the rpm of the drilling process and f_{Feed} is the feed rate. $TORQUE_{DRILL}$ denotes the torque and the $THRUST_{DRILL}$ is the thrust force in the process. As discussed previously, the total thrust force and torque for the drilling process are given in equations (3.62) and (3.63), respectively.

Another way to model AE power in the drilling process is similar to that in modeling the cutting force for the drilling process. Cutting processes at the main cutting lips and secondary cutting lips are presented by classical single-edge oblique

cutting model and orthogonal cutting model, respectively. Each lip is considered to consist of many single edge-cutting elements. To calculate the total power of the entire drilling process, the power of each cutting element on the main cutting lip and on the secondary cutting are first calculated using the equation of the work rate for orthogonal and oblique cutting, respectively. The summation of the elemental power provides the total power expended in the drilling process.

3.6.4 Relationship Between Power of AE Signals and Drill Wear Process

As has been discussed in the previous section, the total power of a drilling process is calculated by summing up the elemental power of elements of both the main and the secondary cutting lips. For simplicity, the summation of one element representing each cutting lip is used here to demonstrate the relationship between AE power and drill wear in an average sense. The summation of the AE power of these two cutting elements can present the total AE power in a drilling process. The relationship of AE power and drill wear of an element on the main cutting lip is given by

$$\dot{W} = C_1\{\tau_k V[C_2\frac{\cos\gamma}{\sin\phi\cos(\phi-\gamma)}tb + C_3\frac{t}{3}(l+2l_l)\frac{\sin\phi}{\cos(\phi-\gamma)} + C_4 W_{area}]\}^m \quad (3.71)$$

The relationship of AE power and drill wear of an element on the secondary cutting lip is expressed as

$$\dot{W} = C_1\{\ \tau_k V\ [\ C_2 \frac{tb}{\sin(\phi_n)} \frac{\cos(\gamma_n)}{\cos(\phi_n-\gamma_n)\cos(\eta_s)} + C_3 \frac{t}{3}(l+2l_l) \frac{\sin(\phi_n)\cos(i)}{\cos(\phi_n-\gamma_n)\cos(\eta_c)} + C_4 W_{area}\ ]\ \}^m \tag{3.76}$$

In the current study, all the cutting parameters are fixed with drill wear as the only variable. In other words, the only force changed in the current experiment setup is friction force in the tertiary zone, which is caused by drill-flank wear. It is indicated from the previous discussion that, since the friction force produced on the tool flank face contributes nothing to removal of the chip, those parameters such as depth of cut, uncut chip thickness, material shear strength, shear plane angle and rake angle remain unchanged. Although the friction force changes in a drilling process, the AE energy generated in both the primary shear and the secondary zones can be assumed constant. The only contribution from the friction force to the change in the energy transmitted by AE signals is on the contact between tool flank and work piece, that is, the tertiary zone. Therefore, combining the two energy terms generated in the primary shear zone and tool-chip interface in equation (3.71) into a constant, the relationship between AE power and drill wear of an element on the main cutting lip (equation (3.71)) can be simplified as:

$$\dot{W}_{main} = C_1\{\ C_2 + C_3 W_{area}\ \}^m \tag{3.79}$$

Similarly, the relationship between AE power and drill wear of an element on the secondary cutting lip (equation (3.76)) can be simplified as:

$$\dot{W}_{Second} = C_1'\{ C_2' + C_3' W_{area}' \}^{m'} \tag{3.80}$$

The above expressions (equations (3.79) and (3.80)) show the relationship between AE power and drill wear of the cutting element, either on the main or on the secondary cutting lip, can be approximated by a polynomial function. The total AE power is the summation of all cutting elements, which indicates that the AE power of an entire drilling process is also a polynomial relationship to the total drill wear. The relationship can be represented as:

$$\dot{W} = C_1\{ C_2 + C_3 W_{area} \}^{m} \tag{3.81}$$

Equation (3.81) will serve as a starting point for the current study. Relationships between the energy calculated from the AE spectrum and drill-flank wear area will be further examined via an experimental approach.

CHAPTER 4. ACOUSTIC EMISSION SIGNAL AND ANALYSIS METHODS

4.1 Introduction to Acoustic Emission Signals

Interest in cutting-tool condition monitoring systems has been growing. It is desirable to have automatic monitoring of tool wear so that a tool can be changed when the quality of the cut is outside of specifications or when the tool is damaged or worn out. The monitoring of tool wear and recognition of tool failure requires sensitive, accurate and reliable methods, which may be either direct or indirect. Because of the difficulties associated with direct and off-line methods, attempts have been made to correlate cutting parameters with tool wear. These parameters include cutting temperature and forces, vibration, and acoustic emission. Temperature measurement is limited to controlled cutting conditions, while force measurement is not sufficiently sensitive to the progression of tool wear and is too sensitive to the prevailing cutting conditions. Numerous attempts have been made to correlate the vibrational behavior of the cutting tool with the progress of tool wear. The main difficulty is in isolating frequency information due to tool wear from that due to machine dynamics.

Acoustic emission (AE), in relation to the cutting process and tool wear, has been under investigation in recent years. AE refers to the stress waves released from materials undergoing deformation, fracture, or both. Since the frequency content of the AE signal is well beyond the range of frequencies generally associated with the dynamic behavior of machine tools, then, the signal should relate to the

cutting process only [3]. There are usually two types of emission signals: (1) a continuous signal with low amplitude and high frequency content, and (2) a burst signal with high amplitude and low frequency content. Both types are observable in metal cutting. Continuous type AE signals are generated in the shear zone, at the chip-tool interface, and at the tool-flank work-piece interface. The burst type AE signals are generated due to chip breakage, chip impact, and tool fracture [1].

4.2 Methods of Acoustic Emission Data Representation

When the AE signal travels from the place where the cutting action is carried to the transducer, it will be changed through several factors. These factors include scattering by structural defects, reflections at interfaces, diffraction by crystal imperfections, and medium changes along the travel path. The wave form might be changed in phase, amplitude attenuation, and so on. Various methods of data representation can be used in AE signal analysis. Analyzing AE signals with different parameters provides useful information about the process. The most popular methods of data representation, count and count rate, amplitude distribution analysis, root mean square value of AE signal, spectrum analysis, distribution moments, and time series and system analysis, are discussed in the following sections.

4.2.1 Count and Count Rate

One of the earliest and most common methods of data representation is the count and count rate. Count is a record of the signals whose amplitude exceed the

present threshold voltage. A threshold is set to some level above background such that when an emission occurs this level is breached and the signal is counted. The purpose of the threshold setting is to eliminate background noise. To calculate the count, the amplified signal is passed to a discriminator, which registers a count each time the threshold is crossed. If a long dead-time between threshold crossings is set, then the equipment counts the total counts registered for a series of events of bursts. If a very short dead-time between threshold crossings is set, then it will give a variable number of counts per burst, the number being in some way related to the amplitude and/or energy of the event. The count rate is chosen reliably for discrete bursts. Each burst above the threshold is counted to obtain the number of bursts per unit time [41].

4.2.2 Amplitude Distribution Analysis

Amplitude distribution analysis is an extension of the count rate method. It is a plot of the number of counts or events for a specified amplitude threshold against the threshold setting. Usually, amplitude distribution analysis had been done by recording AE signals on a videotape recorder, then playing the signal back several times through a counter set each time at a different threshold voltage and a cumulative count taken for each play. This method is reliable for the analysis of AE burst signals. Amplitude distribution analysis of AE may be used to characterize the deformation mechanisms in the process. Each mechanism may generate signals with amplitudes that are considerably different from those of the other mechanisms. For

example, the burst-type signals caused by chip breakage or by chip impact lead to an increase in the number of high amplitudes in the distribution curve. This will deform the symmetry of the distribution curve and create a tail [42]. Hence, a change of the distribution curve provides information about the active mechanisms in the process [37].

4.2.3 Signal RMS (Root Mean Square)

An alternative widely used technique is to pass the signal into a device whose output gives the root mean square (RMS) of the acoustic signal. The RMS value of an AC signal is that value of DC signal which, if applied to the same electrical circuit for the same period of time, produces the same energy dispersion. This is ideal for monitoring a continuous type emission and is also useful for burst emissions. RMS gives a good measure of the energy content of the signal [37].

4.2.4 Spectrum Analysis

The determination of the frequency bands that contain energy or power in a signal is called spectrum analysis. Due to the fact that various source mechanisms produce frequency contents related to the characteristics of the source mechanism, the shape of the spectrum and frequency components contain important information about the process being studied. Changes in the observed spectrum can identify changes in the process. One application example by Noori and Hakimmashhadi was conducted in 1988 [43]. A spectrum of the vibration measurement from a 1/15-hp

electric motor was used to detect a malfunction such as worn out bearings or a loose component. The malfunction is indicated when its corresponding frequency component has too large a magnitude. In the work of Govekar and Grabec [16], components extracted from the two spectrums of the cutting momentum and thrust force were used as an input to a neural network to predict the classified status of drill flank wear. In addition to the amplitude change of certain frequency components, other spectrum characteristics such as frequency shift, ratio of two frequency-band energy changes, and spectrum map which provides a vision of 3-D spectrum are used in past research of different fields.

4.2.5 Distribution Moments

The characteristics of the distribution of recorded data represent the conditions under which those data were produced. Changes in these conditions result in changes in the distribution characteristic. The shape of the distribution can be very useful from the point of view of detecting process changes. To describe the shape of the distribution, distribution moments are used. Distribution moments can quantify useful properties because they provide adequate insight into the distribution of the recorded data. In general, the distribution moments of the first four orders are enough to describe a distribution. The first four order distribution moments, that is average, variance, skewness and kurtosis are introduced below.

When they exist, the moment of a random variable, X, is given by

$$\mu_k = E(X^k), \qquad k = 0,1,2,3,.... \tag{4.1}$$

μ_k is called the k^{th} order moment of X. The first order moment is the mean or average value of the random variable and is given by

$$E(X) = m = \int_{-\infty}^{\infty} Xf(X)dx \tag{4.2}$$

The first order moment, $E(X)$, is certainly the most important of the moments. It is the center of the distribution. If one has to characterize a distribution, to describe it as best as one can, but using just a single number, then the $E(X)$ would be a rational choice. An extended concept for a moment is called the central moment. When they exist, the central moments of a random variable X are given by

$$\mu_k = E[(X - E(X))^k], \quad k = 0,1,2,3,.... \tag{4.3}$$

The central moments are fundamental and they characterize a distribution.

The second order central moment of distribution is the variance, the deviation from the mean, and is given by

$$\sigma^2 = \int_{-\infty}^{\infty} (X-E(X))^2 f(X)dx \tag{4.4}$$

The variance is an important parameter because it indicates the dispersion of the distribution, the scatter about the center.

Other parameters that are useful in interpreting the distribution of the random variable are the skewness and the kurtosis. The skewness is the normalized third-order central moment and is given by

$$S = \frac{\int_{-\infty}^{\infty}(X-E(X))^3 f(X)dx}{\sigma^3} \tag{4.5}$$

The skewness measures the symmetry of the distribution. A negative skew generally indicates a shift of the bulk of the distribution to the left of the mean and a positive skewness indicates a shift to the right.

The kurtosis is the normalized fourth order central moment and is given by

$$K = \frac{\int_{-\infty}^{\infty}(X-E(X))^4 f(X)dx}{\sigma^4} \tag{4.6}$$

A high kurtosis indicates a sharp distribution peak. That is, most of the values are concentrated in a small area near the average. A low kurtosis indicates flat distribution. Distribution moments have been used in the analysis of the tool wear related to the RMS of AE by Kannatey-Asibu and Dornfeld [34,37]. Since the first distribution moment, mean value, of the RMS signal is dependent on the source location, the higher order distribution moments such as variance, skewness and kurtosis, which are more likely to identify useful information inherently hidden in the AE RMS which will be independent of the source location, was used to supplement the direct RMS signal.

4.2.6 Time Series and System Analysis

In general, a signal is a time series. More detailed information about a signal can be obtained if the signal itself can be modeled by using the time series

modeling technique. A formulation, called the autoregressive moving average (ARMA) model, is a typical application of the well-known time-series analysis. An observation variable, $y(t)$, at time, t, can be presented by a stochastic model as:

$$y(t) = \sum_{l=0}^{q} b(l)x(t-l) - \sum_{i=1}^{p} a(i)y(t-i) \qquad (4.7)$$

This is a linear stochastic difference equation referred to as an autoregressive moving average model of order p,q, i.e. $ARMA(p,q)$, where $y(t)$ is the state parameter at time instant t, $a(1)$, $a(2)$,....$a(p)$ are autoregressive parameters, $x(t)$ is the input of the process at time instant t, and $b(0)$, $b(1)$, ...$b(q)$ are the moving average parameters. Two very useful models are simplification of the *ARMA* model. When $a(0)=1$ and $a(i)=0$ for $i >= 1$, the moving average model of order q is produced, MA(q). When $b(0)=1$ and $b(l)=0$ for $l >= 1$, the autoregressive model of order p is produced, $AR(p)$. The q is usually equal to $p-1$, resulting in an $ARMA(p, p-1)$ model. The order of the *ARMA* model is estimated by increasing q from 2 until further increasing in q does not result in a significant reduction in the residual sum of squares. The time-series analysis technique was used by Liang and Dornfeld [44] to model AE signals for monitoring cutting tool wear in turning operations. The AE signal features were encoded into a time-series model parameters vector. Experimental results showed that the parameters vector is not sensitive to the change of cutting parameters such as feed rate, cutting speed, and depth of cut, but showed a strong sensitivity to the progress of cutting tool wear.

4.3 Summary

As has been discussed in chapter 3, the foundation of the current study is the fact that the power of AE signals increases when drill wear increases. Among the AE signal analysis methods and AE parameters mentioned above, the spectrum is the direct measurement of the power of the AE signal. As described in chapter 6, because of the limitations in equipment, spectrum analysis is used in the current study. To consider the changes in the characteristics of the AE spectrum, the distribution moments of the AE spectrum amplitudes are also examined in the present study. The parameters of the AE spectrum and the distribution moments used will be discussed in more detail in chapter 6.

CHAPTER 5. HOLE QUALITY AND CAUSES OF QUALITY ERROR

5.1 Introduction

The major objective of the current study is to establish some performance indices which may describe the state of the quality of a drilled hole. In order to describe the quality of a drilled hole, a qualitative and quantitative assessment is necessary which defines the drilled hole quality with regard to geometrical errors or the errors regarding the hole functions. Recently, GD&T (geometric dimensioning and tolerancing) has captured the attention of industry. GD&T is the broad group of tolerance applied to control part geometry, other than tolerance applied directly to individual dimensions, and is a dual-purpose dimensioning system. First, a set of standard symbols which define part features and their tolerance zones is used. The symbols and their interpretation are documented by the American National Standards Institute Dimensioning Standard, (ANSI Y14.5M-1982). Second, and of equal importance, GD&T is a functional dimensioning philosophy. Functional dimensioning is a philosophy of dimensioning and tolerancing a part based on how it functions. It defines what size and shape the part must be to function as the design intended.

When functionally dimensioning a part, the designer performs a functional analysis. A functional analysis is a process whereby a designer identifies the functions of a part and uses this information to establish the actual part dimensions and tolerances. It provides the designer with better tools to describe the part and it pro-

vides the manufacturer or inspector with a clearer understanding of the design requirements of the part. Since GD&T not only provides the coordinate dimensioning, but also considers what function the part can provide, the assessment of the hole quality in the current study is based on the tolerances used in GD&T. The quality measurements used in the current study are defined according to the philosophy of the functional dimensioning of GD&T and will be discussed in the following section. Following the discussion of defined quality measurements is an examination of the causes of hole quality variation, which provide extended information about how quality measurements change.

5.2 Hole-Quality Definition Based on Geometric Dimensioning and Tolerancing

The most important and common function a hole provides is fit. In fit, under a required level of precision, a mating part needs to be able to insert into the hole. Examples of practical applications of the fitting function are the clearance hole for a rotor shank bearing and the mounting hole for a fastener. To achieve this function, the feature sizes of the mating part and hole as well as the relative position between the axis of the mating part and the hole need to be considered. The best way to describe the functional requirements of fitting hole patterns is the concept of the tolerance of position, which may be viewed in two ways: (1) as a boundary limiting the movement of a surface of a feature, or (2) as a tolerance zone limiting the movement of the axis of a feature. The first way is called the boundary concept and the second way is called as axis concept. Both concepts are useful and in most cases can

be shown to be equivalent [45]. In this section, both the boundary concept and the axis concept are summarized and introduced. Following the introduction of the concepts, the quality measurements for a hole are discussed.

5.2.1 The Boundary Concept

An example of a conventional bolted joint, as shown in Figure 5.1, is given to illustrate the concept. The boundary divides the clearance between the bolt and the hole. Note that the boundary is constructed normal to the interface of the mating parts. Either of the two features can be displaced and the joint will still assemble as long as the interface has not moved beyond the boundary. In this type of application, the specified tolerance of position applies when the hole is at MMC (maximum material condition or minimum diameter). The hole must be maintained within its specified limit of size, and its location must be such that no surface element of the hole will be inside a theoretical boundary. The boundary can be referred to as a gage pin diameter located at true position and its size is independent of hole size.

Because the boundary deals with surfaces, it is obvious that it will always be three dimensional in nature, as shown in Figure 5.2. Figure 5.2 illustrates that the height of the boundary is equal to the height of the considered feature (the plate). The diameter of the boundary for a tolerance of position of the hole is the minimum diameter of the hole minus the tolerance of position value as shown in Figure 5.1.

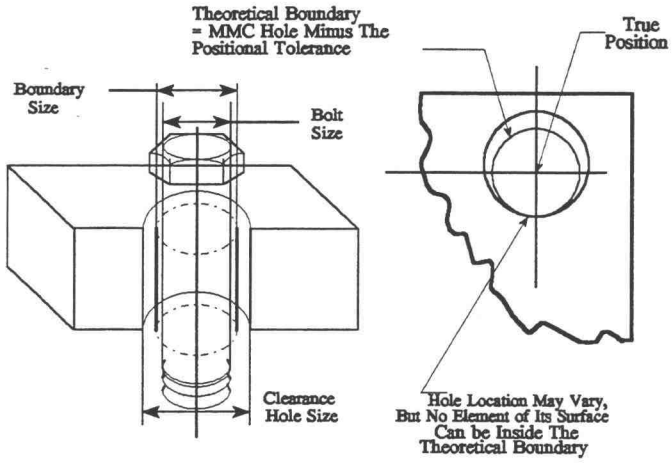

Figure 5.1 Theoretical boundary which limits the movement of hole or bolt to permit normal assembly.

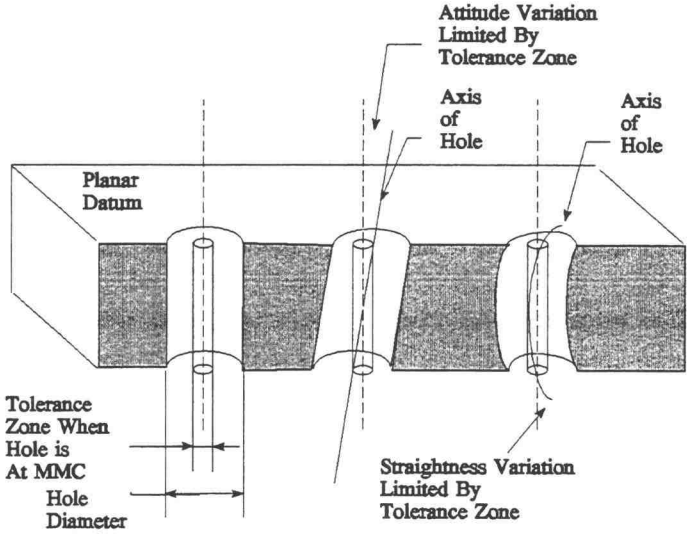

Figure 5.2 Axis concept of the tolerance of position.

As shown in Figure 5.2, the tolerance of position is also an indirect orientation control. The attitude of the boundary produced by the tolerance of position is perpendicular to the primary datum (the plate surface). Since the surface of the hole is limited by this boundary, its attitude will be controlled by this boundary as well. Also, the straightness of the hole is controlled by the boundary established by the tolerance of position [45].

5.2.2 The Axis Concept

When the hole is at minimum diameter, its axis must fall within a cylindrical tolerance zone which is located at the true position as shown in Figure 5.3. The diameter of this zone is equal to the tolerance of position value. This tolerance zone

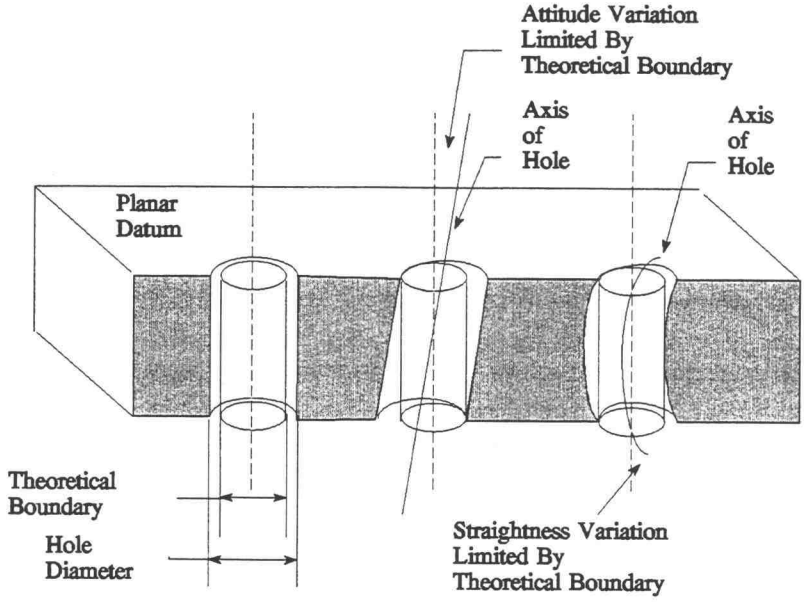

Figure 5.3 Boundary concept of the tolerance of position,

also defines the limits of the attitude of the axis of the hole at minimum diameter in relation to the datum surface. The straightness of the hole is also limited by the cylindrical tolerance zone.

The boundary and the axis concepts can, in most cases, be shown to be equivalent. Figure 5.4 shows how to convert a tolerance of position from a boundary concept to an axis tolerance zone. This can be accomplished by moving the hole until it contacts the boundary in various directions. This causes the center of the hole to generate a diameter tolerance zone about its true position. This zone is the equivalent axis tolerance zone derived from the boundary concept. The diameter of this zone will be equal to the tolerance of position values controlling the hole. Figure 5.5 shows how equivalent axis and boundary tolerance zones limit the location of a hole. It shows that the total amount the hole can be away from its true position is the same in both cases.

The above discussion points out that there are two classes needed for a hole to function normally. The first class is the form which describes the basic geometrical dimensions of the hole and which involves no complex relations between features. This class includes the size (diameter) and cylindricity of the hole. The second class is the axis tolerance zone which provides control of the tolerance of position. The four different tolerance zone requirements which must be met are size (diameter), cylindricity, axis straightness, and perpendicularity of the axis. The actual measurement of these tolerance zones of a hole must be somehow satisfied to achieve the required nominal value. However, to define the quality measurements

of a hole, only the actual measurement of these four tolerance zones is involved [45].

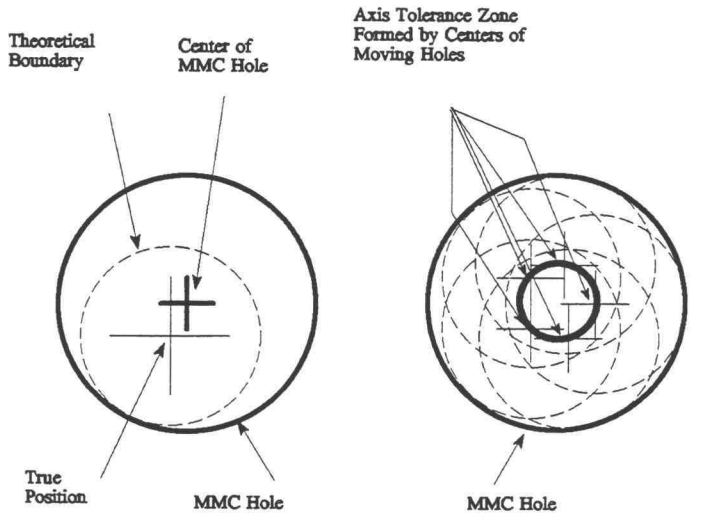

Figure 5.4 Conversion from a theoretical boundary to an axis tolerance zone.

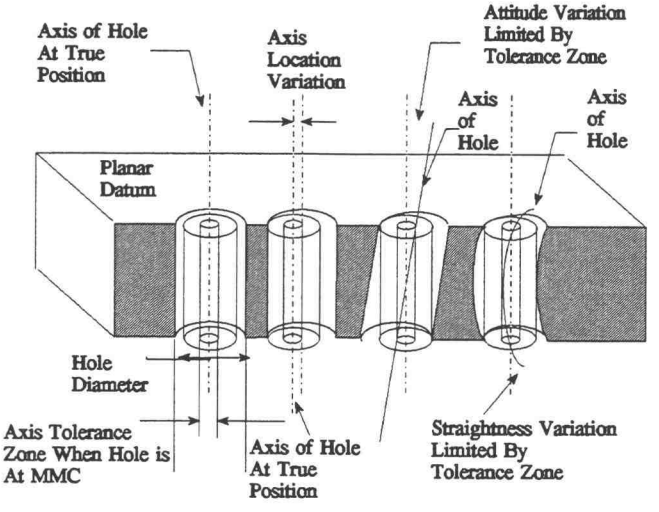

Figure 5.5 Equivalent control of holes by boundary and axis tolerance zone analysis.

5.2.3 Actual Size

The actual size of a hole based on ANSI Y14.5M Standards is shown in Figure 5.6a [46]. The actual size is characterized by two independent dimensions, one dealing with the envelop, called the actual mating size; the other, dealing with individual, opposed-point pairs, called actual local size. The actual mating size of a hole is the diameter of the maximum inscribed balanced cylinder. The actual local size of a hole is the distance between opposed points taken normally to its real axis (spine).

5.2.4 Actual Cylindricity

Cylindricity is the three-dimensional equivalent of roundness. The tolerance zone is created by extending the round tolerance band along the axis of a cylinder as shown in Figure 5.6b. The actual cylindricity of a hole defined by the ANSI Y14.5M Standards [46] is the radial distance between a pair of coaxial cylinders of minimum radial separation, such that they just encompass all points on the surface of the subject.

5.2.5 Axis Straightness

According to the ANSI Y14.5M Standards [46], the axis straightness zone of a hole is cylindrical. The actual overall axial straightness of a hole, as shown in

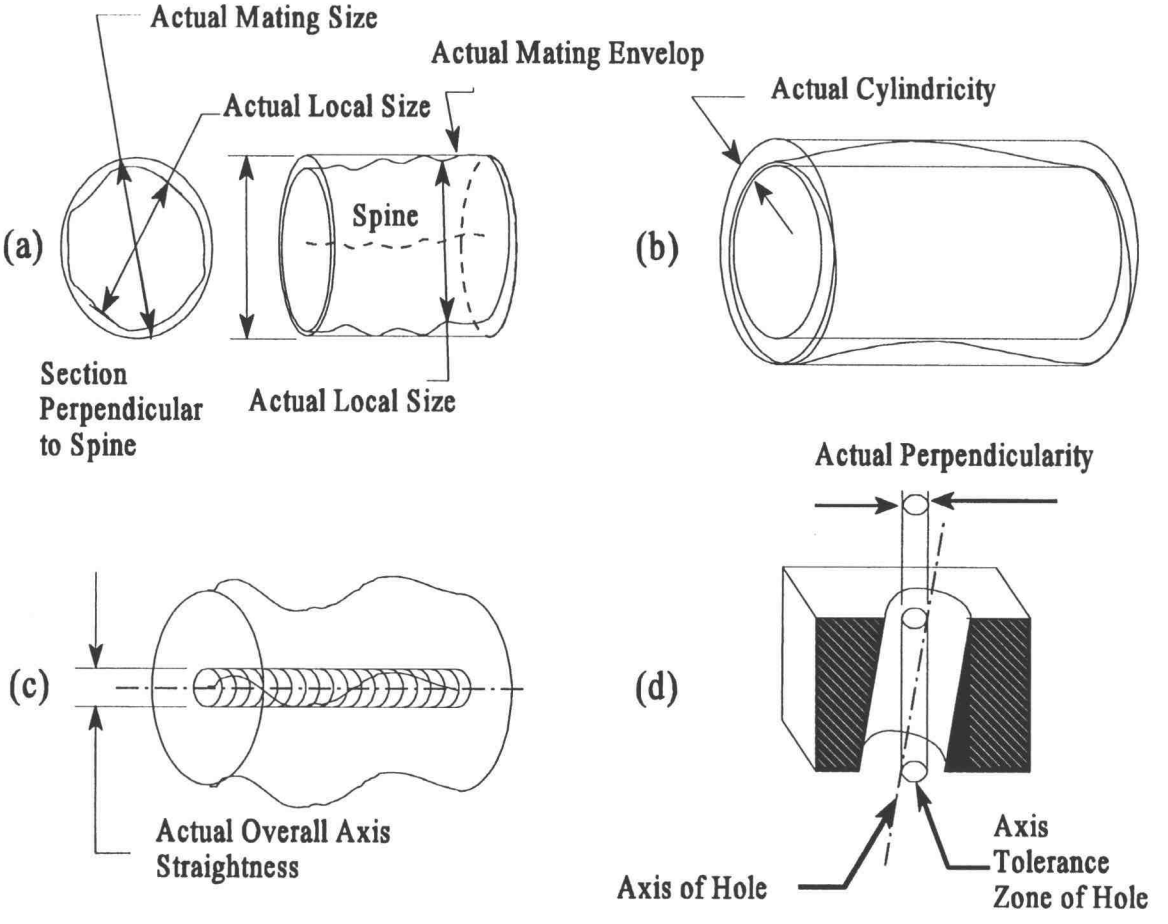

Figure 5.6 Actual measurements of tolerance zones defined for hole quality: (a)actual size, (b) actual cylindricity, (c) actual overall axis straightness, and (d) actual perpendicularity.

Figure 5.6c [46], is the diameter of the smallest cylinder which contains all the center points of each section plane of the hole.

5.2.6 Axis Perpendicularity

In the case of a hole, axis perpendicularity controls the extremes of the axis of the hole. As shown in Figure 5.6d, a planar datum is involved to show that the nominal axis should be perpendicular to this datum plane and the axis tolerance zone is cylindrical. The actual axis perpendicularity, based on ANSI Y14.5M Standards, [46] is the length of the projection of the hole true axis onto the planar datum. The nominal axis perpendicularity is zero.

5.3 The Causes of Hole Quality Variation

The drilling process of a through hole by a twist drill can be divided into three stages, as shown in Figure 5.7. In stage 1, the drill point penetrates the work-piece surface. Stage 1 is completed when the outer corners of the drill have entered the work piece. Stage 2 begins when the full diameter of the drill is in the work piece and is completed when the chisel edge of the drill point starts to break through the underside of the work piece. Stage 3 begins when the drill point breaks through the underside of the work piece and stops when the full diameter of the drill out is through the work piece.

An analysis of drilled hole accuracy was investigated by Galloway [4] and Kahng and Ham [2]. Instead of using the terms perpendicularity, size, and

cylindricity, the alignment (parallelism), oversize, and roundness were used respectively to define hole accuracy. The cutting action in stage 1 is the most important stage and it strongly influences the quality of the drilled hole. In this stage the drilling action was not steady, and drill whirling vibration took place. The force difference is that the two lateral directions cause the bending of the drill which

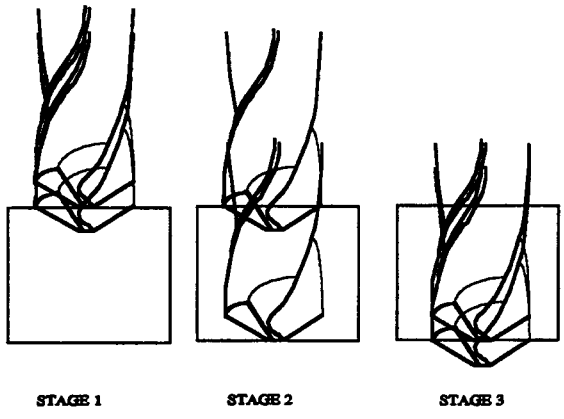

Figure 5.7 Three stages of a through-hole drilling process with twist drill.

consequently causes error in the hole accuracy. The model of hole alignment error developed by Galloway [4] and the experimental observations about the causes of the hole size and roundness errors from Galloway [4] and Kahng and Ham [2] are summarized as follows. Corresponding to the terms used as the hole accuracy variation in their work, the terms based on the GD&T concept are represented in the following discussion. Furthermore, the discussion of the forces status in the drilling action provides the added information for understanding the relationship between the cutting forces and drilled-hole quality variation.

5.3.1 Causes of Hole-Axis Perpendicularity Errors

The deflections of the drill point from the spindle axis suggests that the hole-axis perpendicularity is dependent on the behavior of the drill whirling vibration at the onset of drilling. As reported by Galloway [4], before contacting the work piece, the displacement of the drill point is relatively small. The rotation motion of the drill bit is approximately circular. Later, during the first few revolutions follow-

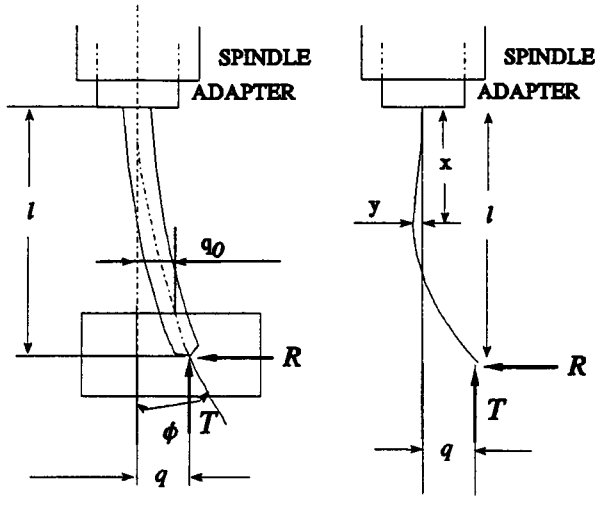

Figure 5.8 Schematic illustration of drill deflection and perpendicularity error for drilled hole.

ing the contact, the drill point was deflected away from the nominal axis. As the drill continued to penetrate into the work piece, the deflection decreased and became centered around a point away the nominal axis. When the outer corner of the drill had just entered the work piece and the full diameter of the hole was reached, the deflection increased again and the initial displacement, q_0 as shown in Figure 5.8,

of the drill point finally became established. This process is called as wandering motion by some researchers (Ema et al. [7, 8], Lee et al. [9]). The evidence from their experiments shows the same pattern of the displacement of the drill point as demonstrated by Galloway [4].

A mathematical model to describe drilled-hole alignment was developed by Galloway [4]. The slope, ϕ, of the drill deflection and the displacement, q, of the drill point away from the nominal rotation axis can be expressed as:

$$\Phi = \frac{R}{T}\frac{3}{2l}\left[l - \frac{1}{k}\tan(kl)\right] \tag{5.1}$$

and

$$q = \frac{R}{T}\left[l - \frac{1}{k}\tan(kl)\right] \tag{5.2}$$

respectively, where l is the length of drill and k is an intermediate variable given by

$$k = \sqrt{\frac{T}{EI}} \tag{5.3}$$

and where E is the system module of elasticity, I the system's moment of inertia, and R and T, respectively, are reaction force and thrust force.

As shown in Figure 5.8, the displacement was initiated by an initial deflection, q_0. Because of this initial deflection, the axis of the drill point will be inclined to the spindle axis. As the depth of the hole increases, the displacement, q, and the deflection slope, ϕ, at the drill point will became progressively larger, so that the drill point will tend to follow a path to drift away further from the nominal axis.

Therefore, the initial penetration condition of twist drilling, at the very beginning of penetration, is the most important stage and it influences the quality of the twist-drilled holes. The experimental relationship between the initial displacement, q_0, and the final displacement, q, was given by the Galloway [4] as:

$$q = q_0 e^{3dp2l} \tag{5.4}$$

where d is the depth the drill point into the work piece and l is the length of the drill. The experimental evidence from Kahng and Ham [2] also shows that as the feed rate increases, the drill point drifts farther off the nominal axis. This is caused by the increased thrust force, which is directly related to the feed rate.

5.3.2 Causes of Hole Size and Cylindricity Error

Again, according to the experimental observations of Galloway [4] and Kahng and Ham [2], in addition to the alignment (perpendicularity), oversize and roundness errors of a drilled hole were also caused by the drill-walking phenomena. As shown in the experimental evidence of Galloway [4], the average hole oversize error is seen to be almost equal to the diameter of the average circle of motion of the drill point. The work of Kahng and Ham [2] shows that the wandering motion during the first stage causes the elliptical motion of the drill axis. This elliptical motion of the drill in turn causes roundness errors in the drilled hole, with an odd number of sides, as shown in Figure 5.9. However, when the drill entered stage 2, the drilling action became much more steady and the drill produced more

symmetrical cutting action in both lips. Hence, the profile of the drilled hole gradually becomes round with increasing hole depth.

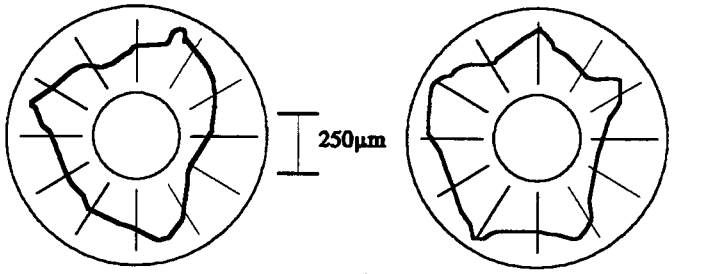

Figure 5.9 Typical roundness errors produced by asymmetric cutting action in drilling stage 1: (a) trigon shape and (b) pentagonal shape.

5.3.3 The Role of Cutting Force in Hole Quality

The schematic illustration of cutting forces in the drilling process is shown in Figure 5.10. The resultant force can be assumed to act as points A and A'. This resultant force can be resolved into three forces, P_X, P_y, and P_Z. The total thrust force is contributed by the two forces acting on both lips at points A and A' and also by the force on the chisel edge of the drill. To determine the thrust force required to achieve a given feed, only the forces in the plane parallel to the axis of drill make a contribution. Thus the force represented by P_y and P_y' must be overcome to allow the drill to penetrate the work piece during drilling. That is, the thrust force ,P, must be greater than $2P_y+P_y'$. To determine the torque required to rotate the drill only the forces in the plane horizontal to the axis of the drill are considered. In an ideal condition, as shown in Figure 5.10, the radial forces, P_X, acting on the lip of

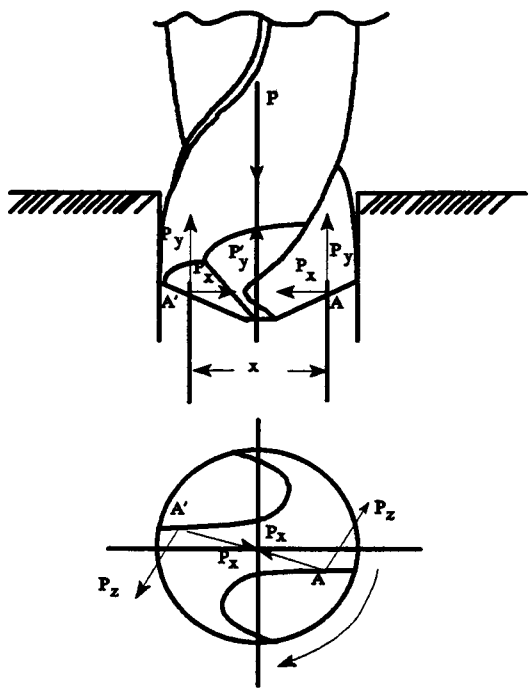

Figure 5.10 Cutting force elements in a twist-drill drilling process.

the drill, are equal in magnitude, but opposite in direction along the same line, and thus, cancel each other. The force, P_Z, is also of equal magnitude and opposite in direction, but does not act along the same line. Hence, there is no resultant radial force, but a couple, $P_Z \bullet x$, which must be overcome. Since there is no resultant radial force, no cutting action is effected in the radial direction. However, in a practical situation, the ideal cutting condition will never happen and hence, the difference in the two radial forces causes bending of the drill, which consequently causes errors in hole accuracy. The experimental evidence from Kahng and Ham [2] shows that the difference of the radial forces is manifested in variations of the recorded cutting force diagram. Since the unbalanced radial force causes an

unsteady drilling operation, the variation can be used to indicate an unsteady drilling operation. Also, since the torque is a linear function of the lateral forces, the unsteady drilling operation also exhibits itself in the variation of the recorded cutting torque diagram. Therefore, an unsteady drilling operation will be indicated by recorded thrust force, radial force and the torque. The change in the cutting force and corresponding hole roundness error was also studied by Kahng and Ham [2]. This research showed that variation in the recorded radial force and torque diagram in the first drilling stage was a good indicator of roundness error. The variation in thrust force was also found to be useful as an indication of hole quality by Radhakrishnan and Wu [26].

These unbalanced cutting actions are caused by factors such as improper installation of the drill, unbalanced force due to difference in lip height and half point angles, different degrees of sharpness on the cutting edges, and the traverse deflection of the drill. No matter that the original error is from the drill bit or from the system, the effect of these error will be reflected on the hole qualities and be manifested in the radial force, torque, and the thrust force. Hence, the characteristics of the cutting force signals could be useful as indications of both hole quality and steadiness of the drilling process.

CHAPTER 6. PRIMARY EXPERIMENT METHODOLOGY

The purpose of the current study was to investigate the possibility of building a system for measuring the quality of drilled holes on-line by using acoustic emission (AE) signals as an indicator. For this purpose, an experiment was conducted using a radial-arm drilling machine. Results from this experiment are employed in this study to qualitatively validate the possibility of predicting both drill-wear and drilled-hole quality through the AE spectrum and to guide additional future analysis of the practical model.

Determining the relationships between AE signals, drill-wear and drilled-hole quality are the priorities of this study. Therefore, to accomplish the experiment, three questions were considered: (1) how and in which form an AE signal is collected; (2) how drill wear is measured; and (3) how the quality measurements for drilled holes are obtained. These considerations are discussed in the following sections. The experimental setup and procedures followed in collecting samples, and the parameters used to paramatize the spectral information are discussed first. Following those discussions, the definition of drill-wear measurement and the arrangement of the vision system used to measure drill wear are introduced. Finally, general information on using the coordinated measuring machine to measure hole quality is given.

6.1 Monitoring Acoustic Emissions

Considering the AE analysis methods discussed in chapter 4, most methods require that AE signals be recorded first and then an off-line analysis be conducted. Since the AE signal contains many very high frequencies and hence high data rates, a digital device with limited memory is not suitable to record a series of raw AE signals. In AE signal analysis, the AE signals are usually recorded by a modified video tape recorder and played back several times to extract the desired information. For real world applications, this method, recording first and examining later, may not be practical.

Moreover, the observations reported by past investigations in tool-wear sensing show that, when the cutting tool gets worn, the AE energy generated at the interface of the tool flank and work piece increases [25,33,34]. As the cutting tool is heavily worn, this AE source will become dominant. This observation became the basis of the current study. The AE spectrum can be detected by a spectrum analyzer and presents the energy distribution with respect to the frequencies of AE signals. To evaluate the validity of using the energy content embedded in the AE spectrum to predict both drill wear and the drilled-hole quality, an experiment was conducted.

6.1.1 Experimental Setup for AE Spectrum Collection

The schematic illustration of the experiment set up is shown in Figure 6.1. Through the experiment the sequential spectrums of AE signals generated under fixed cutting conditions were obtained for subsequent analysis. Different hardware for both the radial arm drilling machine and instrumentation were developed and arranged for running the experiment. In this subsection, a special fixture, as shown in Figures 6.2, 6.3, and 6.4, designed for the experiment in the current study, is introduced. Following the discussion of the fixture, the material, drill bit, chosen drilling speed and feed rate are discussed. Then, the devices and signal flow control for the instrumentation are discussed.

The special fixture was designed to be mounted on the existing vise of the radial-arm drilling machine through four existing taped holes. Two functions provided by this special fixture were AE sensor mounting and work-piece holding.

The transducer, DEC model SE900MWB, was located on back of the wall of main body of the fixture, as shown in Figures 6.2 and 6.3. The transducer was separated from the work piece by a wall of only 0.2 inch thickness and fixed as close as possible to the cutting lips in the drilling operation. As shown in Figure 6.4, with a rubber sheet covering the whole fixture except the contacting point between the work piece and fixture, the sensor was protected against mechanical impacts from material chips.

For the function of holding the work piece, two different drilling processes in the experiment were considered in designing the fixture: (1) the sample collecting

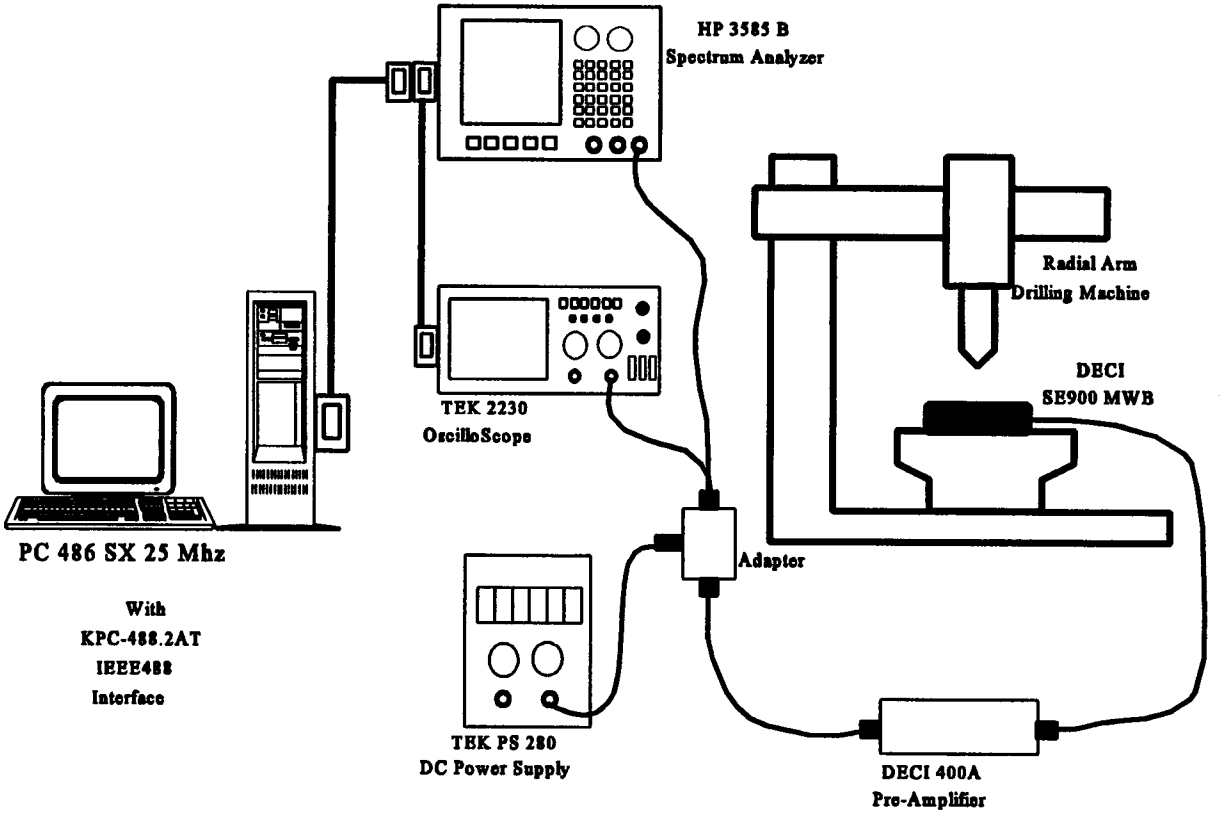

Figure 6.1 Experimental setup for collection of AE spectrums generated in a drilling process.

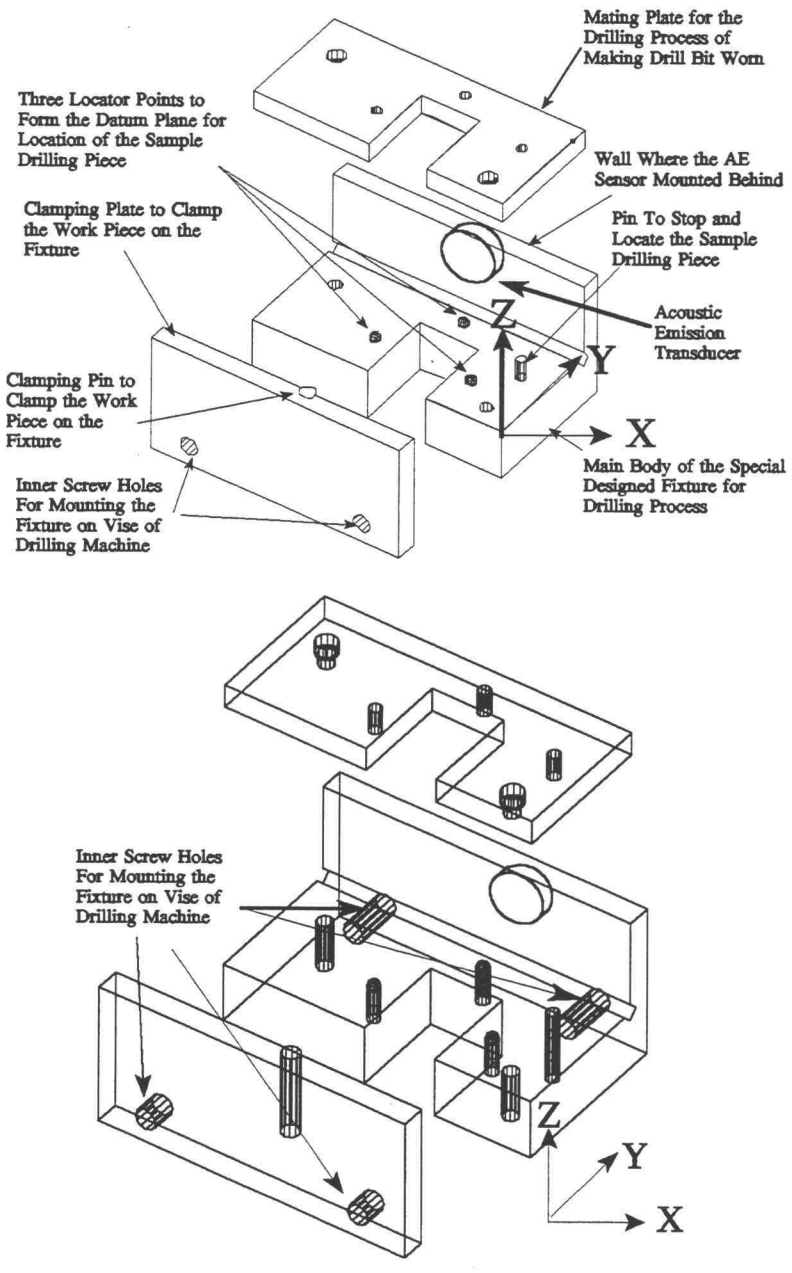

Figure 6.2 Structure and mating parts of specially designed fixture.

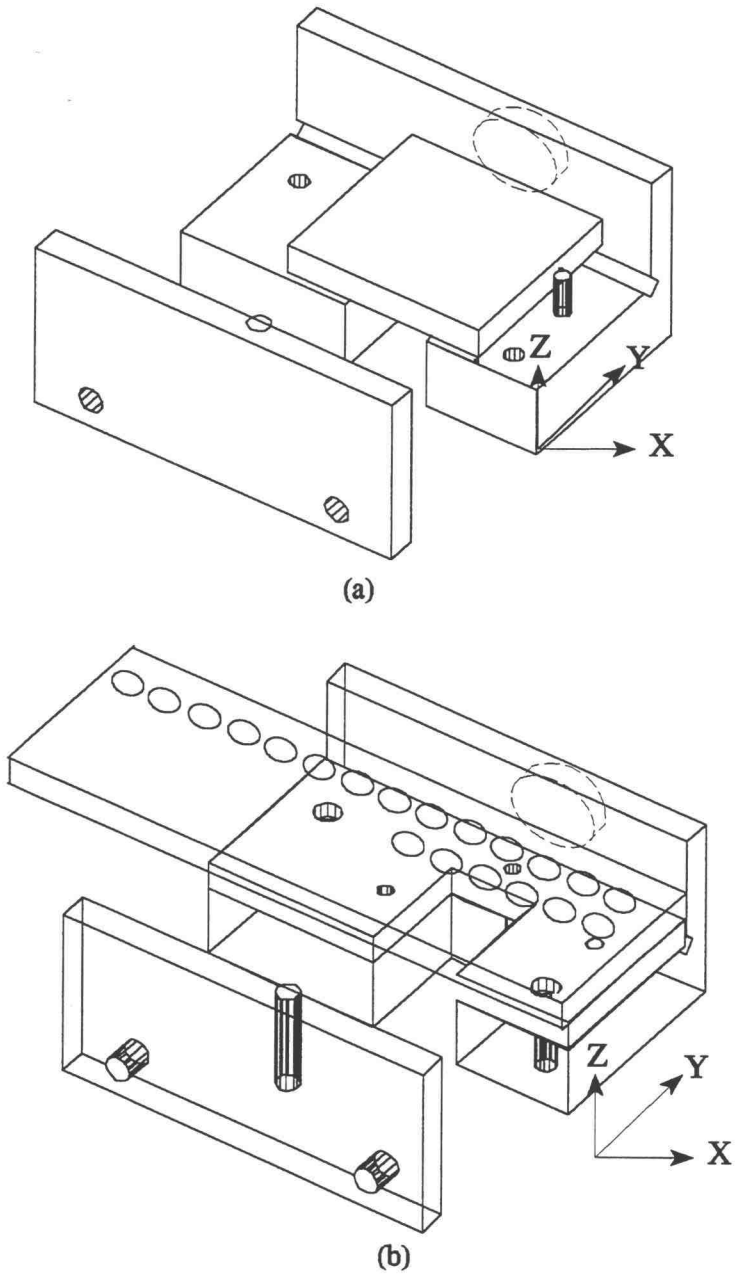

Figure 6.3 Designed fixture usage for experimental processes: (a) in sample work pieces and AE spectrum collection process, and (b) in drill-flank wear production process.

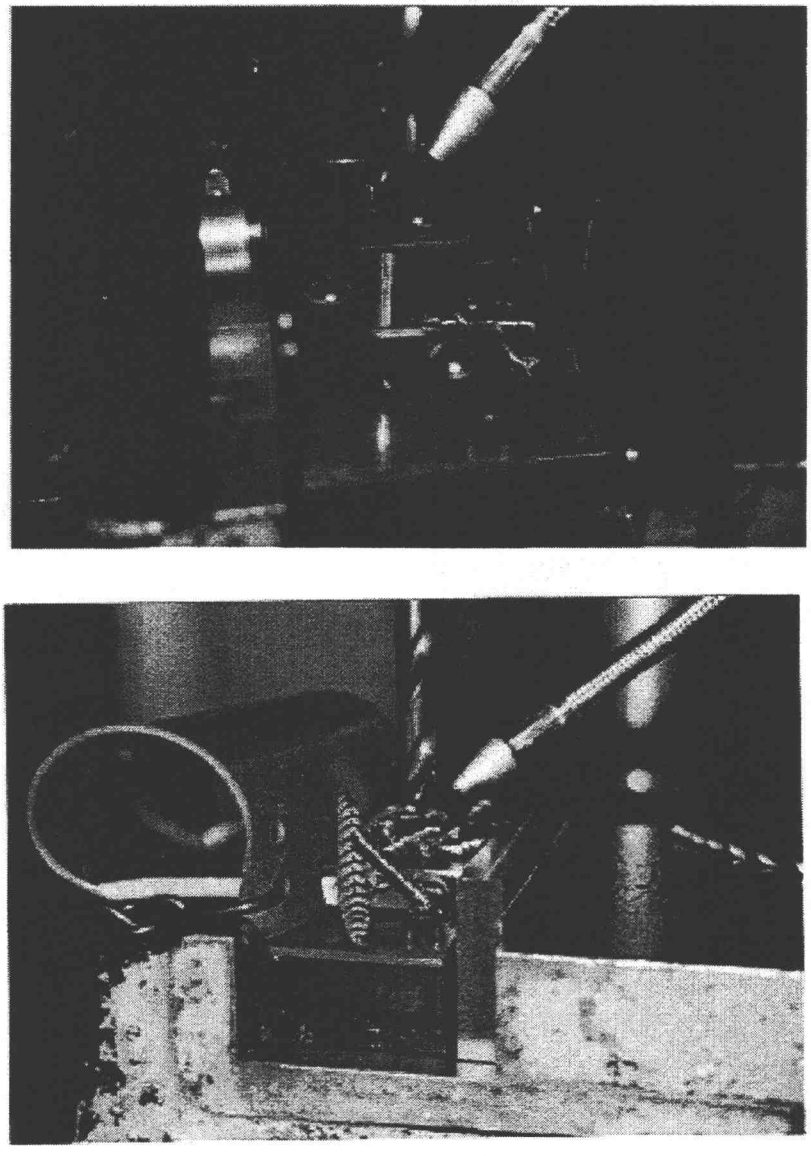

Figure 6.4 Fixture rubber sheet cover for elimination of chip impact on AE signals.

process and (2) the drill-wear producing process. During the sample collecting process, one hole was drilled on the work piece, and the work piece and the spectrums generated in the hole-drilling process were collected. During the drill-wear producing process, the work piece and the AE spectrum were not collected and the purpose of this process was only to produce the wear area on the drill flank face.

Since, the purpose of the sample collecting process was to collect the work piece and AE spectrums for later analysis, the accuracy and repeatability of locating the work piece were important. To assure the position accuracy and repeatability, the 3-2-1 principle was used in the fixture design [47]. As shown in Figures 6.2 and 6.3a, the work piece was located at the same position every time through point contact by using three balls and two pins. The three locator points form a datum plane for locating the work piece on the same plane, that is in the same Z position, each time. The pin on the main fixture body was used as a stopping locator to fix the work piece in the same position in the X-direction each time. Both the pin on the clamping plate and the wall on the main fixture body work together to fix the work piece in the Y-direction.

Considering that the purpose of the drill-wear producing process was to produce wear area on the drill flank face only, the accuracy of the work piece location was not important. However, this is a time consuming process. To make the process effective, a mating plate was designed as shown in Figures 6.2 and 6.3b. During the process, this mating plate was fastened onto the main fixture body by two screws. The clearance holes provided space to receive the locator balls and pin. As shown in Figure 6.3b, with this mating plate fixed on the main fixture body, the

scrap work piece could be moved continuously from left to right, and many holes could be continuously drilled. Since no precise location was needed, this method saved time for locating the work piece.

For drilling, a work piece of 4140 high strength steel with hardness of 197-Bhn and dimension of 3-inch length x 2-inch width x 0.5-inch thickness was used. The top surfaces of the work piece perpendicular to the drill was flattened by milling to minimize the effects of surface roughness on drill wandering motion. The side surfaces of the work piece contacting the wall behind which the AE transducer was mounted was flattened by milling to minimize the effects of surface roughness on signal noise in transmitting AE signals. The R10HD drill bit, manufactured by Precision Twist Drill Co., with 135° split point, 0.5-inch diameter and 6-inch average length was employed in this experiment. Drilling was performed with 20:1 water soluble cutting fluid. Drilling feed rate and speed recommended by the company for this drilling condition are 0.007-0.009 in/rev and 50-70 fpm (382–535 rpm).

During the drill-wear producing process, considering the default choices of speed and feed rate provided by the drilling machine, drilling speed and the feed rate are set as 441 rpm and 0.009 in/rev respectively.

During the process of collecting spectrums for AE signals, to eliminate the influence of randomly appearing bursts AE signals generated by chip breakage, cutting speed was changed to 163 rpm to make the chip in drilling operations as continuous as possible, because the increasing drilling speed makes the chip break more easily. The reduction of drilling speed also allowed collection of as many spectrum

as possible in a single hole-drilling operation. The feed rate during the collecting process was fixed at 0.009 in/rev.

In a single hole drilling process, a total of 34 AE signal spectrums could be collected. As shown in Figure 6.1, the signal from the transducer was first pre-amplified with a DECI model 400A AE preamplifier. A PC, model SX25MHz, with a program written in the C programming language, was used to control the collecting process with a KPC-488.2AT GPIB interface. The first amplified AE signal, generated as the drill contacted the work piece, was detected by the TEK 2230 scope. The oscilloscope informed the PC computer, and then the computer controlled the HP3585 spectrum analyzer to send the sequential 34 spectrums to the memory of the PC. Those spectrums were then modified as ASCII data, stored in the computer, and later analyzed.

6.1.2 Collecting Procedure for AE Spectrum

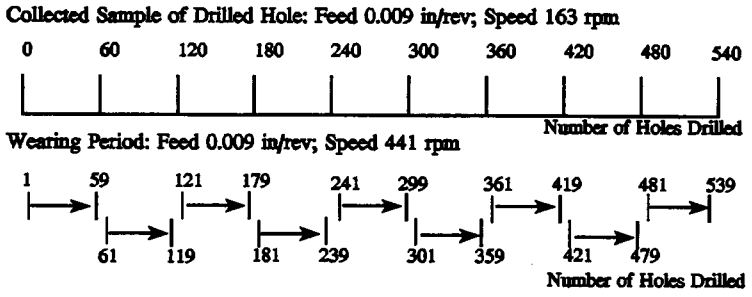

Figure 6.5 Experimental processes for: (a) work piece samples and spectrum collecting process, and (b) drill-flank wear producing process.

As shown in Figure 6.5, in the experiment, flank wear areas were measured every 60 holes. The spectrums of the drilled holes of numbers 0, 60, 120, 180, 240, 300, 360, 420, 480 and 540 were collected at a cutting speed of 163 rpm and a feed rate of 0.009 in/rev. In one collection loop, each of the 59 holes between the two collected holes was drilled continuously on the scrap material at a cutting speed of 441 rpm and at a feed rate of 0.009 in/rev. After 59 holes were finished, the drill-wear image was taken and measured using a machine vision system. After changing the cutting speed to 163 rpm and drilling in a individual fixed size work-piece, the AE spectrum of the next hole-drilling process was recorded and the work piece was collected at the end of each collection loop. The collection loop was repeated until when an audible vibration occurred during the drilling operation. At this time, the life of the drill bit was assumed to be at an end. With a new drill bit of the same type, the whole collection process was repeated to check the repeatability of the experimental results. Altogether, using two drill bits of the same type under the same drilling conditions, 1080 holes were drilled and among them, the spectrum data for 20 drilled holes were collected.

6.1.3 AE Spectrum-Processing Technique

The AE signal spectrums generated during stage 2 of the drilling process were used to characterize the drilling process. When drilling through-holes, the operation can usually be divided into three distinct stages, as discussed in chapter 5. In stage 1, as the drill contacts and penetrates the work piece, the cutting action is

unsteady, and the cutting forces rapidly increase. During stage 3, the cutting forces rapidly decrease as the drill point breaks through the underside of the work piece, and again the cutting action becomes unsteady until the point of the drill has completely come out of the hole. On the other hand, throughout stage 2, the cutting action becomes much more steady, the drill produces a symmetric cutting action in both lips, and the cutting forces remain quite constant. Therefore, the total of 19 spectrum generated during the second drilling stage were used in analysis.

To eliminate the influence of randomly appearing burst AE signals, a new spectrum, which was the average of the 19 spectrums, was proposed to describe the drilling process. It was observed that during metal cutting, plastic deformation and fracture of the material are the major sources of AE. The plastic deformation in the primary, secondary, and tertiary zones generates continuous-type AE signals. These continuous-type AE signals which carry the tool-state information are the main focus in machining process monitoring. The burst type AE signals generated by chip impact, chip breakage, and the hard material particle were considered as interference effects and needed to be eliminated. A special fixture discussed in the previous section was designed to eliminate the chip impact with a rubber sheet covering the whole fixture except the contacting points of the location surface for positioning the work piece at the same datum plane on the fixture and the contacting area between the work piece and a wall behind which the AE transducer was mounted. The effect of eliminating the chip impact by using this rubber sheet was checked and found to cause no changes in the spectrum. Additionally, the effect of burst type AE signals

generated by chip breakage and hard material particles was reduced to minimal levels by using an average spectrum strategy.

6.1.4 AE Spectrum Parameters

The energy content embedded in the AE spectrums was investigated to find the possible correlations with both tool wear and drilled-hole quality. The typical averaged AE spectrums and the histograms of their spectral amplitudes from the initial experiment are shown in Figure 6.6. Three observations in Figure 6.6 are discussed and the potential indicator variables of drill wear and drilled-hole quality in a drilling process are examined.

From Figure 6.6a the frequency shift of the amplitude peak was examined. There are no evident changes in the frequencies of the four amplitude peaks; that is, the amplitude peaks happened at the same frequency points. This means that the mechanisms driving inside the drilling process are basically of the same type. It indicates that the frequency shift might not be a useful indicator variable in the current study.

Figure 6.6a shows that, as total machining time increases (that is, as drill wear progresses) the amplitude of the spectrum increases. That is the energy released from the drilling process increases as the drill wear increases. It also shows there are basically four main peaks in the spectrum. Based on these four peaks, four frequency bands are defined. Band #1 is the frequency interval from 74 kHz to 200 kHz. Band #2 is defined as the frequency interval between 200 kHz and

(a)

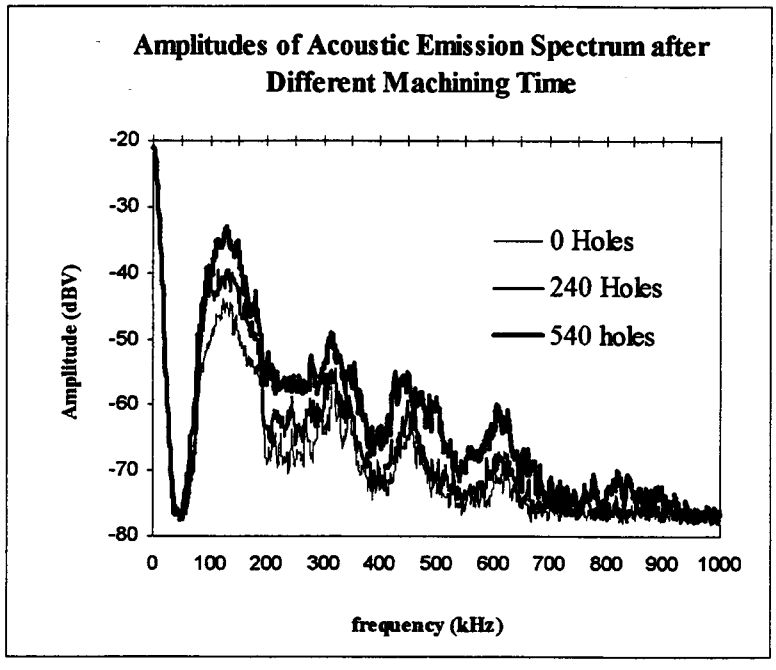

(b)

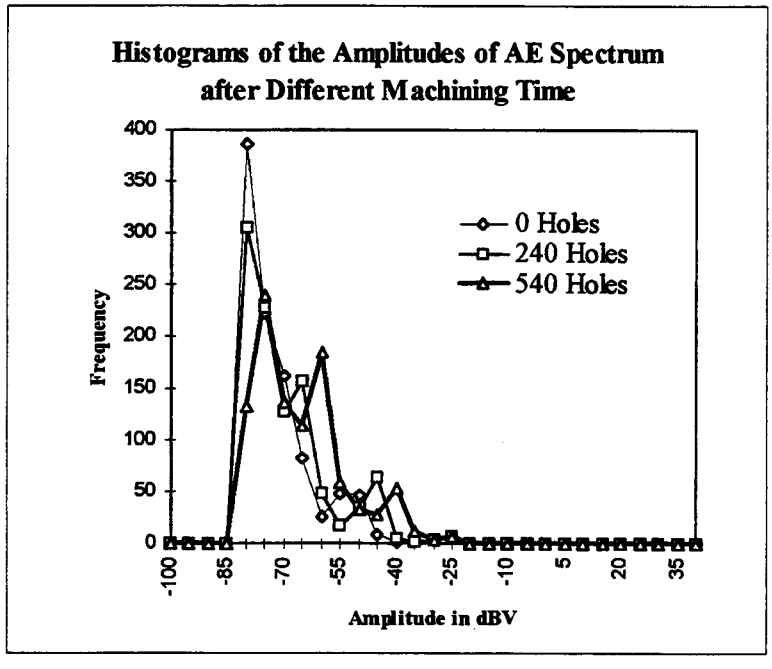

Figure 6.6 (a) Typical AE spectrum generated following set machining time; (b) histogram of changes in machining time.

374 kHz. Band #3 and band #4 are defined as the frequency interval from 376 kHz to 550 kHz and from 550 kHz to 676 kHz, respectively.

To choose the possible parameters as the indicator variables for drill-wear and drilled-hole quality in the drilling process, energy embedded beneath the four frequency bands was calculated and used as possible indicators in the current study. In addition to the energy content in a single frequency band, the energy ratios of each two frequency bands was also investigated.

Moreover, Figure 6.6a shows that the spectrum amplitudes increase as a result of drill-wear propagation not only at those four main frequency bands but also at each frequency point all over the AE spectrum. The histogram (i.e. distribution) of the spectral amplitudes provides some information about the relative change of the AE spectrum shape, as shown in Figure 6.6b. As the drill wears, the amplitude of the entire spectrum seems to increase and the count of the frequency points which have lower amplitudes decreases. This result is indicated by the frequency drop at the left side of the histogram. Another observation of the change in distribution is that, since entire spectral amplitudes increase, the new highest spectral amplitudes will be produced. Therefore, those points which have new highest amplitudes will appear at the right side of the histogram. This means that the count of frequency points at the right side of the histogram, which have higher amplitudes increases and the tail of the histogram propagates to the right. Based on this observation, the distribution parameters of AE spectrum amplitudes were employed as indicators in the current study to see whether they could provide a potential picture which describes the change in energy for the overall spectrum.

The distribution parameters used in the current study are the first four moments of the amplitude distribution of the spectrum. The first one is the average, which describes the widespread increment in the amplitude of the AE spectrum. The second moment of distribution is the variance, the deviation from the mean. The variance indicates the dispersion of the distribution, the scatter about the center. In general, variance provides the range change from the lowest AE amplitude to the highest AE amplitude. The skewness is the third moment, a measurement of the symmetry of the distribution. A positive skewness generally indicates a shift of the bulk of the distribution to the right of the mean. Figure 6.6b indicates that a positive skewness might be expected in the current study. The kurtosis is the fourth moment and a high kurtosis indicates a sharp distribution peak. That is, most of the amplitudes are concentrated in a small area near the average amplitude. On the opposite, a low kurtosis indicates a flat distribution characteristic.

Finally, eight parameters developed from the averaged spectrum were employed in the current study as predictor variables to investigate possible correlations with both tool wear and drilled-hole quality. The parameters can be grouped into two categories: (1) energy embedded beneath four dominant peak frequencies, and (2) distribution parameters of spectral amplitudes within the frequency range considered, 0 to 1 MHz. Four of the eight parameters, B1, B2, B3 and B4, represent the energy under the four peak frequencies, which are calculated with selected frequency bandwidths (i.e., [74 200] kHz, [200 374] kHz, [376 550] kHz and [550 676] kHz, respectively). The other four parameters, A, V, S and K are obtained by computing

the moments of the spectral amplitude distribution: average, variance, skewness and kurtosis. The eight AE parameters are thus defined as follows:

B1 = embedded AE energy in band #1,

B2 = embedded AE energy in band #2,

B3 = embedded AE energy in band #3,

B4 = embedded AE energy in band #4,

A = average, the first order distribution moment of AE amplitude distribution,

V = variance, the second order distribution moment of AE amplitude distribution,

S = skewness, the third order distribution moment of AE amplitude distribution, and

K = kurtosis, the fourth order distribution moment of AE amplitude distribution.

The ratios of energy embedded beneath four dominant peak frequencies, B1/B2, B1/B3, B1/B4, B2/B3, B2/B4 and B3/B4, are also analyzed to investigate the relationships between these ratios and drill-wear propagation.

6.2 Machine Vision System for Drill-Flank Wear Measurement

Progressive tool wear takes place by a process of attrition on both the rake and flank faces of the drill. Wear on the tool face is characterized by the formation of a cavity or a crater which is produced by the attrition of the chip flowing along

the tool face. The rubbing action on the newly generated work-piece surface causes wear on the flank face extending back from the cutting edge. This flat surface is called a wear land. When tools are used under normal and economical conditions, the flank wear of the tool is usually the controlling factor. Wear on the flank face of a cutting tool is caused by friction between the newly machined work-piece surface and the contact area on the tool flank face. The worn area, referred as the wear land, on the flank face is approximately parallel to the new work-piece surface being machined. The width of the wear land is usually taken as a measure of the amount of wear and can be determined by means of a toolmaker's microscope.

As discussed in section 3.3, no fixed criterion for the characterization of drill-wear condition has been determined, and different investigators have used different measurements to define drill-flank wear. However, as previously discussed, the growth in both the cutting forces and the cutting energy are functions of the wear area. Moreover, as has been discussed earlier, the wear on the flank face of a cutting tool is caused by friction between the newly machined work-piece surface and the contact area on the tool flank face. Consequently, the worn area on the flank face was used as the drill-wear measurement for this study. Figure 6.7 shows typical drill-flank wear obtained from the current experiments. The wear area on one lip was calculated as the summation of the areas of both trapezoid and rectangle. Since there were two cutting lips, the total flank wear was found by multiplying the wear area on one lip by 2.

In the current study, drill wear was determined by means of a machine vision system. The image of wear on the flank surface of the drill, as shown in

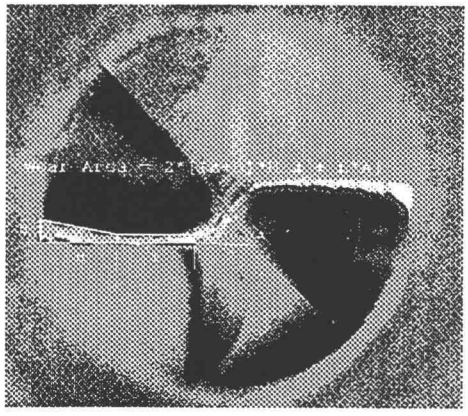

Figure 6.7 Typical flank-wear pattern for a split-twist drill and wear measurement definition used in current study.

Figure 6.7, was obtained by Accumen 2000 Vision System with a routine in the C programming language prepared by Farkas [48]. When using the vision system, three requirements need to be considered: First, the measured object must be put at the same altitude level as the calibration object; Second, the measured object must be put back in the same position every time; Third, the geometrical relationship between the camera and object must be both consistent and known. The camera lens needs to be as parallel to surface of the object as possible. In Farkas's work, these requirements are not provided, and hence a special calibration bar and fixture were designed to accomplish the first two requirements and a calibration method was developed to calibrate the relative position of the camera to the measured object. Figure 6.8a shows that the specially designed calibration bar has the same dimensions as the drill bit, and the hole on the holder has the same diameter as the diameter of the drill bit. Therefore, the drill bit can replace the calibration bar on

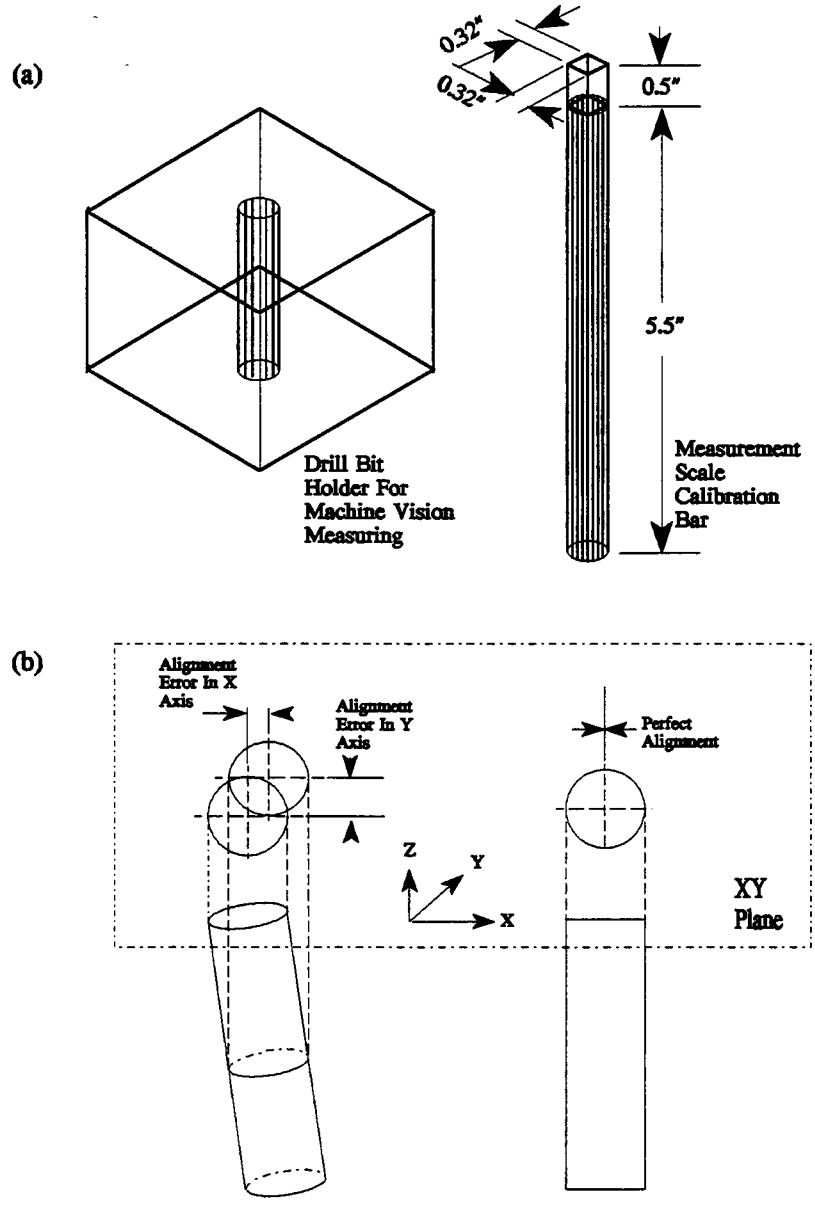

Figure 6.8 Calibration method used for machine vision measurement of drill wear, including (a) the designed drill-bit holder and bar used to calibrate measuring scale and (b) the alignment algorithm.

the holder without affecting the calibration setting. Figure 6.8b shows that if a cylinder is not located perpendicularly, the alignment will be reflected as position difference between centers of two top views of cross sections. In the other word, if a cylinder is located perfectly, there will be no position difference between centers of two top views of cross sections and the top views will overlap each other. Therefore, two cylinders having the same diameter but different lengths could be used to calibrate the camera alignment. To check the alignment, the shorter cylinder will be put into the holder first. After adjusting focus and having the image of the top view of the cylinder on the monitor, the center point of the top view image will be marked. Then, using the same procedure, replace the shorter cylinder with the longer cylinder to get the top view image of the longer cylinder on the monitor. The previous mark from the shorter cylinder can then be used to compare with the center point of the top view image of the longer cylinder. If the mark is located at the same spot of the center point, good alignment will be achieved.

6.3 Coordinate Measuring Machine for Hole-Quality Measurement

A Mitutoyo coordinate measuring machine (CMM), model BHN305, was used to measure drilled-hole quality. Each drilled hole was measured at five levels, with depths of 0.05, 0.15, 0.25, 0.35, and 0.45 inches respectively. The points around the inscribed circle were recorded and the hole quality was measured. The hole quality measurements discussed in chapter 5 were modified to present drilled-hole quality for the present study. Experimental results from Galloway [4] show

that the variation in hole diameter beyond some certain depth will change little. Therefore, attention was confined to measurements taken at the middle three layers of each drilled hole. The size of a hole was taken as the average diameter of the inscribed circles at the middle three layers. Since cylindricity is the three-dimensional equivalent of roundness, to simplify the cylindricity measurement of the drilled hole, the cylindricity was measured as the average roundness of the cross sections at the middle three layers. Straightness and perpendicularity were measured by the machine automatically.

6.4 Summary

This chapter introduces the experiment conducted in the current study. After the original 34 AE spectrums were collected, the averaged spectrum was calculated and those indicator variables were extracted from the averaged spectrum. Then, different statistical analyses were performed to determine feasibility of tool-wear monitoring and hole-quality prediction by statistical software, *StatGraphics Plus 2.0*. The results of the experiment and the statistical analysis and the possible usage of those results are discussed in the next chapter.

CHAPTER 7. RESULTS AND DISCUSSION

To establish some useful predictor variables from AE spectrums to use in predicting both drill wear and drilled-hole quality, an experiment was carried out to collect AE spectrums after different amounts of machining time had elapsed. In a nominal drilling process with constant drilling speed, feed rate, type of work-piece material, and type of drill bit, the remaining input parameter to the drilling process is only drill wear. Drill wear is empirically shown to be the cause for both hole quality variation and on-line AE energy increase. Therefore, the relationship between drill wear and AE energy increases and between drill wear and drilled hole quality variations are investigated. How AE energy changes along with drill wear propagation is examined first. Since drill wear is not measurable on-line during a drilling process, the prediction of drill wear using AE parameters is discussed. Moreover, in order to investigate the possibility of on-line drilled-hole quality prediction using on-line measurable AE parameters instead of using drill wear which is not measurable on-line, the correlations between the quality measurements of drilled hole and AE energy parameters become important and are also discussed.

7.1 Drill-Wear Propagation Versus Elapsed Machining Time

By plotting drill wear against the elapsed machining time, a wear curve was observed as shown in Figure 7.1. In the figure, the drill wear area is shown to increase as the machining time increases. The three distinct wear stages discussed

in the previous chapter are only slightly observable. At the beginning of the wear curve, there is a big jump in drill wear after several holes (1 to 60 holes) have been

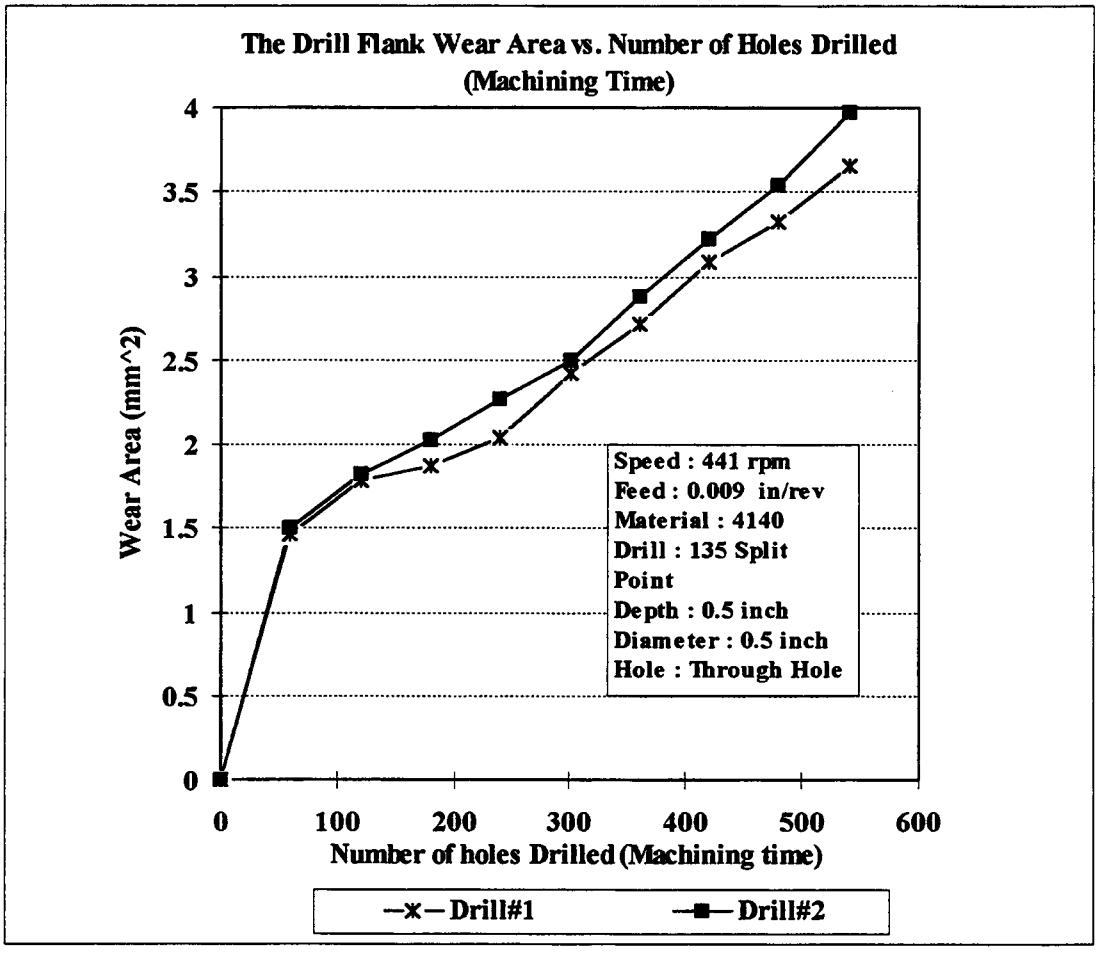

Figure 7.1 Characteristic pattern curve of drill-flank wear versus machining time.

drilled. During the period from 60 holes to 330 holes, the wear curve slope remains relatively constant. Also, the wear curve slope seems constant from 330 holes all the way to the end. Recall the theoretical wear curve; the slope at this stage should be higher than the current result. The possible reason for this result is due to the

vision system used in the current study. Since the vision system is a two-dimensional system, the lighting situation and projection plane become the main effects in measurement results. Moreover, both the accuracy and repeatability of the vision system are low, estimated as 0.010 to 0.020 inch. Due to the limitation of the lighting situation and 2D projection plane, as well as the low accuracy and repeatability of the vision system, the dimensions of the image at the outer corner of the drill bit, where the wear progresses much faster than in other positions, can only be approximately measured.

7.2 AE Parameter Changes Versus Drill-Wear Propagation

Eight parameters developed from the averaged AE spectrum were employed as predictor variables to investigate possible correlations with drill wear. The parameters, B1, B2, B3 and B4, represent the energy under the four peak frequencies which are calculated with selected frequency bandwidths (i.e., [74 200] kHz, [200 374] kHz, [376 550] kHz and [550 676] kHz, respectively). Parameters, A, V, S and K, are the distribution moments of the spectral amplitude distribution (average, variance, skewness and kurtosis). Figure 7.2a-d shows the plots for AE energy embedded in each frequency band against drill wear, indicating that energy increased along with the increased drill wear. The solid line in each plot represents the fitted polynomial function of the energy increasing along with drill wear increasing. The high values of the coefficient of multiple determination, R^2, suggest that

(a)

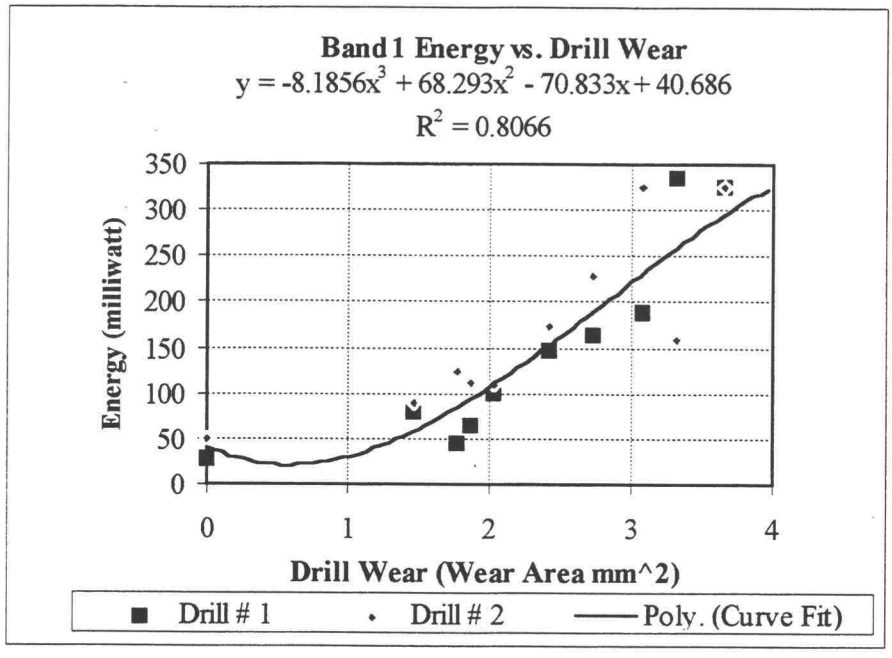

(b)

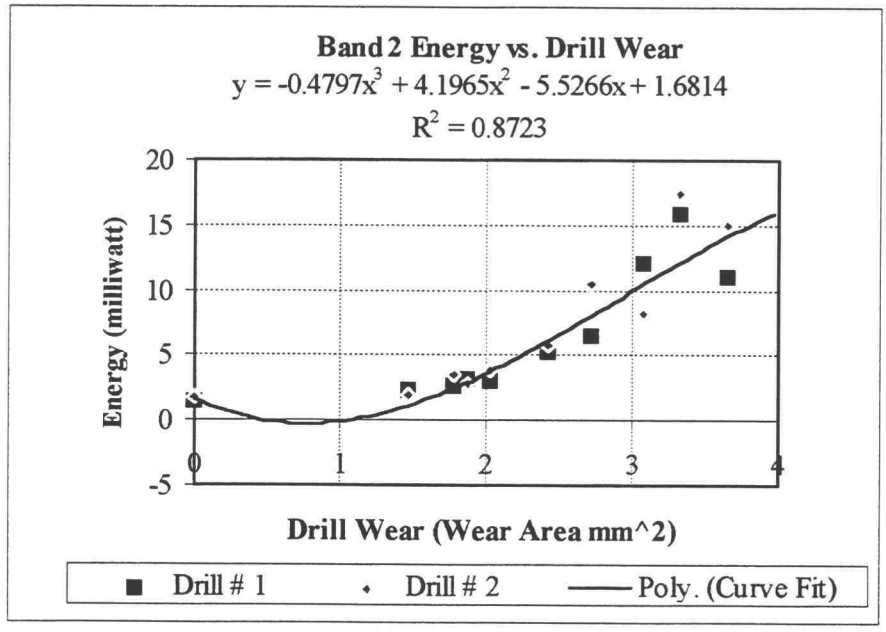

Figure 7.2 AE energy changes in single frequency band versus drill-flank wear for: (a) frequency band 1, (b) frequency band 2 (c) frequency band 3, and (d) frequency band 4.

(c)

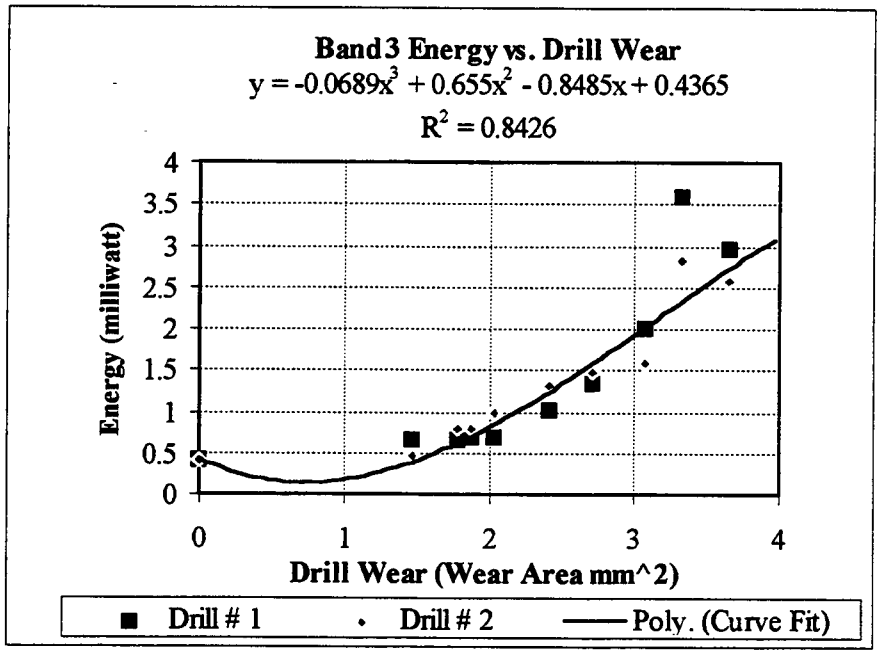

(d)

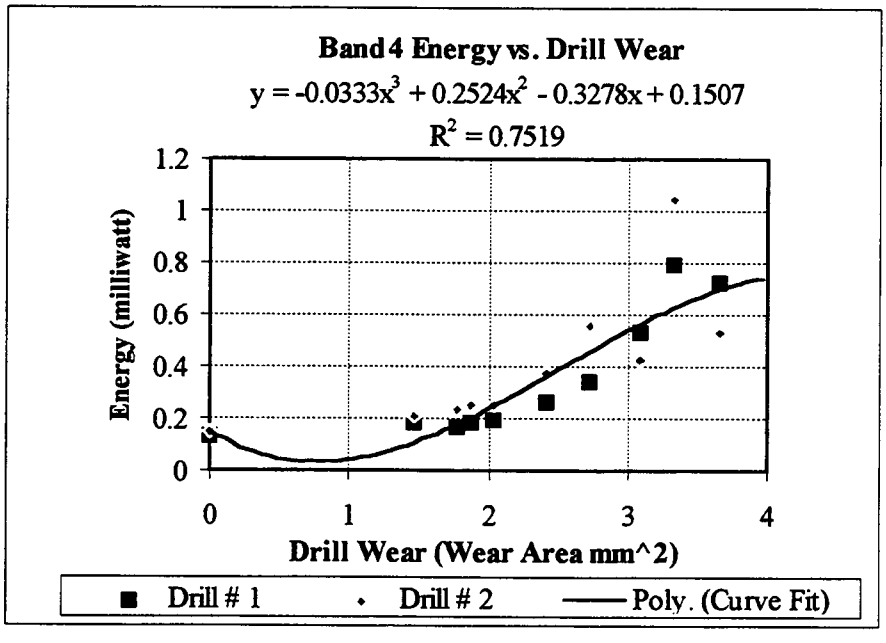

Figure 7.2 (Continued).

the fitted polynomial function for each frequency band has been very successful in relating the embedded AE energy in the frequency band to the drill wear area.

Comparing the degree of the relationships between drill wear and the energy of four frequency bands, three predictor variables (the first, second and third power of drill flank wear) were used in each fitted polynomial function. Among the four plots, the highest R^2 value, 0.8723, for the chosen polynomial function of B2 indicates that the embedded AE energy in the band #2 has the highest correlation with the drill wear area.

This observation tends to confirm the theoretical relationship, $\hat{W} = C1\ \{\ C2 + C3W_{area}\}^m$, between AE energy and the drill-wear area, as developed in chapter 3. The factor, m, of that equation could be taken as 3. Those fitted polynomial functions such as $\hat{W} = 0.4797W_{area}^3 + 4.1965W_{area}^2 - 5.5266W_{area} + 1.6814$, are similar to the form as $\hat{W} = C1\ \{\ C2 + C3W_{area}\}^3$.

The plots in Figure 7.3a-f indicate that there is no apparent relationship between the energy ratio of any two frequency bands and the drill-wear area. The possible reason for the observation is that there is a high correlation between the energies in any two bands. Energy in one frequency band increases as energy in another frequency band increases. Therefore, the ratio of any two band energies may remain approximately constant throughout the increasing drill wear.

The plots of the distribution moments versus drill wear were obtained and are shown in Figure 7.4a-d. By examining the R^2 values of these plots, it is obvious that there were strong correlations between each of the distribution moments with orders from 1 to 4 and drill wear. Figure 7.4a shows an agreement to the condition

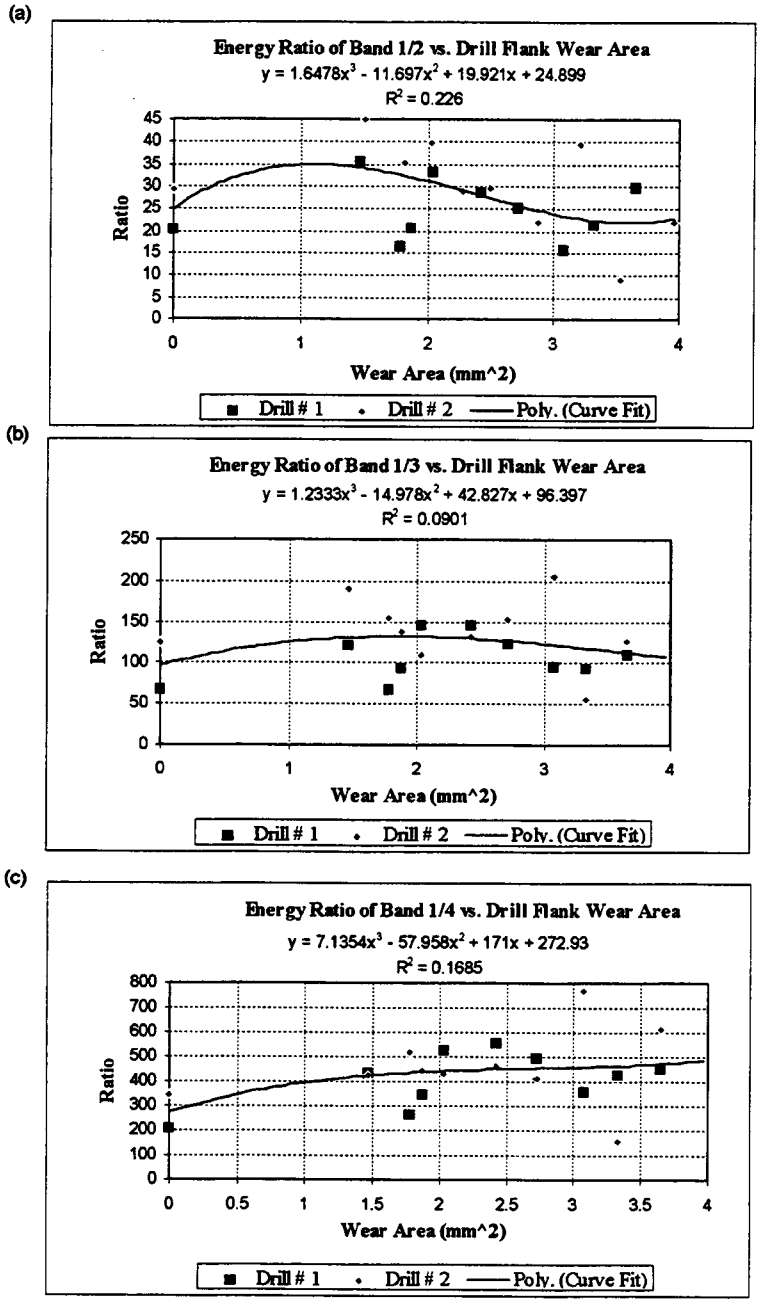

Figure 7.3 Changes of energy ratio for each two frequency bands versus drill-flank wear area: (a) Band 1 to 2, (b) Band 1 to 3, (c) Band 1 to 4, (d) Band 2 to 3, (e) Bank 2 to 4, and (f) Band 3 to 4.

(d)

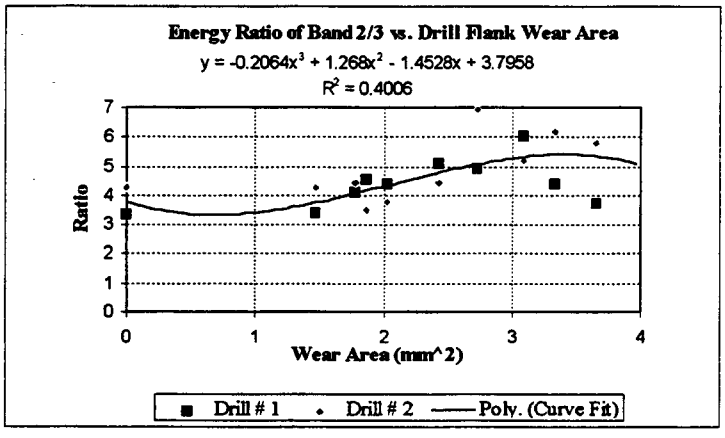

(e)

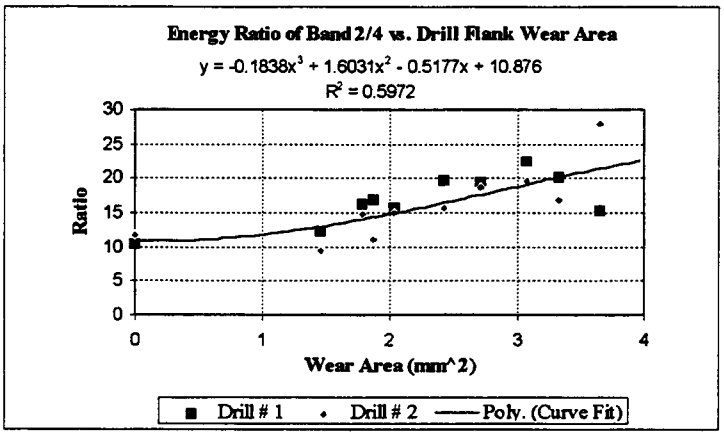

(f)

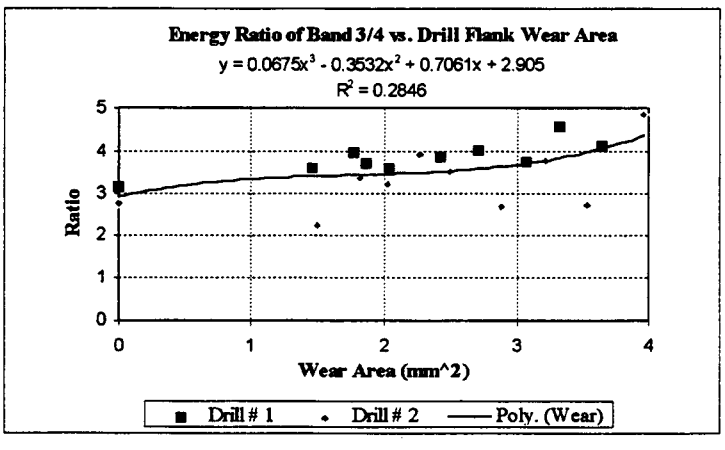

Figure 7.3 (Continued).

(a)

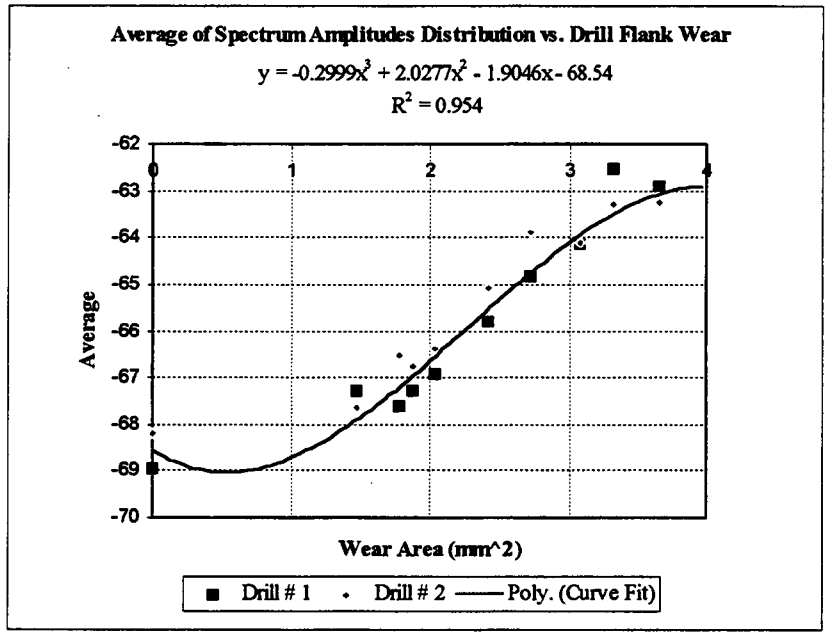

(b)

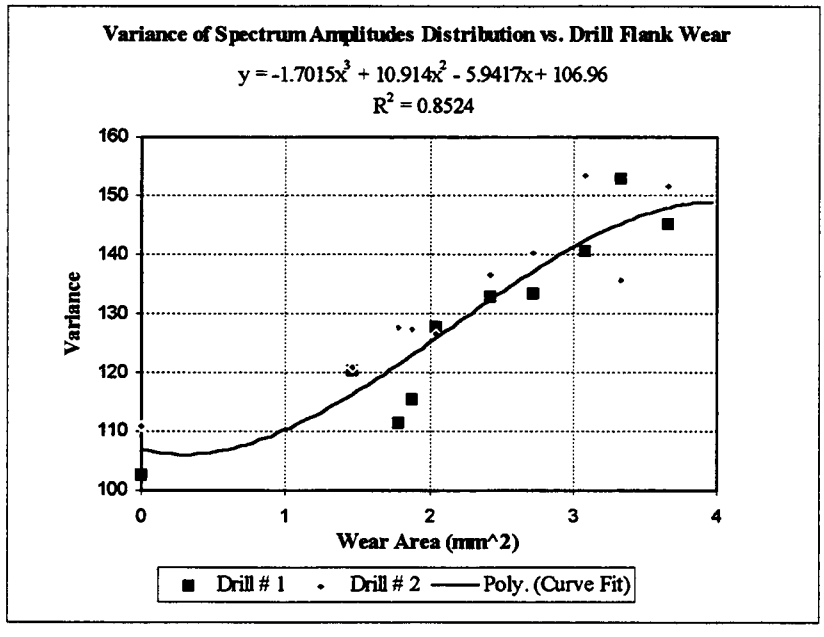

Figure 7.4 Changes of distribution moments for AE spectrum amplitudes versus drill-flank face wear: (a) first order, amplitude average, (b) second order, amplitude variance, (c) third order, amplitude skewness, and (d) fourth order, amplitude kurtosis.

(c)

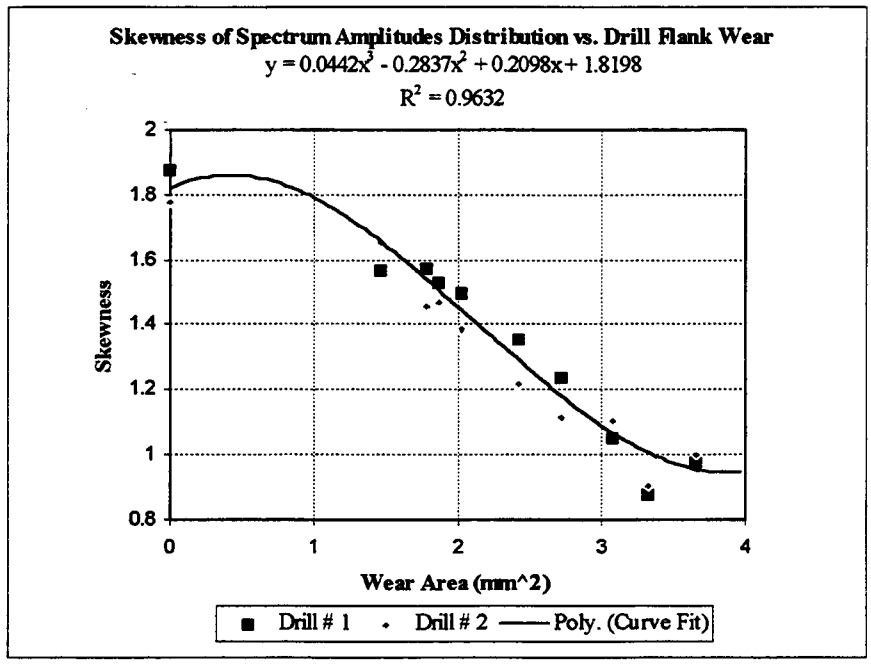

(d)

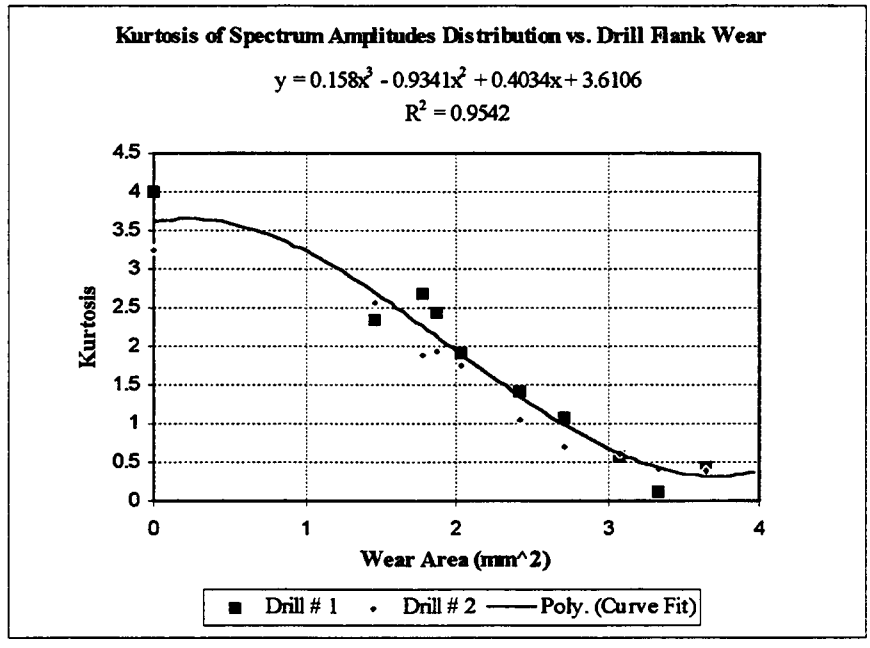

Figure 7.4 (Continued).

of that AE energy increases as drill wear increases. Since the amplitude at each frequency point over a whole spectrum increased, the average of AE spectrum amplitudes should have increased accordingly. The plot in Figure 7.4b shows that as drill wear increased, the variance of the AE spectrum amplitudes increased. The plots in Figures 7.4c-d show that the skewness and kurtosis, in contrast to variance, decreased as drill wear increased.

7.3 Hole-Quality Change Versus Drill-Wear Propagation

Figure 7.5a-d shows the plots of quality measurements of drilled holes versus drill wear. The plot in Figure 7.5a shows that there is a suggestive relationship between the hole straightness measurement and drill wear. The straightness measurement for drilled holes tended to increase as drill wear increased. Figure 7.5b indicates that there was no apparent relationship between the change in the perpendicularity measurement of drilled holes and drill wear. The evidence in Figure 7.5c shows that there is a strong relationship between the change in the roundness measurement of drilled holes and drill wear. The roundness error in drilled holes tended to get larger as drill wear proceeded. The plot in Figure 7.5d shows that there is a relationship between the diameter measurement of drilled holes and drill wear. The plot indicates that the diameter measurement of the drilled holes tended to be oversized either when using a new drill bit or when the drill bit reached a certain degree of wear. The diameter measurements of the holes drilled between

(a)

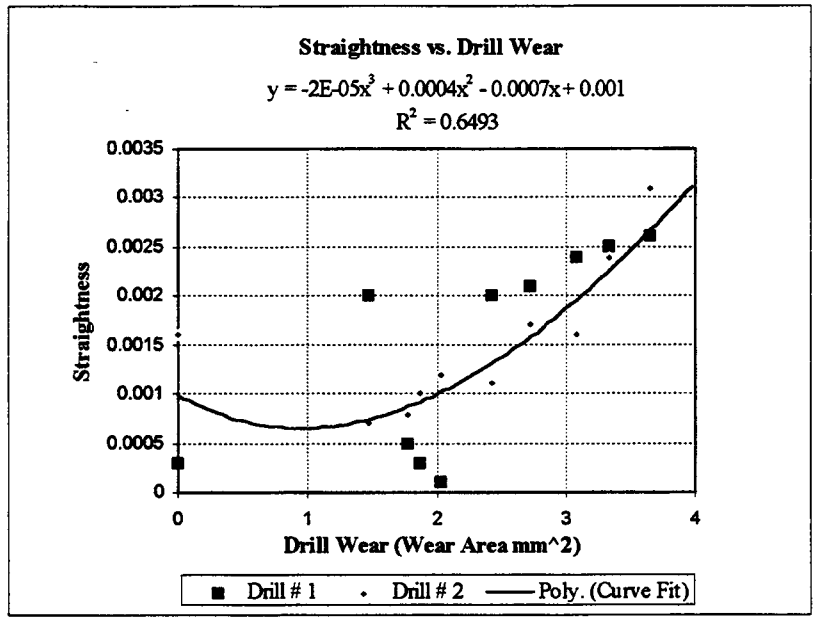

(b)

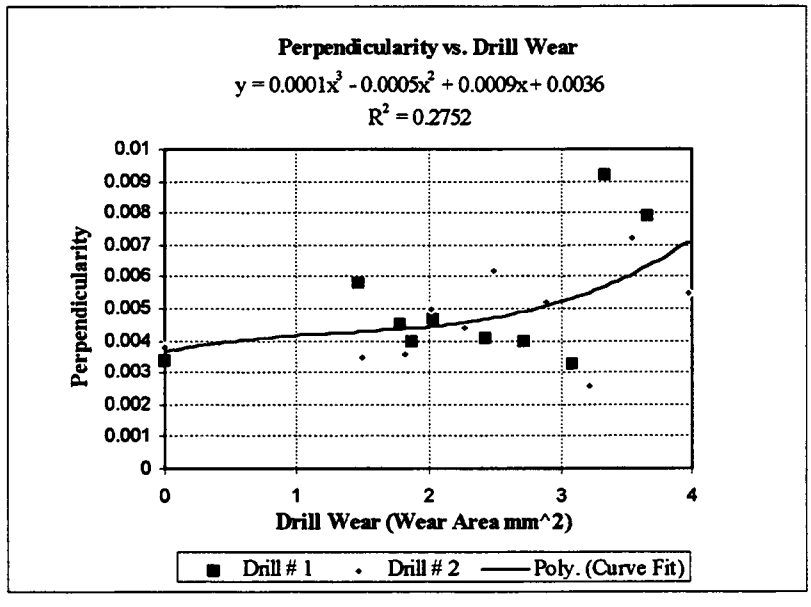

Figure 7.5 Quality measurements versus changes in drill-flank face wear: (a) straightness, (b) perpendicularity, (c) averaged hole roundness, and (d) averaged hole diameter.

(c)

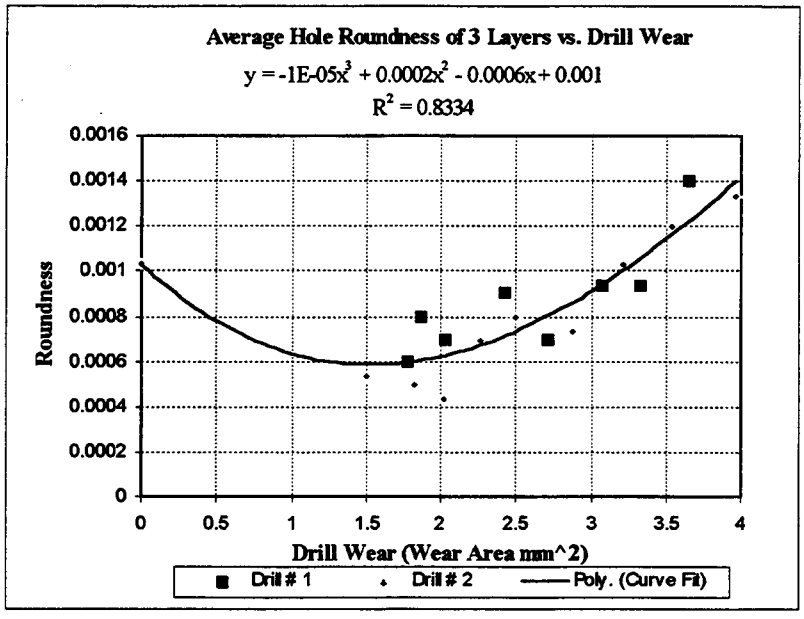

(d)

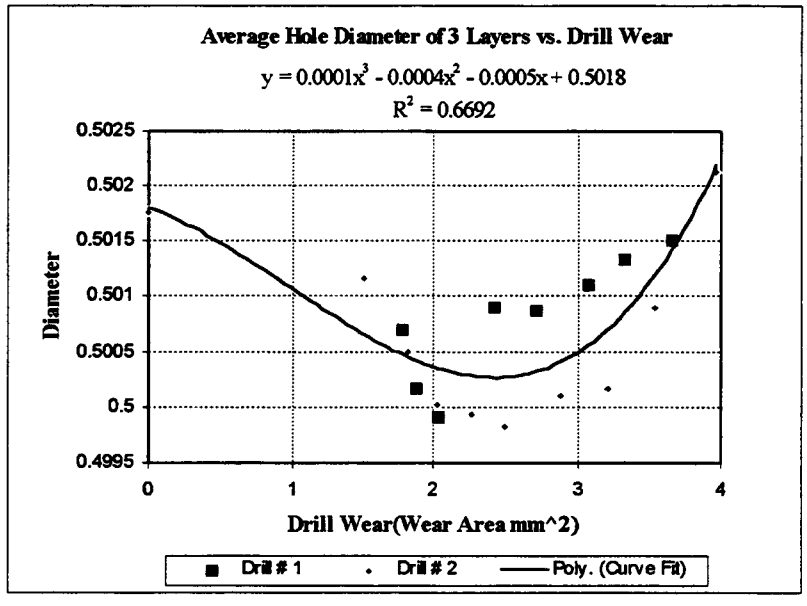

Figure 7.5 (Continued).

these two extremes do not change much. The big gap shown in Figure 7.5a-d indicates the fact that the initial drill wear was built up only after several holes (1 to 60 holes) were drilled. This evidence shows agreement with the drill wear curve shown in Figure 7.1.

7.4 AE Parameters and Drill-Wear Prediction

As discussed in section 7.2, there were strong relationships between drill wear and embedded AE energy in each frequency band as well as between drill wear and distribution moments. Those strong relationships provide the possibility of using AE energy of specific frequency bands or the AE spectrum amplitude distribution moments to predict drill wear. To investigate the possibility of using AE parameters to predict drill wear, drill wear was set as the dependent variable whereas the AE parameters were treated as the independent variables. By switching the axis of the plots in Figure 7.2, new plots of drill wear versus those AE parameters were obtained and are shown in Figures 7.6a-d and 7.7a-d. It is observed that a general additive multiple regression model with three predictor variables, which are the first, second and third powers of a single AE parameter, was sufficient for the prediction of drill wear through any one of those eight AE parameters, that is, AE energies embedded in the four frequency bands and the four distribution moments of the AE amplitude distribution for the first four orders. The high R^2 values suggest that the chosen models successfully related drill wear area to those eight AE parameters.

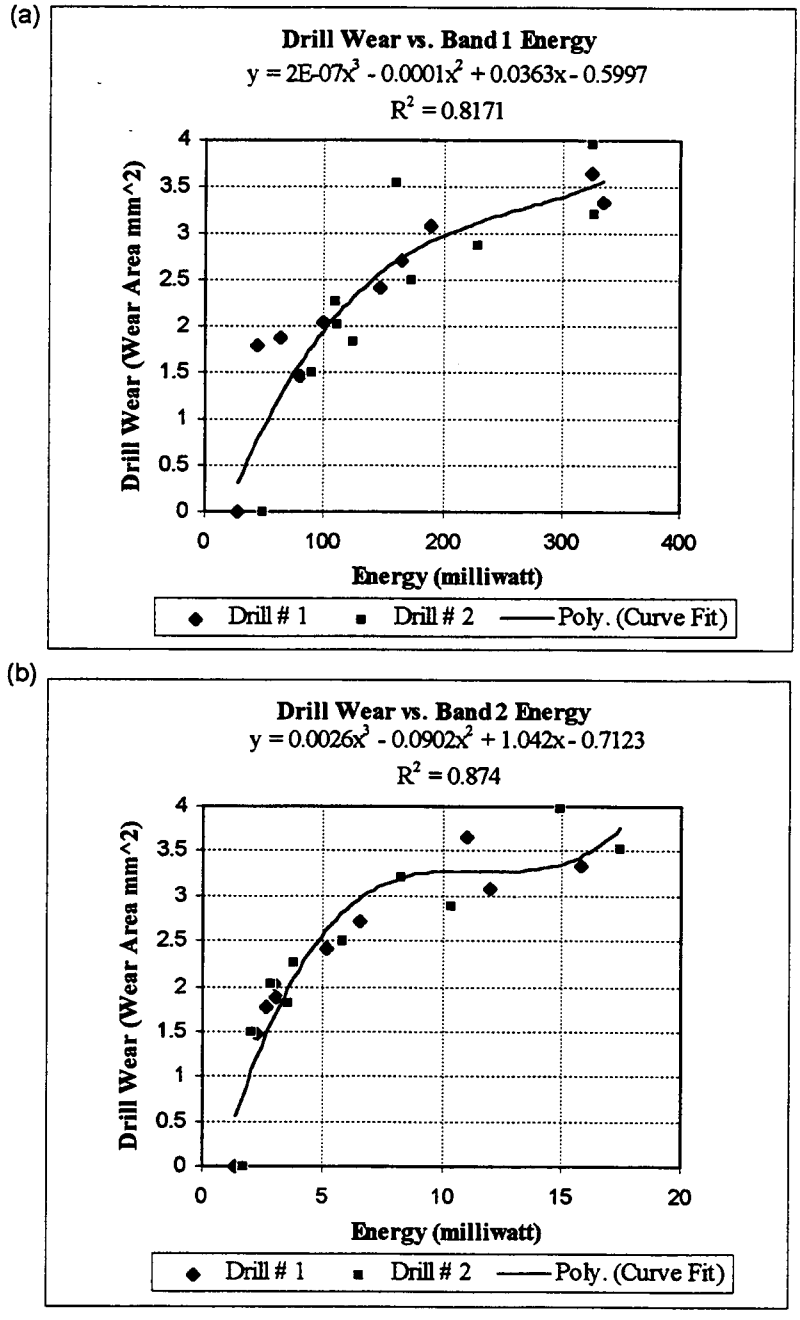

Figure 7.6 Drill-flank wear curve-fitting model for AE energy embedded in frequency bands: (a) Band 1, (b) Band 2, (c) Band 3, and (d) Band 4.

(c)

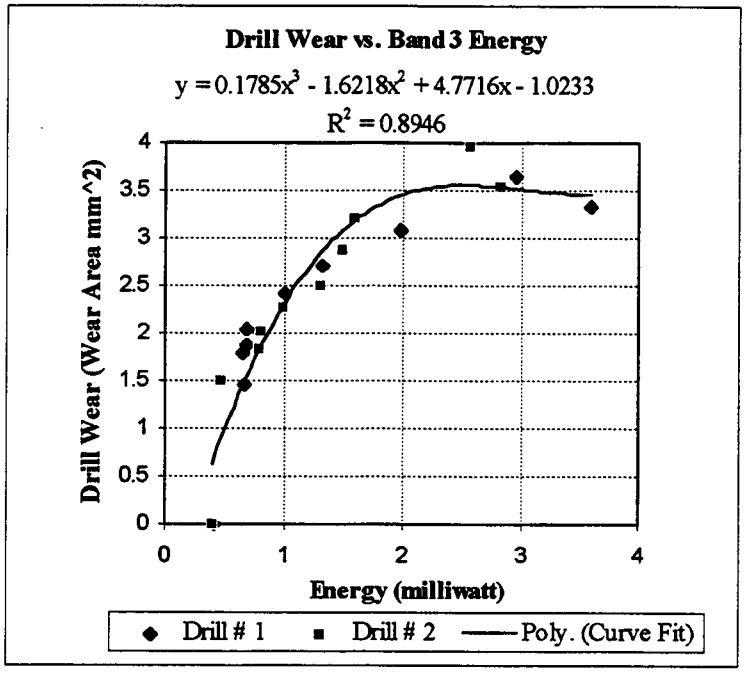

(d)

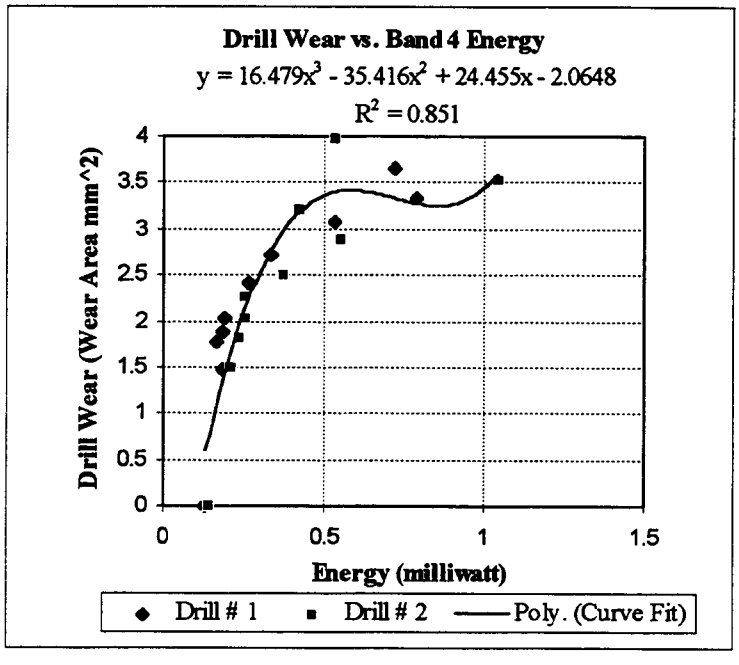

Figure 7.6 (Continued).

(a)

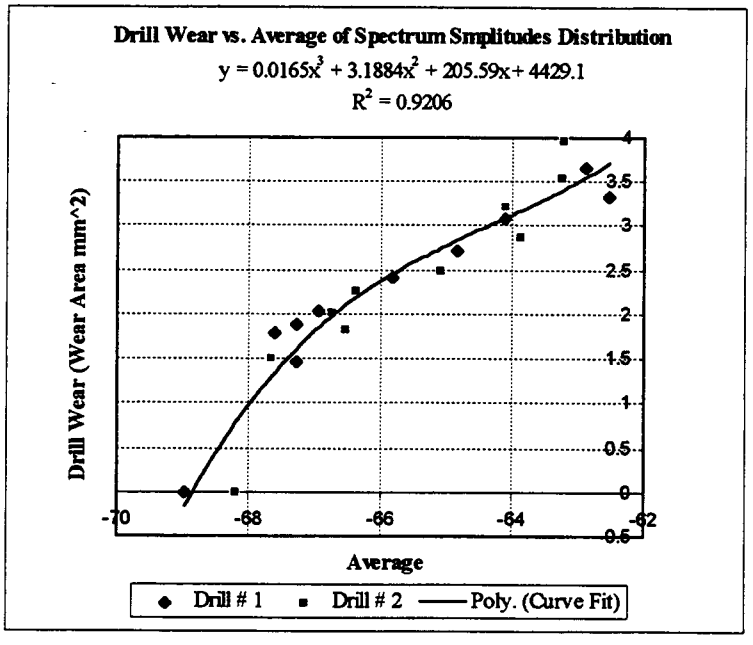

(b)

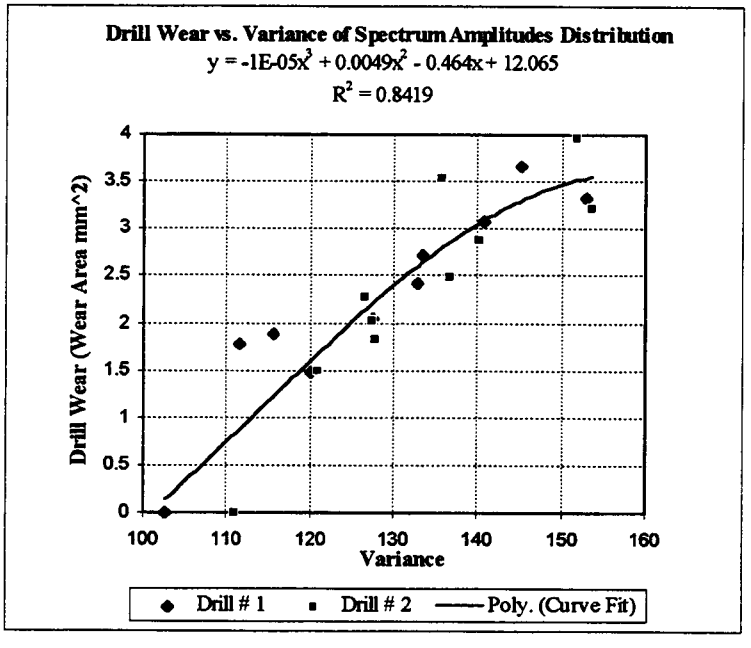

Figure 7.7 Drill-flank wear curve-fitting model for different order distributions of AE spectrum amplitude moments: (a) first order average, (b) second order variance, (c) third order skewness, and (d) fourth order kurtosis.

(c)

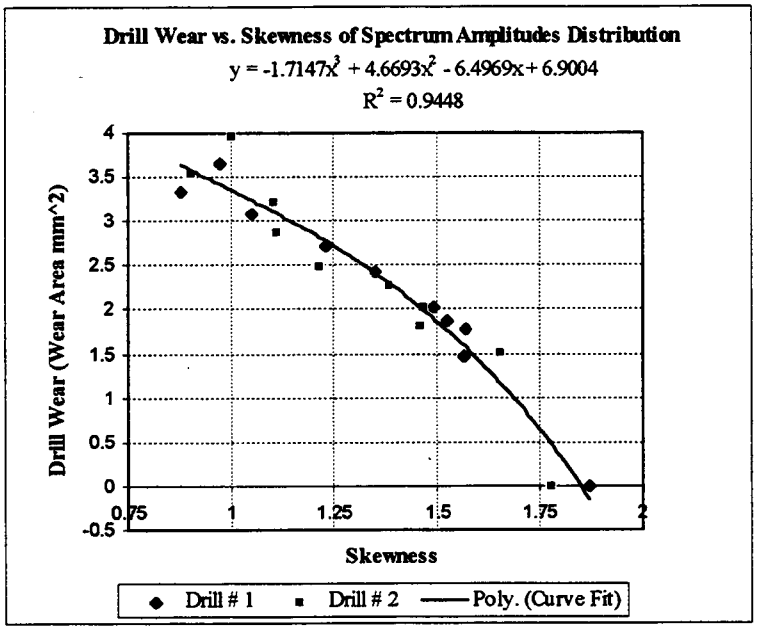

(d)

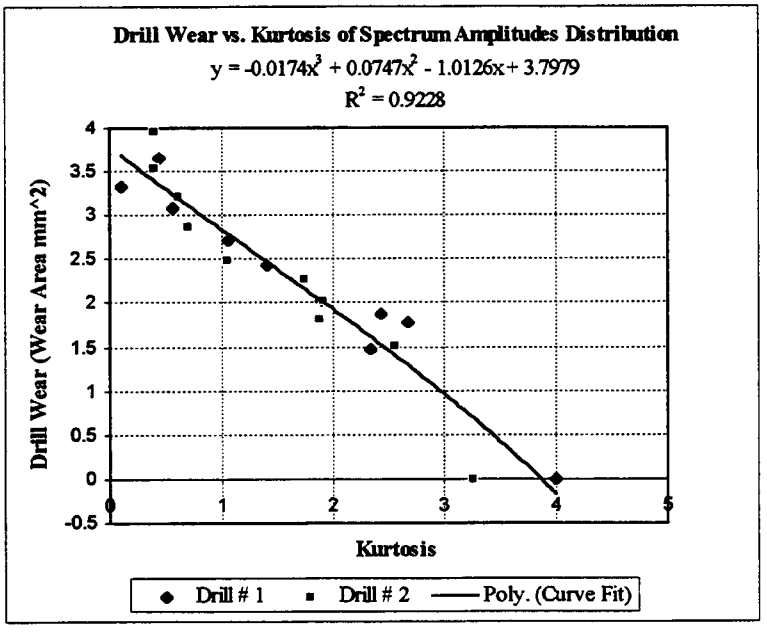

Figure 7.7 (Continued).

7.5 Hole Quality Prediction Using AE Parameters

Since both drill wear and quality measurements of drilled holes are not measurable on-line, the feasibility of using AE parameters to predict drill wear and quality measurements of drilled holes becomes important. As discussed in section 7.4, the AE parameters such as the energies embedded in the four frequency bands and the distribution moments of the first four orders could be used to predict drill wear. Moreover, the experimental evidence in section 7.3 shows that there are suggestive relationships between the quality measurements of drilled holes and drill wear. These observations tend to signify the potential for using AE parameters to predict hole quality.

To obtain those correlations for the relationship of drilled-hole quality to the possible predictor variables from among the AE parameters, a regression analysis was used to fit a regression model for each quality measurement for drilled holes. The forward-stepwise variable selection procedure was used to find the best-fit regression model [49]. The objective of the forward-stepwise selection procedure was to select the best-fitted model for significant variables selected from a set of provisional variables. The forward selection procedure begins with no variables in the model, other than the constant. The first variable to enter the model is the one which lowers the residual sum of squares the most. The next variable selected to enter the model is the one which lowers the residual sum of squares the most, when included in a model which already includes the first variable. At each step, an F-to-enter is calculated for each variable not yet included in the model. If some variables

have F-to-enter scores in excess of a pre-determined cutoff (usually 4.0), the one with the largest F is entered. This process is repeated until all F's are all less than the cutoff [49].

There are two reasons to choose only one AE parameter and the set of that AE parameter raised to different powers to be the provisional explanatory variables in each fitting procedure. One reason is that the objective of the current study is to find as many potentially useful predictor parameters which can apparently be closely related to hole-quality measurements. Another reason is that there were high correlations between any two of the AE parameters used in the current study. For reason of these high correlations, only one AE parameter could be selected to fit the regression model. In the other words, for the forward-stepwise selection procedure, different AE parameters were not pooled to determine the best-fit regression model for each quality measurement.

Through forward-stepwise multiple linear regression analysis, the final models for estimated drilled hole quality measurements associated with each AE parameter were obtained and are shown in Tables 7.1-7.4. The best-fit regression models of hole-quality measurement (i.e., straightness, perpendicularity, roundness and diameter) for each AE parameter (B1, B2, B3, B4, A, V, S, or K) are presented in Tables 7.1, 7.2, 7.3, and 7.4, respectively. In each table, the related statistics for each regression model of the quality measurement for each AE parameter are summarized. For example, the regression model of the straightness measurement on B4 is as follows:

Table 7.1 Regression models, significant predictor variables and related statistics from stepwise multiple regression analysis of hole straightness measurement on different AE parameters

Estimated Mean Straightness Error of Drilled Hole Versus AE Parameters						
AE Parameters		**Regression Model**			**Two Sided P-Value**	
					Model Variables	p-value
Released AE Energy of Single Frequency Band	Band#1 (B1)	Mean {Straightness}= 0.000498 + 0.00000632(B1)			B1	0.0003
		SE--> (0.000268) (0.00000144)				
		ADJ. R-square:0.491	σ: 0.000629; on 18df	p-value:0.0003		
	Band#2 (B2)	Mean{Straightness}= 0.000600 + 0.000135(B2)			B2	<0.0001
		SE---> (0.000209) (0.0000250)				
		ADJ. R-square:0.596	σ: 0.000560; on 18df	p-value<0.0001		
	Band#3 (B3)	Mean{Straightness}= 0.000511 + 0.000725(B3)			B3	0.0001
		SE---> (0.000227) (0.000138)				
		ADJ. R-square:0.583	σ: 0.000569; on 18df	p-value:0.0001		
	Band#4 (B4)	Mean{Straightness}= -3.99E-6 + 0.00487(B4) - 0.00240$(B4)^3$			B4	0.0016
		SE---> (0.000371) (0.00129) (0.00120)				
		ADJ. R-square:0.549	σ: 0.000592; on 17df	p-value:0.0004	$(B4)^3$	0.0616
AE Signal Spectrum Amplitudes Distribution Moments	1st Order Average (A)	Mean{Straightness}= 0.0249 + 0.000356(A)			A	<0.0001
		SE---> (0.00429) (0.0000654)				
		ADJ. R-square:0.601	σ: 0.000556; on 18df	p-value<0.0001		
	2nd Order Variance (V)	Mean{Straightness}= -0.00137 + 1.66E-$7(V)^2$				
		SE---> (0.000690) (3.909E-8)			$(V)^2$	0.0005
		ADJ. R-square:0.473	σ: 0.000640; on18df	p-value:0.0005		
	3rd Order Skewness (S)	Mean{Straightness}= 0.00450 - 0.00226(S)			S	0.0001
		SE---> (0.000634) (0.000466)				
		ADJ. R-square:0.542	σ: 0.000596; on 18df	p-value:0.0001		
	4th Order Kurtosis (K)	Mean{Straightness}= 0.00244 - 0.000598(K)			K	0.0002
		SE---> (0.000248) (0.000131)				
		ADJ. R-square:0.509	σ: 0.000617; on 18df	p-value:0.0002		

Table 7.2 Regression models, significant predictor variables and related statistics from stepwise multiple regression analysis of hole perpendicularity measurement on different AE parameters

Estimated Mean Perpendicularity Error of Drilled Hole Versus AE Parameters						
AE Parameters		**Regression Model**			**Two Sided P-Value**	
					Model Variables	p-value
Released AE Energy of Single Frequency Band	Band#1 (B1)	Mean {Perpendicularity}= 0.00364 + 0.00000792(B1) SE--> (0.000645) (0.00000346)			B1	0.0345
		ADJ. R-square:0.182	σ: 0.00151; on 18df	p-value:0.0345		
	Band#2 (B2)	Mean{Perpendicularity}= 0.00426 + 7.011E-7(B2)^3 SE---> (0.000346) (1.986E-7)				
		ADJ. R-square:0.376	σ: 0.00132; on 18df	p-value=0.0024	(B2)^3	0.0024
	Band#3 (B3)	Mean{Perpendicularity}= 0.00412 + 0.000113(B3)^3 SE---> (0.000253) (0.0000186)				
		ADJ. R-square:0.656	σ: 0.000982; on 18df	p-value<0.0001	(B3)^3	<0.0001
	Band#4 (B4)	Mean{Perpendicularity}= 0.00403 + 0.00432 (B4)^2 SE---> (0.000349) (0.00106)			(B4)^2	0.0007
		ADJ. R-square:0.450	σ: 0.000124; on 18df	p-value:0.0007		
AE Signal Spectrum Amplitudes Distribution Moments	1st Order Average (A)	Mean{Perpendicularity}= 0.0377 + 0.000500(A) SE---> (0.0108) (0.000164)			A	0.0007
		ADJ. R-square:0.302	σ: 0.00140; on 18df	p-value:0.0007		
	2nd Order Variance (V)	Mean{Perpendicularity}= -0.00161 + 0.0000497(V) SE---> (0.00325) (0.0000247)			V	0.0597
		ADJ. R-square:0.138	σ: 0.00155; on18df	p-value:0.0597		
	3rd Order Skewness (S)	Mean{Perpendicularity}= 0.00927 - 0.00329(S) SE---> (0.00149) (0.00109)			S	0.0077
		ADJ. R-square:0.296	σ: 0.000140; on 18df	p-value:0.0077		
	4th Order Kurtosis (K)	Mean{Perpendicularity}= 0.00614 - 0.000793(K) SE---> (0.000596) (0.000315)			K	0.0215
		ADJ. R-square:0.219	σ: 0.00148; on 18df	p-value:0.0215		

Table 7.3 Regression models, significant predictor variables and related statistics from stepwise multiple regression analysis of hole roundness measurement on different AE parameters

Estimated Mean Roundness Error of Drilled Hole Versus AE Parameters						
AE Parameters		**Regression Model**			**Two Sided P-Value**	
					Model Variables	p-value
Released AE Energy of Single Frequency Band	Band#1 (B1)	Mean {Roundness} = 0.000675 + 4.524E-9 $(B1)^2$ SE--> (0.0000704) (1.189E-9)			$(B1)^2$	0.0029
		ADJ. R-square:0.399	σ: 0.000213; on 16df	p-value:0.0029		
	Band#2 (B2)	Mean{Roundness} = 0.000581 + 0.0000370(B2) SE---> (0.0000848) (0.00000967)			B2	0.0015
		ADJ. R-square:0.446	σ: 0.000204; on 16df	p-value:0.0015		
	Band#3 (B3)	Mean{Roundness} = 0.000553 + 0.000202(B3) SE---> (0.0000885) (0.0000513)			B3	0.0012
		ADJ. R-square:0.461	σ: 0.000201; on 16df	p-value:0.0012		
	Band#4 (B4)	Mean{Roundness} = 0.000564 + 0.000709(B4) SE---> (0.0000986) (0.000210)			B4	0.0040
		ADJ. R-square:0.377	σ: 0.000217; on 16df	p-value:0.0040		
AE Signal Spectrum Amplitudes Distribution Moments	1st Order Average (A)	Mean{Roundness} = 0.120 + 0.00269(A) - 2.0268E-7 $(A)^3$ SE---> (0.0528) (0.00121) (9.478E-8)			A	0.0424
		ADJ. R-square:0.503	σ: 0.000193; on 15df	p-value<0.0020	$(A)^3$	0.0494
	2nd Order Variance (V)	Mean{Roundness} = 0.000311 + 2.225E-10$(V)^3$ SE---> (0.000201) (8.0068E-11)				
		ADJ. R-square:0.283	σ: 0.000232; on16df	p-value:0.0134	$(V)^3$	0.0134
	3rd Order Skewness (S)	Mean{Roundness} = 0.00361 - 0.00300(S) + 0.000460$(S)^3$ SE---> (0.000784) (0.000931) (0.000177)			S	0.0056
		ADJ. R-square:0.519	σ: 0.000190; on 15df	p-value:0.0016	$(S)^3$	0.0202
	4th Order Kurtosis (K)	Mean{Roundness} = 0.00130 - 0.000507(K) + 0.0000386$(K)^3$ SE---> (0.000100) (0.000107) (0.0000109)			K	0.0003
		ADJ. R-square:0.574	σ: 0.000179; on 15df	p-value:0.0006	$(K)^3$	0.0030

Table 7.4 Regression models, significant predictor variables and related statistics from stepwise multiple regression analysis of hole diameter measurement on different AE parameters

Estimated Mean Diameter of Drilled Hole Versus AE Parameters						
AE Parameters		**Regression Model**			**Two Sided P-Value**	
					Model Variables	p-value
Released AE Energy of Single Frequency Band	Band#1 (B1)	Mean{Diameter} = 0.500722 SE---> (0.000162)				
		ADJ. R-square:0.0	σ: 0.000690; on 17df	p-value:		
	Band#2 (B2)	Mean{Diameter} = $0.500463 + 0.00000337(B2)^2$ SE---> (0.000193) (0.00000161)			$(B2)^2$	0.0531
		ADJ. R-square:0.165	σ: 0.000630; on 16df	p-value:0.0531		
	Band#3 (B3)	Mean{Diameter} = $0.500445 + 0.0000932(B2)^2$ SE---> (0.000189) (0.0000409)			$(B3)^2$	0.0368
		ADJ. R-square:0.198	σ: 0.000618; on 16df	p-value:0.0368		
	Band#4 (B4)	Mean{Diameter} = 0.500722 SE---> (0.000162)				
		ADJ. R-square:0.0	σ: 0.000690; on 17df	p-value:		
AE Signal Spectrum Amplitudes Distribution Moments	1st Order Average (A)	Mean{Diameter} = 0.500722 SE---> (0.000162)				
		ADJ. R-square:0.0	σ: 0.000690; on 17df	p-value:		
	2nd Order Variance (V)	Mean{Diameter} = 0.500722 SE---> (0.000162)				
		ADJ. R-square:0.0	σ: 0.000690; on 17df	p-value:		
	3rd Order Skewness (S)	Mean{Diameter} = 0.500722 SE---> (0.000162)				
		ADJ. R-square:0.0	σ: 0.000690; on 17df	p-value:		
	4th Order Kurtosis (K)	Mean{Diameter} = 0.500722 SE---> (0.000162)				
		ADJ. R-square:0.0	σ: 0.000690; on 17df	p-value:		

Mean{straightness} = -3.99E-6 + 0.00487(B4) - 0.00240$(B4)^3$
SE--> (0.000371) (0.00129) (0.00120),

ADJ. R-square: 0.549,

$\hat{\sigma}$: 0.000592; on 17df,

p-value:0.0004,

p-value for B4: 0.0016, and

p-value for $(B4)^3$: 0.0616.

These statistics show the results of fitting a multiple linear regression to describe the relationship between straightness and band #4 energy. In the example, it shows that two predictor variables, B4 and $(B4)^3$, are selected as significant variables for fitting the model. The estimated coefficients for B4 and $(B4)^3$ are 0.00487 and -0.0024, respectively. With the constant -3.99E-6, the equation for the fitted model is as follows: $Straightness = -3.99E\text{-}6 + 0.00487(B4) - 0.00240(B4)^3$. The p-values, 0.0016 and 0.0616 for the two variables, generally determine whether the variable is significantly related to the straightness measurement. The smaller the p-value, the greater the signficance attributed to the variable. Usually, 0.05 is the boundary value for the p-value to conclude whether the variable is significant or not. Although, as seen in this example, the p-value, 0.0616, for $(B4)^3$ is a somewhat larger than 0.05, for preservation purposes $(B4)^3$ was still included in the model for the current study.

Another important statistic is the p-value of the regression model, 0.0004. It determines whether the chosen model is justified or not when using selected variables to fit this model. The adjusted R-square statistic generally indicates that the

fitted model explains 54.9% of the variability in straightness measurement. The SE values present the standard errors for those estimated regression coefficients of the constant and of the two predictor variables. The $\hat{\sigma}$ on $17df$ is the standard error of estimate based on 17 degrees of freedom. The $\hat{\sigma}$ is the standard deviation of the residuals and can also be used to construct prediction limits for new observations [50].

Table 7.1 shows the result of regression analysis for the straightness measurement of drilled holes associated with each AE parameter. Convincing evidence was provided that the mean straightness measurement of drilled holes is associated with each AE parameter in each single model. The mean straightness measurement of drilled holes is associated with the AE energies embedded in different frequency bands, including band#1_energy(B1), band#2_energy(B2), band#3_energy(B3), band#4_energy(B4), and the squared band#4_energy($B4^2$) (the two-sided p-values were 0.0003, <0.0001, 0.0001, 0.0016, and 0.0616, respectively). Along with AE energy, the mean straightness measure was strongly associated with all four distribution moments, including average(A), squared variance(V^2), skewness(S), and the kurtosis(K) (the two-sided p-values were <0.0001, 0.0005, 0.0001, 0.0002, respectively). The adjusted R-square statistic generally indicates what percentage of the variability for straightness measurements can be explained by the fitted model. Among the eight models, the highest R-square value, 0.601, for the model of straightness on AE parameter A indicated that this model was the best for the prediction of straightness measures. However, the R-square value for each model

was close to the others (i.e., a range of 0.474 to 0.601); no one model was significantly better than others.

In Table 7.2, the final models of estimated mean perpendicularity measurement for each AE parameter are presented. Again, there was strong evidence that the mean perpendicularity measurement of drilled holes is associated with each AE parameter. The mean perpendicularity measurement is associated with the AE energies embedded in different frequency bands, including band#1_energy(B1), cubed band#2_energy($B2^3$), cubed band#3_energy($B3^3$), and the squared band#4_energy($B4^2$) (the two-sided p-values were 0.0345, 0.0024, <0.0001, and 0.0007, respectively). Mean perpendicularity measurement was also associated with distribution moments, including average(A), variance(V), skewness(S), and the kurtosis(K) (the two-sided p-values were 0.0007, 0.0597, 0.0077, 0.0215, respectively). Similarly, among the eight models, the highest R-square value, 0.656, for the model of perpendicularity measurement on the AE parameter B3, indicates this model is the best model to predict perpendicularity measurement by using that AE parameter, B3. The small R-square values for other models indicated that no other models were relevant for the prediction of perpendicularity measurement.

Again, through forward-stepwise multiple linear regression analysis, the final models of estimated mean roundness measurement for each AE parameter were obtained and are shown in Table 7.3. There was convincing evidence that the mean roundness measurement of drilled holes is associated with both the energies embedded in different frequency bands and the distribution moments. The significant predictor variables included squared band#1_energy($B1^2$), band#2_energy(B2),

band#3_energy(B3), the band#4_energy(B4), average(A), cubed average(A^3), cubed variance(V^3), skewness(S) and cubed skewness(S^3), and kurtosis(K) and cubed kurtosis(K^3) (the two-sided p-values were 0.0029, 0.0015, 0.0012, 0.0040, 0.0424, 0.0494, 0.0134, 0.0056, 0.0202, 0.0003, and 0.0030, respectively). The highest R-square value, 0.574, for the model of roundness measurement of the AE parameter K, indicated that this was the best model for predicting roundness measurements with two predictor variables, such as the first and the third powers of AE parameter K.

For the diameter measurement of the drilled hole, the regression models chosen from forward-stepwise variable selection procedures are shown in Table 7.4. Except the AE energies embedded in the second and the third frequency bands, there was no strong evidence that there is a relationship between any one of the rest of the AE parameters and hole diameter. There is suggestive evidence that hole-diameter measurement is associated with either the squared energy of the second frequency band($B2^2$) or the squared band#3_energy($B3^2$) (the two-sided p-values were 0.0531, 0.0368, respectively). Although there was suggestive evidence that hole diameter measurement is associated with either the squared band#2_energy($B2^2$) or the squared band#3_energy($B3^2$), the low R-square values for the two models indicates that the models are not good enough to predict hole-diameter measurement.

Except for hole diameter, these results show that there is a certain relationship between each quality measurement of a drilled hole and each AE parameter. Therefore, each AE parameter, accompanied by the regression models for different quality measurements, could be used to predict on-line straightness, perpendicu-

larity, and roundness errors of drilled holes. Only two AE parameters, the AE energies embedded in the second and the third frequency bands, could be used to predict the diameter measurement of drilled holes on-line. The usage of these regression models to predict hole quality on-line is like the question, "How large are those quality measurements for a drilled hole having an on-line measured AE energy of 1.334 milliwatt released in the third frequency band?" In terms of the regression models of hole quality measurements of AE energy released in the third frequency band, the estimated mean of each quality measurement for the drilled hole with 1.334 milliwatts measured as band#3_energy is presented.

For B3 = 1.334 milliwatt, the calculations for the estimated mean straightness, perpendicularity, roundness and diameter measurements are as follows:

$$\text{mean \{straightness\}} = 0.000511 + 0.000725(1.334)$$
$$= 0.00148,$$
$$\text{mean \{perpendicularity\}} = 0.00412 + 0.000113(1.334^3)$$
$$= 0.00439,$$
$$\text{mean \{roundness\}} = 0.000553 + 0.000202(1.334)$$
$$= 0.000822 \text{ and}$$
$$\text{mean \{diameter\}} = 0.500445 + 0.0000932(1.334^2)$$
$$= 0.50061.$$

The predictive quality of drilled holes may be considered as follows: "the quality measurements of the current finished hole are straightness: 0.00148", perpendicularity: 0.0439", roundness: 0.000822" and the diameter: 0.50061".

7.6 Categorized Quality Measurement Information of Drilled Holes versus AE Parameters

As discussed in the previous section, almost all of the AE parameters have apparent relationships associated with hole-quality measurements. However, the adjusted R-squares for these models were not high. In this sense of the R-square, the estimate was the percentage of the variability in hole quality measurements, explained by variation in the current model. The median size R^2-value in each plot suggests that the chosen models for hole-quality measurements could not be successfully in relating the hole-quality measurements to AE parameters. Moreover, considering that during most manufacturing process operations, the information an operator needs to know is not numerical but is categorical. Examples of categorical information needed are "the drill wear is low," "the drill wear is high," "hole straightness is acceptable," or "straightness is unacceptable." Since the regression model gives us the estimated mean of the quality measurement as a real number, the other usages of these predictor variables were considered to provide categorized information that could help operators evaluate a drilling process.

To categorize the drilled holes into different groups and to use selected AE parameters as variables for the prediction of which group a drilled hole falls into, appropriate data was subject to cluster and discriminant analysis. Cluster analysis is a technique for grouping objects so that objects within the same cluster are more like each other than they are like objects in other clusters [51]. This grouping method is a primitive technique in that no assumptions are made concerning group structure.

Before the analysis, no known groups existed. Grouping was done on the basis of similarity or dissimilarity [51]. By using the cluster analysis, all of the drilled holes could be characterized in two groups, "acceptable" and "unacceptable," according to their similarity or dissimilarity in quality measurements.

Discriminant analysis differs insofar as its use is appropriate only when two or more groups exist. Two goals were involved in this analysis. One was to find one or more functions, the discriminant functions, from several known quantitative measurements of the members in both groups. The found function can help to discriminate among known groups. A second goal, the principal objective of discriminant analysis, was to provide a method for predicting which group a new object would most likely fall into by using the developed function of known quantitative measurements [51,52].

In the current study, a computer statistical analysis tool, *StatGraphics Plus 2.0* was used for both cluster and discriminant analyses. With no presumed cut-off value, the drilled holes were classified into either "unacceptable" or "acceptable" groups using cluster analysis. After the drilled holes had been characterized as "acceptable" or "unacceptable," discriminant analysis was conducted to use AE parameters to build a discriminant model for the allocation of new drilled holes to previously defined groups for future use.

Two grouping considerations were involved in the current study. At first, the drilled holes were characterized into the two groups, "acceptable" and "unacceptable", by considering all four hole-quality measurements in conjunction as a four-dimensional space. The drilled holes which were spatially close to each other

were characterized into one group. With respect to grouping, "Acceptable" simply meant that the holes in this group, in general, had smaller quality errors; "Unacceptable" meant that the quality measurements (straightness, perpendicularity, and roundness errors) of the holes in this group were over a certain limit.

After holes were characterized into the two groups by considering all four hole-quality measurements, forward-stepwise discriminant analysis was used to select the significant AE parameter variables which could be used to select the best discriminant model for further prediction. The results of grouping, prediction, and the degree of accuracy for the classifications are presented in section 7.6.1.

Since a four-dimensional space is invisible, the drilled holes were again characterized into two groups by considering only one hole quality measurement at a time. After the drilled holes were grouped, forward-stepwise discriminant analysis was used to select the significant AE parameter variable to find the best discriminant model for further prediction. The results of grouping, prediction, and the degree of accuracy are presented in section 7.6.2. However, most of the discriminant models obtained in the previous section, 7.6.1 and 7.6.2, involve several AE parameters. The discriminant function graphically describes the differential features of objects in two or more dimensions. As the dimensions increased, it was more difficult to imagine the relationship between the objects and explanatory variables. Therefore, in section 7.6.3, with help of a plot for each quality measurement versus individual AE parameters, the attempt to use a single AE parameter to categorize a single quality measurement is discussed.

7.6.1 Grouping All Four Quality Measurements

Using cluster analysis and considering all four quality measurements together, the drilled holes were characterized into the two groups, "acceptable" and "unacceptable". The results of cluster analysis from *StatGraphics Plus 2.0* show that there is the most similarity among the 16 holes drilled before 480 holes were finished and that the remaining 4 holes drilled after 480 holes were finished are more similar to each other. Therefore, the 16 holes drilled before 480 holes were finished were classified as "acceptable" and the 4 holes drilled after 480 holes were finished were classified as "unacceptable." The discriminant model generated and used to classify the drilled holes, is as follows [51,52]:

$$DFS\{hole\} = -9.3791 + 4.50243*B3 + 2.03014*K\ .$$

This equation gives each drilled hole a discriminant function value by substituting AE energy embedded in frequency band#3 and the Kurtosis of the hole into it. If the discriminant function value of one drilled hole was larger than zero the hole was characterized as an unacceptable hole. On the other hand, if the discriminant function value of one drilled hole was negative when the Kurtosis and AE energy embedded in frequency band#3 were substituted into the above equation, this hole was characterized as an acceptable hole. The results of using the derived discriminant functions to classify all drilled holes show that among the 18 drilled holes, 100% were correctly classified.

7.6.2 Grouping One Quality Measurement At a Time

The above section describes the characterization of drilled holes for the current study by considering all four quality measurements. However, it is beneficial to know the condition of each quality measurement for one drilled hole after the hole is characterized as either an unacceptable hole or an acceptable hole. In this part of the study, each drilled hole was characterized by considering only one quality measurement at a time. The main consideration here was whether the "unacceptable" group according to only one of the four quality measurements was also found to be "unacceptable" when considering to four quality measurements.

The results of cluster analysis based on straightness measurements alone are shown in Figure 7.8, arranged by the number of clusters. For example, Figure 7.8b is a plot of the drilled holes divided into three clusters. An examination of the plots shows that cluster 3 in Figure 7.8.b and cluster 4 in Figure 7.8.c have the same drilled holes as members. Therefore, these five drilled holes were included in the "unacceptable" group, including all four holes chategorized as "unacceptable" based on four quality measurements. Therefore, characterized by hole straightness errors, five holes were defined as "unacceptable" and the other 15 as "acceptable." By using *StatGraphics Plus 2.0*, the forward-stepwise discriminant analysis with the provisional variables, either the AE parameters or all variables found to be significantly associated with hole straightness measurement in the previous regression analysis, was conducted and gave the best discriminant model as follows [51,52]:

$$\text{DFS } \{\text{hole}\} = -86.5086 + 0.35532*B2 + 3.28602*B3 - 1.21314*A \ .$$

(a)

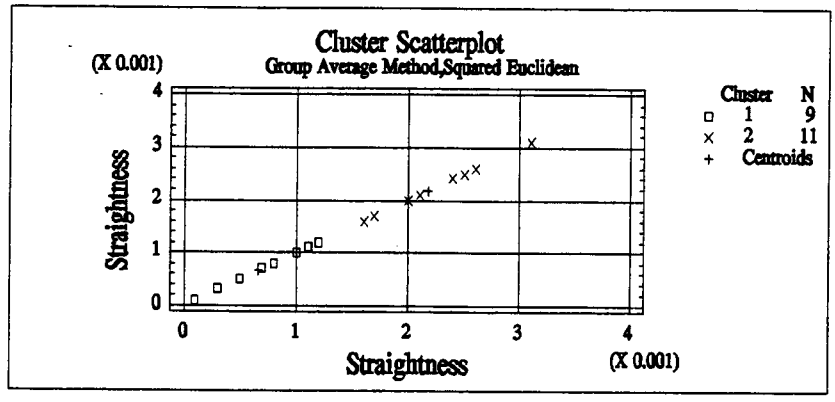

(b)

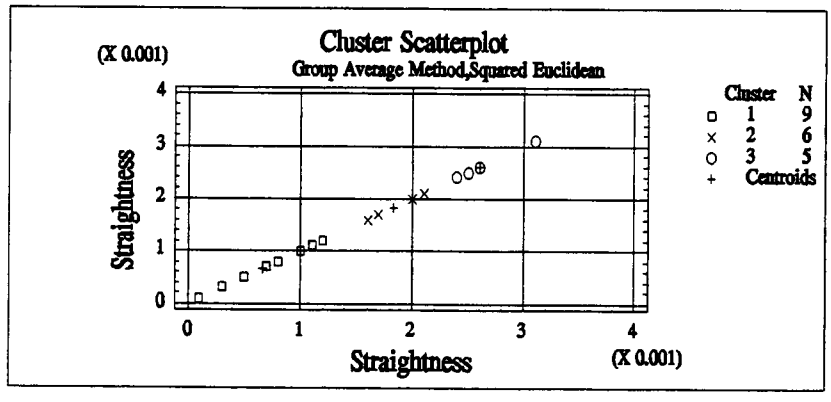

(c)

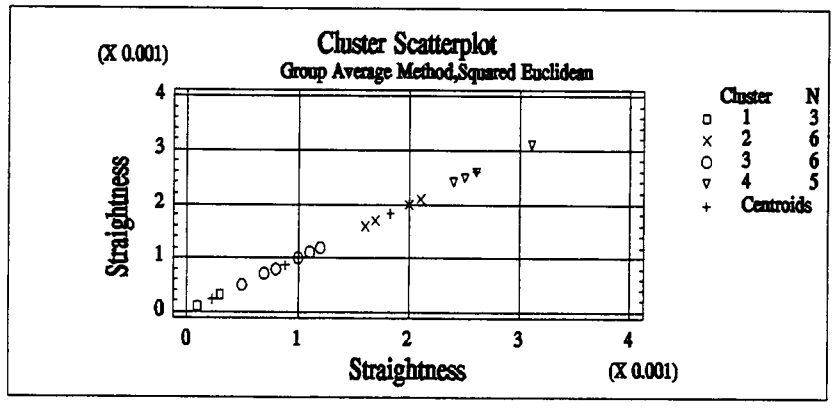

Figure 7.8 Cluster analysis plots for the straightness of drilled holes, (a) with two clusters, (b) with three clusters, and (c) with four clusters.

The results of using the derived discriminant functions to classify all drilled holes show that among the 20 drilled holes, 100% were correctly classified.

The results of using cluster analysis with perpendicularity as the similarity criterion are shown in Figure 7.9. Examining the plots, the three holes in cluster 2 in Figure 7.9.a, in cluster 3 in Figure 7.9.b, and in the combination of clusters 3 and 4 in Figure 7.9.c seem to be distinct from the other 17 holes. Besides, all three holes are also members of the "unacceptable" group chosen when considering all four quality measurements. Therefore, characterized by hole perpendicularity error, these three holes are defined as "unacceptable" and the remaining 17 holes are defined as "acceptable." Again, through forward-stepwise discriminant analysis with the provisional variables, either the AE parameters or all the variables found to be significantly associated with hole perpendicularity measurement in the previous regression analysis, the best discriminant model was derived as:

$$\text{DFS } \{\text{hole}\} = -4.2637 - 2.16955\mathbf{B2} + 7.91347\mathbf{B3} + 0.228751\mathbf{B3}^3 + 32.0538\mathbf{B4}^2.$$

The results of using the derived discriminant functions to classify all of the drilled holes show that among the 20 drilled holes, 100% were correctly classified.

The plots in Figure 7.10 show the results of cluster analysis according to roundness error. From the plots we see that whether divided into two, three, or four clusters, the group of three holes (cluster 2, 3 or 4 in Fig 7.10a-c, respectively) which have the highest roundness values is distinct from the others. Upon further examination of the comparison between the "unacceptable" group chosen according to all four quality measurements and the current group also shows that they have

(a)

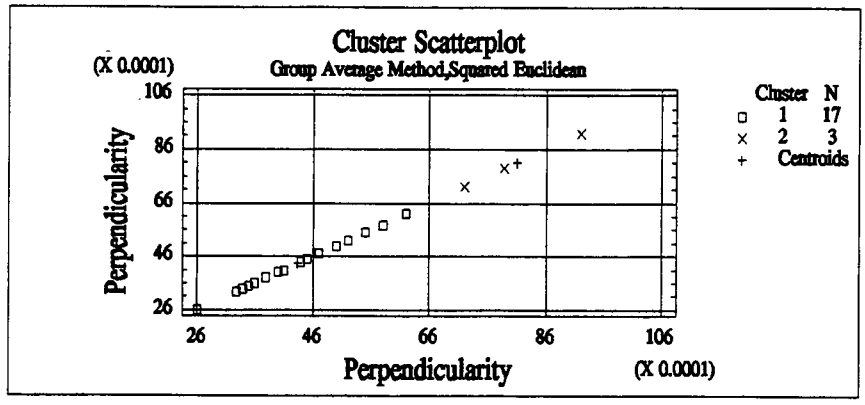

(b)

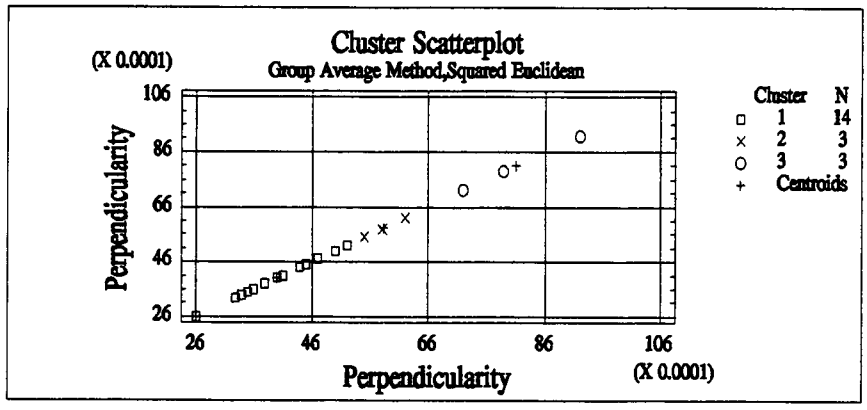

(c)

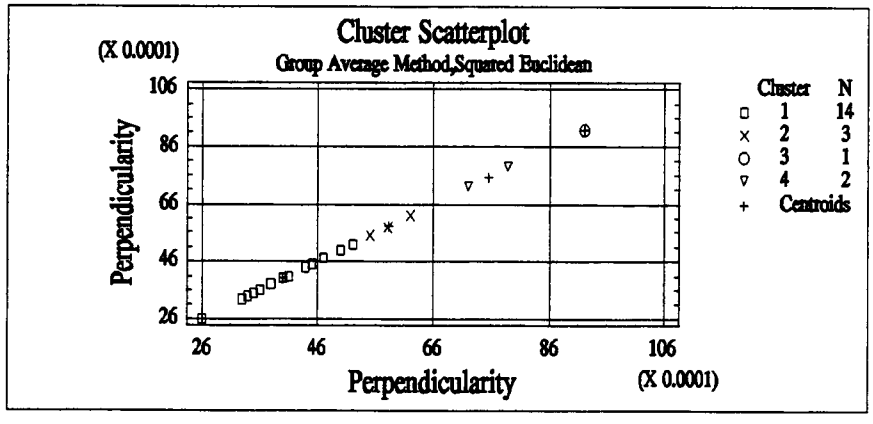

Figure 7.9 Cluster analysis plots for the perpendicularity of drilling holes, (a) with two clusters, (b) with three clusters, and (c) with four clusters.

(a)

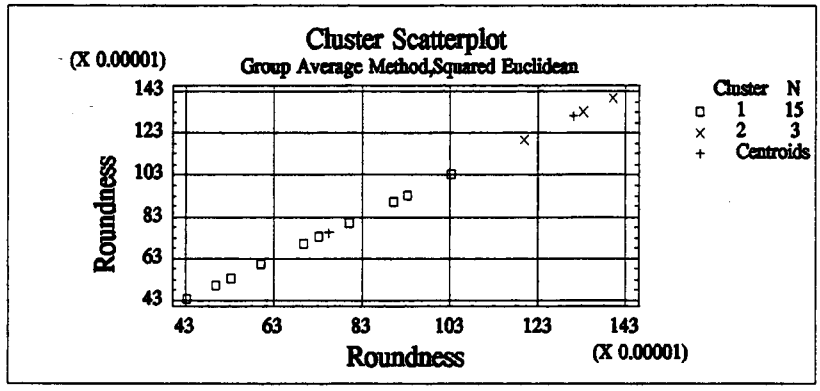

(b)

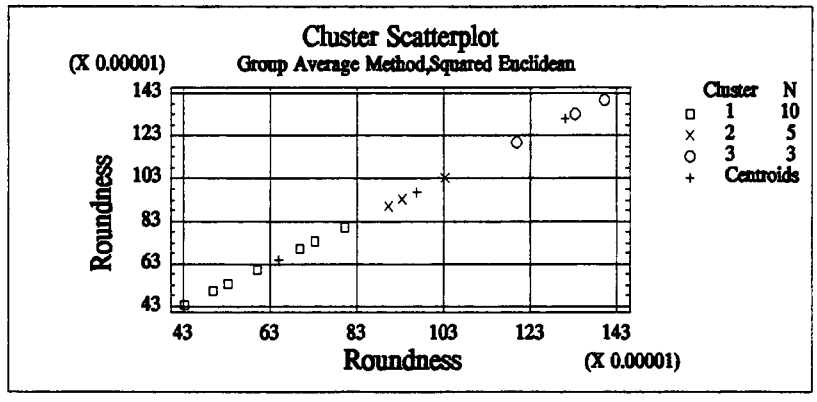

(c)

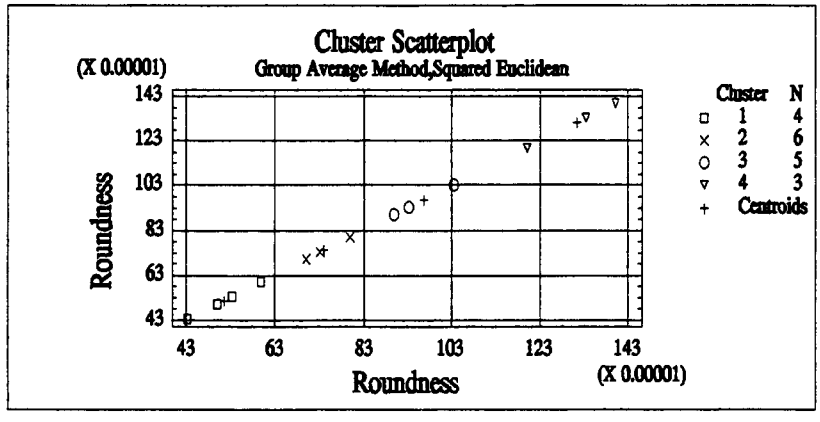

Figure 7.10 Cluster analysis plots of roundness for drilled holes, (a) with two clusters, (b) with three clusters, and (c) with four clusters.

three identical members. Therefore, characterized by hole roundness error, these three holes were defined as "unacceptable" and the other 15 holes were defined as "acceptable." Likewise, through forward-stepwise discriminant analysis with those significant variables chosen as provisional variables (B1, $B1^2$, B2, B3, B4, A, A^3, V, V^3, S, S^3, K and K3), the best discriminant model was derived as:

$$\text{DFS } \{\text{hole}\} = -2.09405 + 5.23659\mathbf{B4} \, .$$

The results of using the derived discriminant functions to classify all the drilled holes show that 2 out of the 3 drilled holes in the "unacceptable" group and 13 out of the 15 drilled holes in the "acceptable" group were correctly classified. It means that among the 18 holes, 15 holes could be correctly classified by this discriminant model. The percentage of cases correctly classified is 83%.

The plots in Figure 7.11 show the results of cluster analysis considering only diameter measurement as the similarity criterion. The plots, Figure 7.11a, show that the cluster presented as "x" consisted of 7 holes and was distinct from the rest of the holes. Considering the match between the group chosen as "unacceptable" according to only one quality measurement and the "unacceptable" group chosen according to four quality measurements together, the cluster, "□," in Figure 7.11a was further divided to sort out the similarity. As shown in Figure 7.11b, we further divided the rest of the 11 holes into two different clusters. The cluster presented as "o" which consisted of two holes was separated from the others. Further examination of the comparison between this group and the "unacceptable" group chosen according to all four quality measurements shows that they had only one shared member. This suggested that some drilled holes which are members of the

(a)

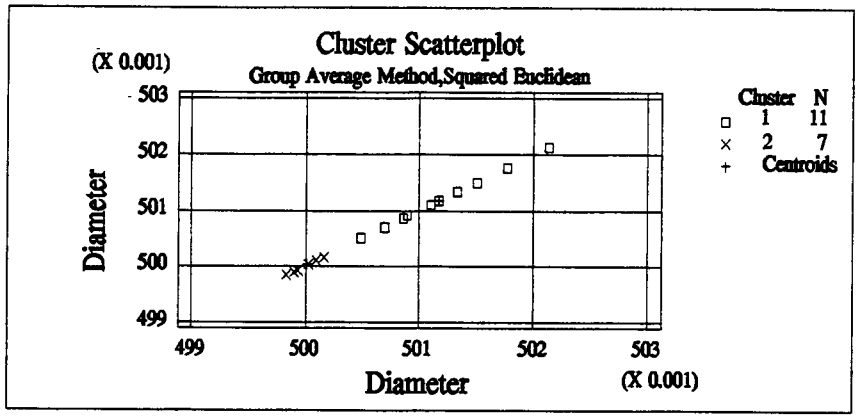

(b)

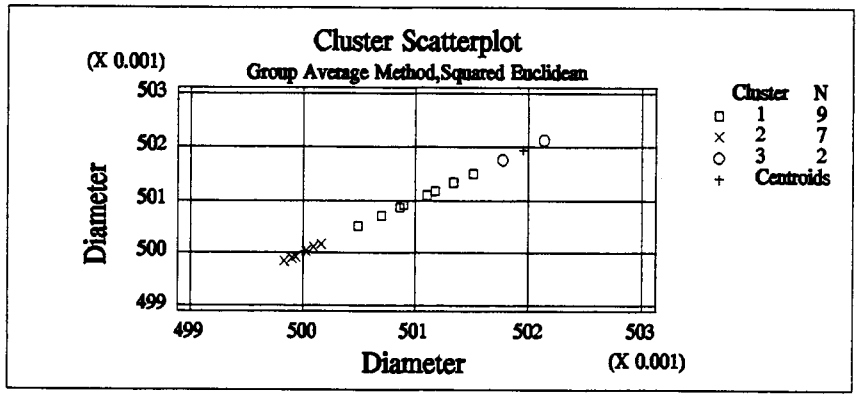

(c)

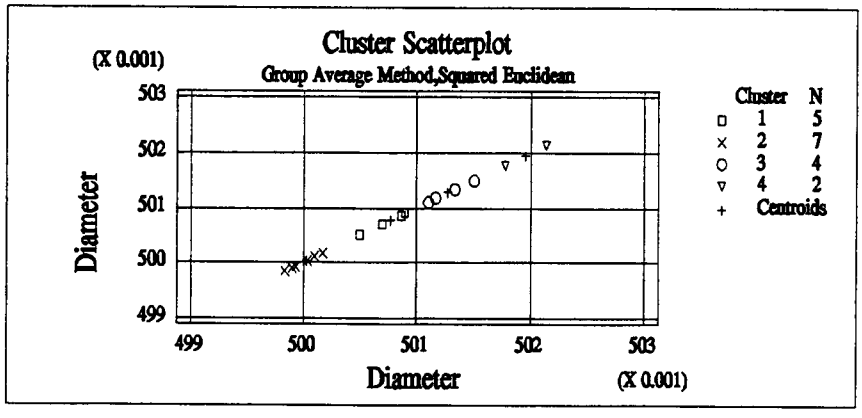

Figure 7.11 Cluster analysis plots for diameter of drilled holes, (a) with two clusters, (b) with three clusters, and (c) with four clusters.

"unacceptable" group chosen according to all four quality measurements needed to be adopted into the current group. Therefore, further small clusters presented as "o" and "□" in Figure 7.11c were obtained. The four drilled holes presented as cluster "o" and the two drilled holes presented as the cluster "∇ " in Figure 7.11c were combined in the "unacceptable" group. This combined result shows that among these six holes of this group, four holes were shared with the "unacceptable" group chosen when considering all four quality measurements, and hence the comparison check was satisfied. The forward-stepwise discriminant analysis with those significant variables chosen as provisional variables gave the best discriminant model as:

$$\text{DFS } \{\text{hole}\} = -19.439 + 3.72316\mathbf{B3} + 10.9006\mathbf{S} \ .$$

The results of using the derived discriminant functions to classify all the drilled holes show that 5 holes out of the 6 holes in the "unacceptable" group and 11 out of the 12 holes in the "acceptable" group were correctly classified. This means that among the 18 holes, 16 holes could be correctly classified using this discriminant model. The percent of cases correctly classified was 89%.

7.6.3 Quality Measurement Categorization for a Single AE Parameter

The discriminant analysis discussed in the previous section gives good results for predicting drilled hole categorical information. However, most of the discriminant models obtained in the previous section graphically describe the differential features of objects in two or more dimensions. As the dimensions increase, it

becomes more difficult to imagine the relationship between the objects and the explanatory variables. In this section, with the help of plots for each quality measurement versus individual AE parameters, the attempt to use a single AE parameter to categorize single quality measurement is discussed. Examples of this attempt are given by using each AE parameter to categorize hole straightness errors. The groups defined in the previous section are also used here.

Figure 7.12 shows of the straightness error plots of drilled holes versus different AE parameters; thus, Figure 7.12a is the straightness error plot versus the AE energy embedded in the first frequency band. Different from the regression model derived from section 7.5.1, the solid line in each plot represents the curve fitting model from a third-order polynomial function. The same horizonal line in each plot divided the straightness error into two groups. The holes with a straightness error under the line are categorized as "acceptable." The holes with a straightness error over the line were categorized as "unacceptable." The cut-off value, 0.0022, of the horizonal line was set as the average of the centroids of two subclusters which have about the same size of spread. The two subclusters were the "unacceptable" group and the "acceptable" group, i.e., clusters 4 and 2 in Figure 7.8c, respectively. Moreover, another perpendicular line was incorporated into each plot. This perpendicular line is located at the values equal to the intersection point of the horizonal line and the fitted polynomial line. The perpendicular lines in the plots of Figure 7.12a-h are located at B1=227, B2=10.2, B3=1.91, B4=0.525, A= -62.85, V=143, S=1.03 and K=0.525, respectively. Since the hole-straightness error is not measurable on-line, each of these values is treated as the boundary which

(a)

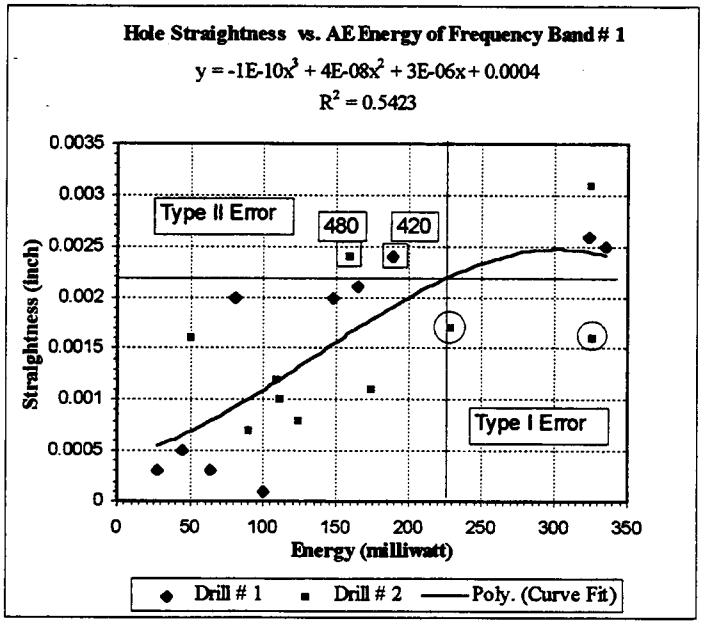

(b)

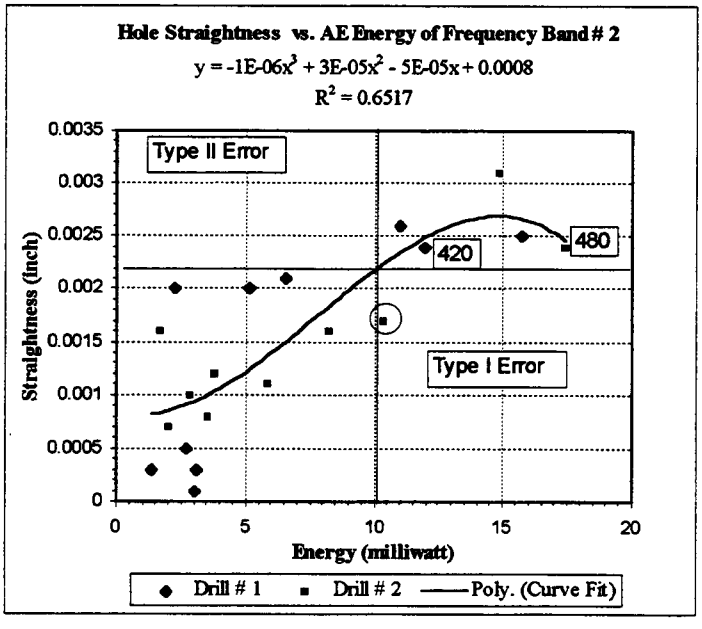

Figure 7.12 Schematic characterization of drilled-hole acceptable and unacceptable groups using different AE parameters to predict straightness measurements: (a) AE energy embedded in frequency band #1, (b) AE energy embedded in frequency band #2.

(c)

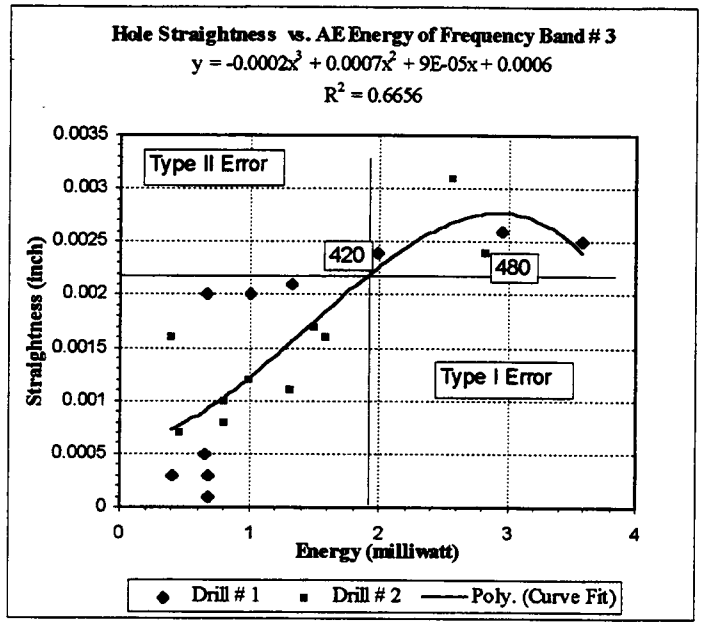

(d)

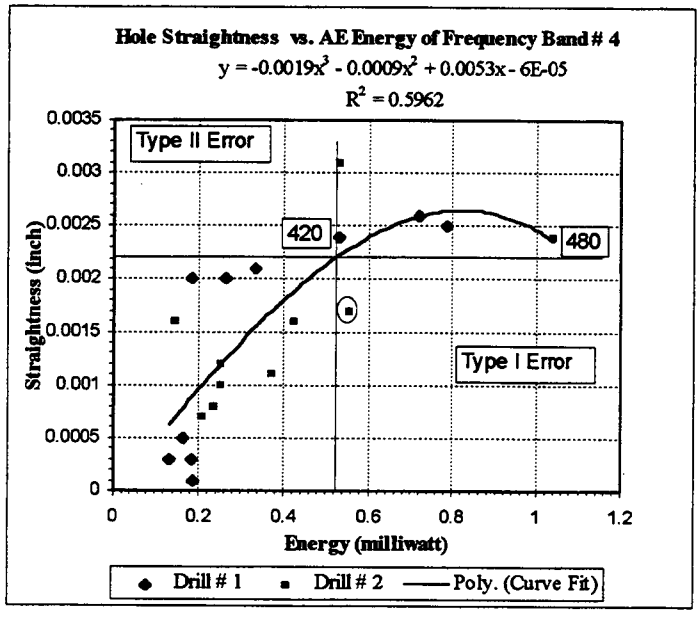

Figure 7.12 (Continued) (c) AE energy embedded in frequency band #3, (d) AE energy embedded in frequency band #4.

(e)

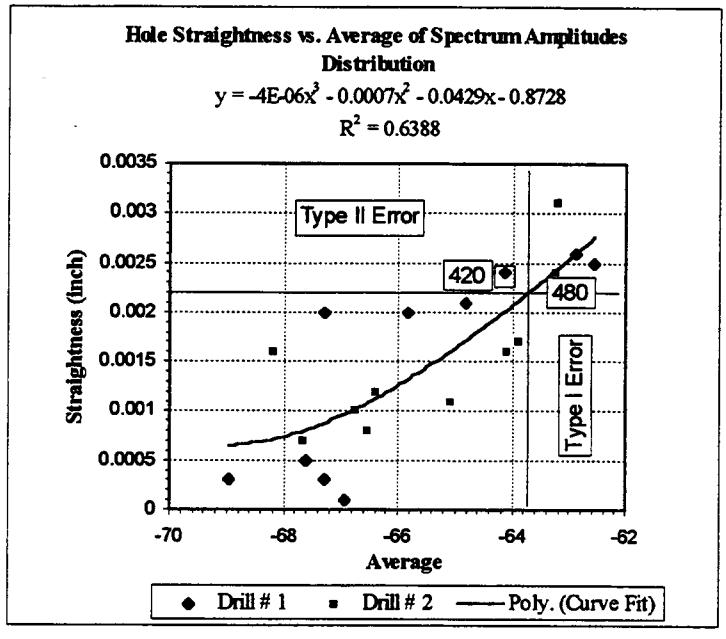

(f)

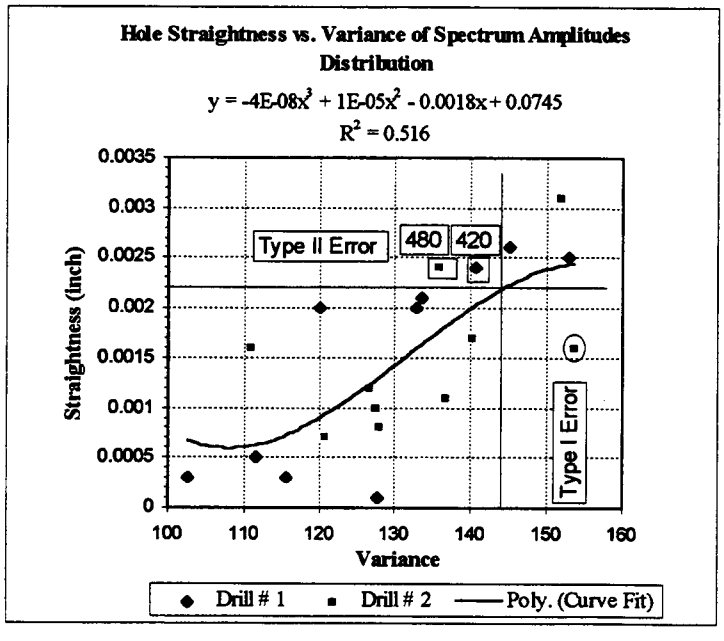

Figure 7.12 (Continued) (e) average of AE spectrum amplitudes for first-order moments, (f) variance among AE spectrum amplitudes for second-order moments.

(g)

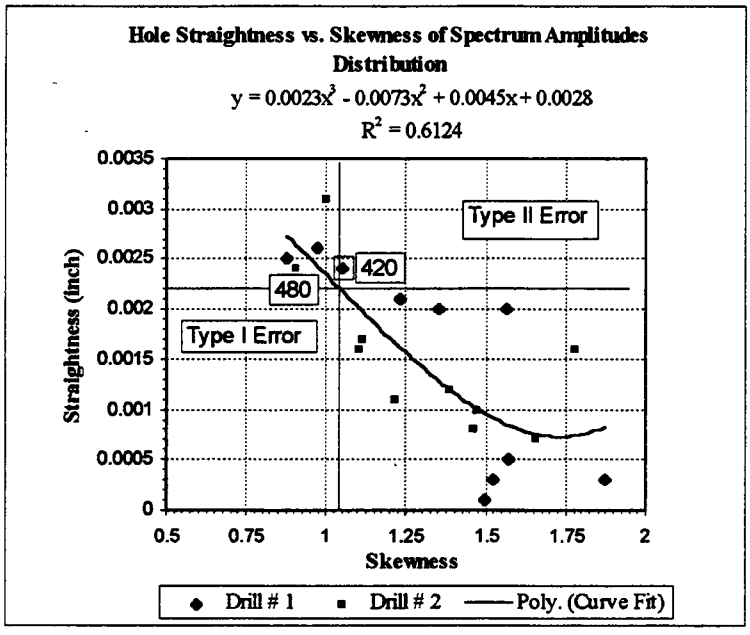

(h)

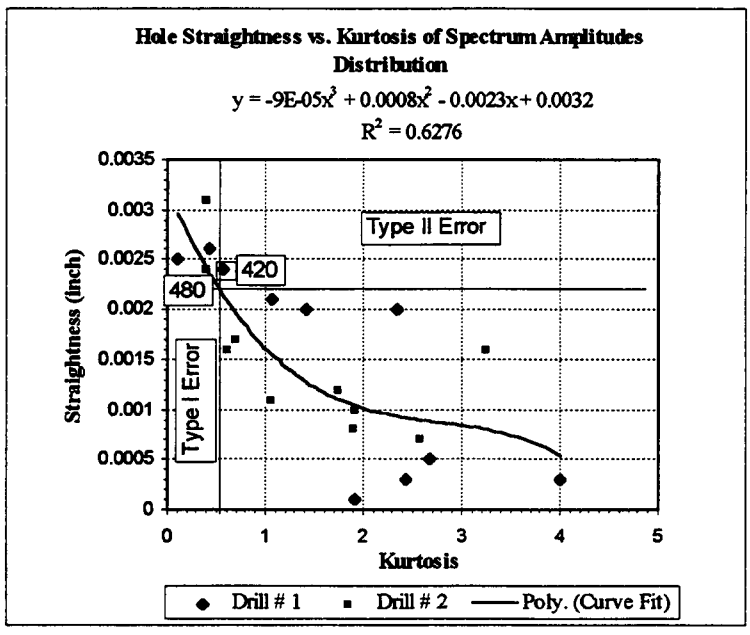

Figure 7.12 (Continued) (g) skewness of AE spectrum amplitudes for third-order moments, (h) kurtosis of AE spectrum amplitudes for fourth-order moments.

separates the acceptable straightness error and the unacceptable straightness error for a drilled hole. A hole with the AE parameter measurement larger or less than the value (larger or less chosen based on different AE parameters) was characterized as an unacceptable hole, which means the straightness error was over the cutoff value. Conversely, a hole with AE parameter measurement less or larger than these values was characterized as an acceptable hole. The horizonal line and the perpendicular line divide the each plot area into four small areas which represent the different categories. The four categories are "unacceptable holes", "acceptable holes", "type I error" and "type II error." The "unacceptable holes" category represent drilled holes which are not acceptable because the straightness error is over the cut-off. The "acceptable holes" category represents drilled holes which are acceptable because the straightness error was under the cut-off value. In a perfect condition, there are no holes located in the areas of "type I error" and "type II error." These terms refer to different types of predicting errors. The error types are dependent on the location of the hole. Type I errors occur when a hole is predicted as acceptable but it turns out to be unacceptable. Type II errors occur when a hole is predicted as unacceptable but turns out to be acceptable.

From these plots, information and control algorithms could be provided. An application example using Figure 7.12c is: If the band#3 energy is larger than 1.91 milliwatt, the drilled hole is unacceptable (straightness error is larger than 0.0022); or: If the band#1 energy is less than 1.91 milliwatt, the drilled hole is acceptable (straightness error is less than 0.0022). Moreover, since drill wear is the only variation of the drilling process in the current study, the information and control algor-

ithm could also be provided as "If the band#3 energy is larger than 1.91 milliwatt, the drill bit should be changed" or "If the band#1 energy is less than 1.91 milliwatt, the drill bit can continue to be used." The evaluation of this algorithm shows that among these, 5 holes were assigned as unacceptable holes, 5 holes or 100% were correctly predicted using band#3 energy. Neither type I error nor type II errors occurred. However, by using band#1 energy for the prediction, among the 5 holes assigned as unacceptable holes, only 3 holes or 60% were correctly predicted. Two type II errors occurred. This means that by using the same algorithm, these two holes were predicted as good holes and the drill bit could still be used but the actual straightness errors of drilled holes was not acceptable and the drill bit should have been changed. There are also two type I errors. This means that, by using the same algorithm, these two holes were predicted as bad holes and the drill bit should have been changed but it turned out that the actual straightness error of the drilled holes was acceptable and the drill bit could still have been used.

For a single drilled hole, as in the above discussion, using different AE parameters may result in different conclusions for that hole. In the present circumstance, a different weight was assigned to each AE parameter. It presents the probability of using this AE parameter to predict the status of a drilled hole correctly, i.e. evaluation of the current conclusion. Since the R^2 value suggests how successful the chosen model was in relating the quality measurement to the AE parameter, the R^2 value of each chosen model was assigned to be the weight of the probability to each AE parameter. Three rules were developed in the current study to combine all eight AE parameters for predicting a drilled-hole group membership and

for assigning the weight to the predicted conclusion. The rules for assigning a weight to a final prediction for a drilled hole are as follows:

Rule 1: The positive weight is assigned to the prediction that concludes the hole is a bad hole. The negative weight is assigned to the prediction that concludes the hole is a good hole.

Rule 2: **If**
{the conclusions for a single hole given by using each AE parameter are all the same}

Then
{the maximum R^2 value among these R^2 values will be the weight assigned to the conclusion}.

Rule 3: **If**
{one of the conclusions for a single hole given by using each AE parameter is different from others}

Then
{the average of the weights of predictions made from all AE parameters will be the final weight assigned to the final conclusion}.

An example of using these rules is given for the hole marked by " " in Figure 7.12a, which is the 480th hole drilled by drill#2. From the band#1 energy, the prediction is that the hole is acceptable and -0.5423 is assigned to be the weight of this conclusion. From the band#2 energy, the prediction is that the hole is not acceptable and 0.6517 is assigned to be the weight of this conclusion. Using the same rules, the conclusions given by all eight AE parameters and the final conclusion and its weight are given in Table 7.5.

Therefore, the final prediction from the AE parameters will be "with weight 0.33, the hole is not acceptable and a new drill bit should be used." Comparing to the actual straightness measurement of this hole, 0.0024, which is greater than 0.0022, the final prediction was correct.

Table 7.5 Hole straightness error prediction through all AE parameters for hole # 480 drilled by drill # 2

The Hole Straightness error Prediction For Hole # 480 Drilled by Drill # 2		
AE Parameter	Prediction	Weight
Band#1 Energy (B1)	Acceptable	-0.5423
Band#2 Energy (B2)	Not Acceptable	0.6517
Band#3 Energy (B3)	Not Acceptable	0.6656
Band#4 Energy (B4)	Not Acceptable	0.5962
Average (A)	Not Acceptable	0.6388
Variance (V)	Acceptable	-0.516
Skewness (S)	Not Acceptable	0.6124
Kurtosis (K)	Not Acceptable	0.6176
Final Conclusion	Not Acceptable	0.328

Table 7.6 Hole straightness error prediction through all AE parameters for hole # 420 drilled by drill # 1

The Hole Straightness error Prediction For Hole # 420 Drilled by Drill # 1		
AE Parameter	Prediction	Weight
Band#1 Energy (B1)	Acceptable	-0.5423
Band#2 Energy (B2)	Not Acceptable	0.6517
Band#3 Energy (B3)	Not Acceptable	0.6656
Band#4 Energy (B4)	Not Acceptable	0.5962
Average (A)	Acceptable	-0.6388
Variance (V)	Acceptable	-0.516
Skewness (S)	Acceptable	-0.6124
Kurtosis (K)	Acceptable	-0.6176
Final Conclusion	Acceptable	-0.1392

Another example is given for the hole marked by "◈" in Figure 7.12a, which is the 420th hole drilled by drill#1. Using the same rules, the concluded results for each AE parameter and the final conclusion and weight are given in Table 7.6. The final prediction from those AE parameters will be "with weight 0.14, the hole is acceptable and a new drill bit will not be necessary." Comparing this to the the actual straightness measurement of this hole, 0.0024, which is greater than 0.0022, the final prediction was incorrect and a type II error occurred. However, since the weight for this final conclusion, 0.14, is quite low, the type II error should not be a big surprise.

Schematization of the characterization of drilled holes into "acceptable" and "unacceptable" groups, and the usage of different AE parameters to predict errors of perpendicularity, roundness and diameter of drilled holes are shown in Figures 7.13, 7.14, and 7.15, respectively. Similar to Figure 7.12, when a hole's quality measurement was larger than a cut-off value, the hole was characterized as unacceptable according to that quality measurement. The cut-off value for characterizing a hole as "unacceptable" varies for different quality measurements. For example, the cut-off values for perpendicularity, roundness and diameter were 0.0067, 0.00114 and 0.501 inches, respectively. For a specific quality measurement, after the cut-off value was decided, the boundary value of each AE parameter for that quality measurement could be decided. Then, each one of the eight AE parameters were used to predict to which group a drilled hole belongs with regard to specific hole quality error using the boundary value of the AE parameter. Type I and type II errors occurred occasionally. The boundary values for different AE parameters predicting

(a)

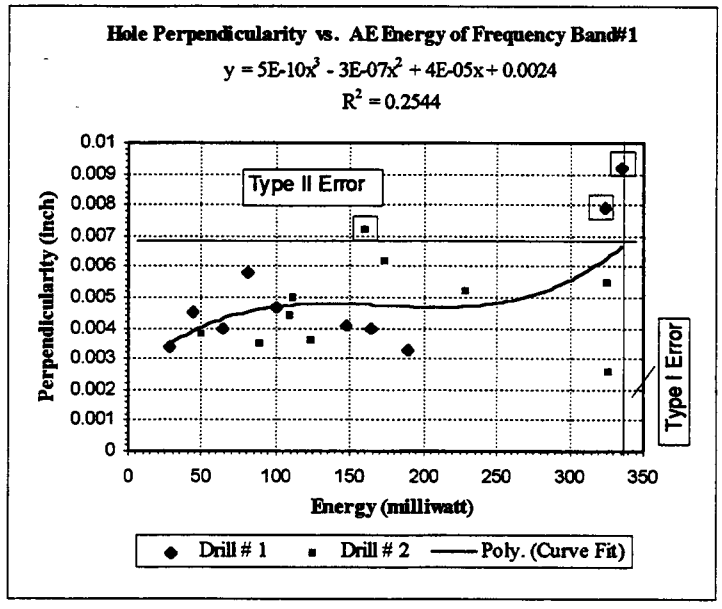

(b)

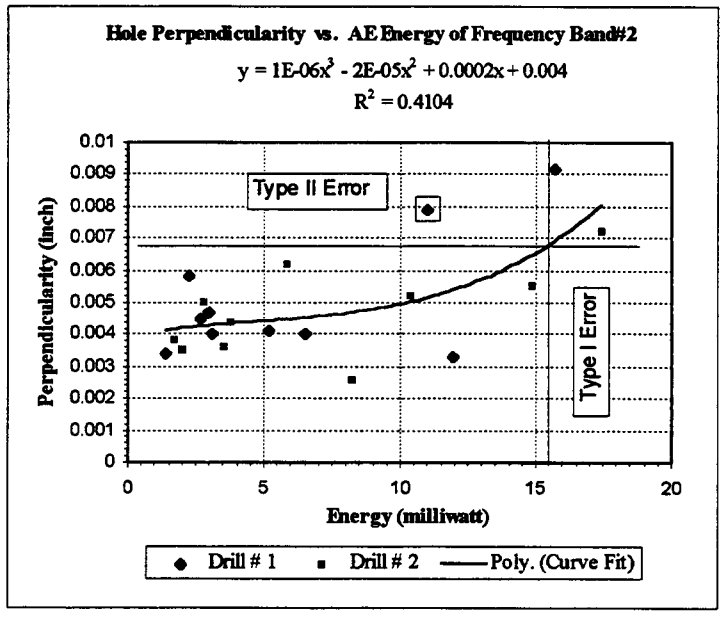

Figure 7.13 Schematic characterization of drilled-hole acceptable and unacceptable groups using different AE parameters to predict perpendicularity measurements: (a) AE energy embedded in frequency band #1, (b) AE energy embedded in frequency band #2.

(c)

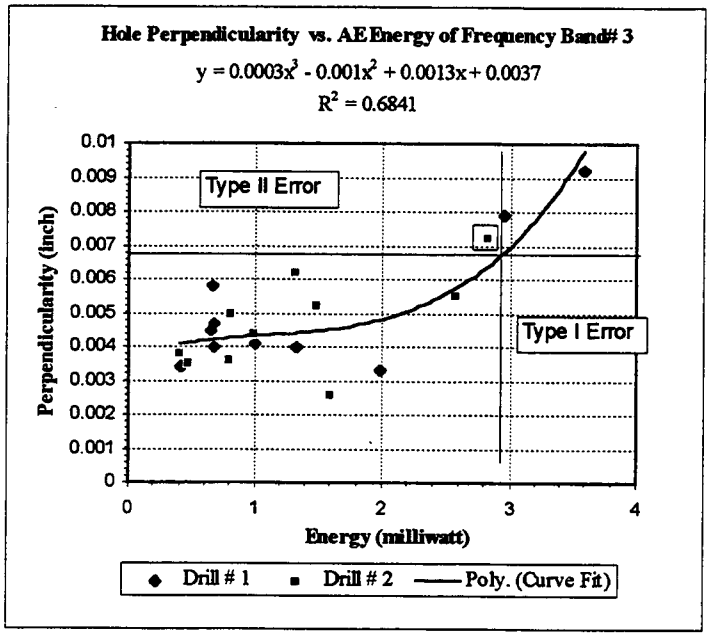

(d)

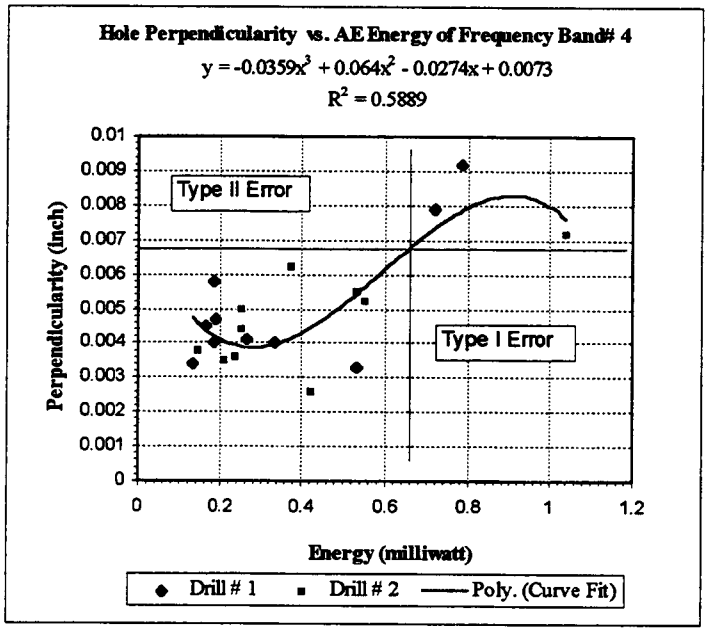

Figure 7.13 (Continued) (c) AE energy embedded in frequency band #3, (d) AE energy embedded in frequency band #4.

(e)

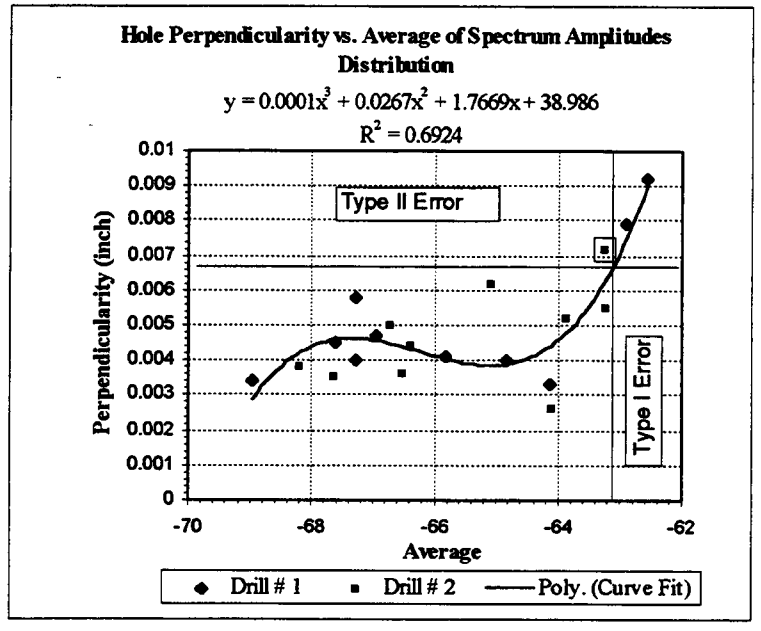

(f)

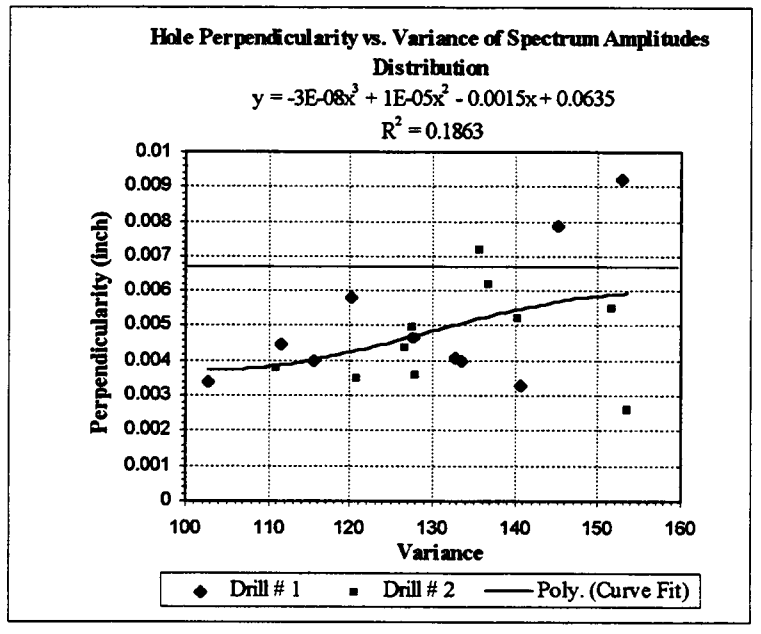

Figure 7.13 (Continued) (e) average of AE spectrum amplitudes for first-order moments, (f) variance among AE spectrum amplitudes for second-order moments.

(g)

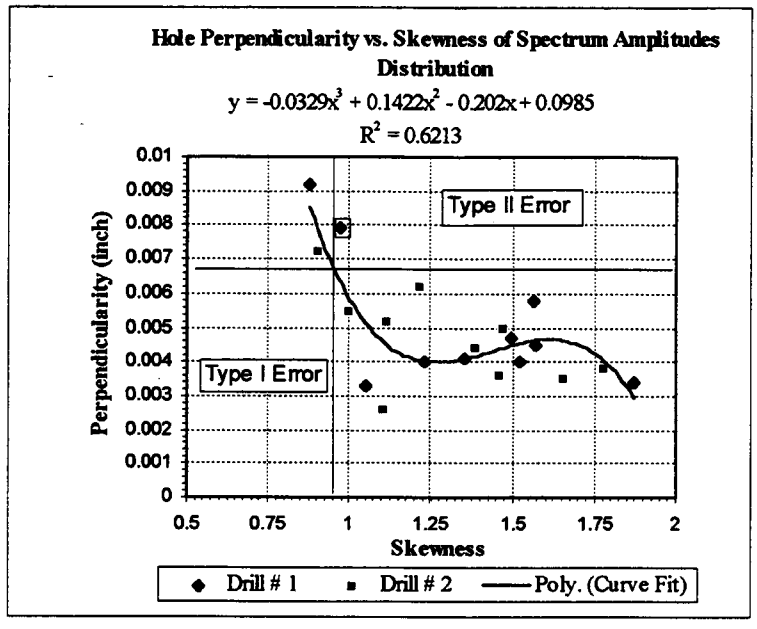

(h)

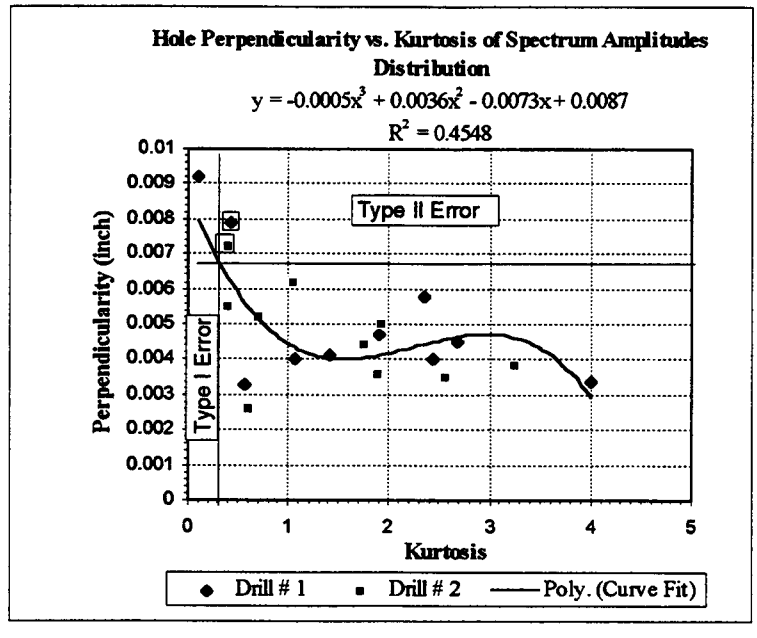

Figure 7.13 (Continued) (g) skewness of AE spectrum amplitudes for third-order moments, (h) kurtosis of AE spectrum amplitudes for fourth-order moments.

(a)

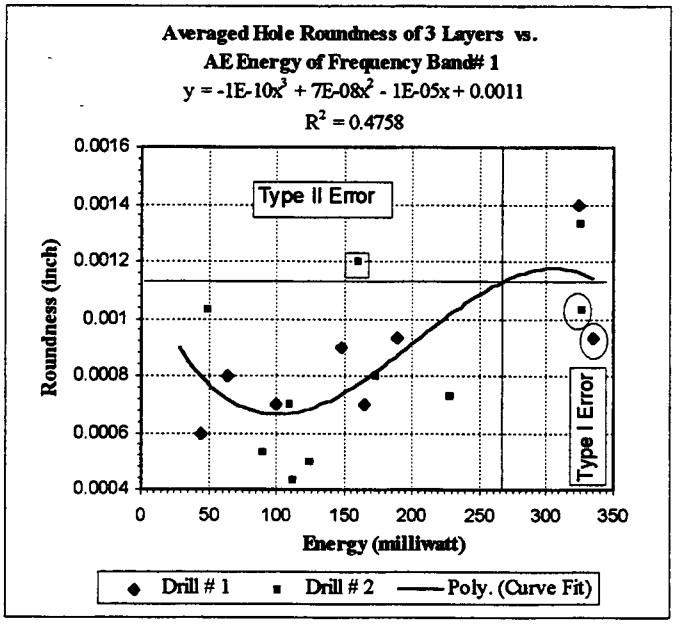

(b)

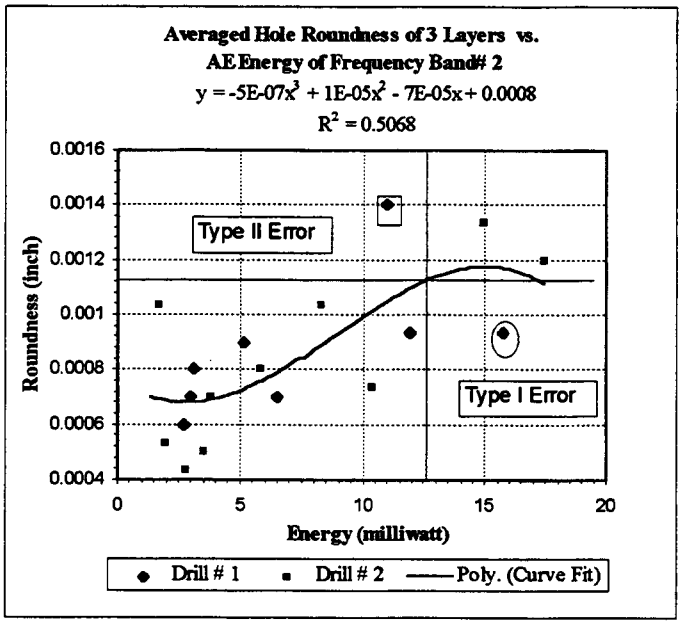

Figure 7.14 Schematic characterization of drilled-hole acceptable and unacceptable groups using different AE parameters to predict roundness measurements: (a) AE energy embedded in frequency band #1, (b) AE energy embedded in frequency band #2.

(c)

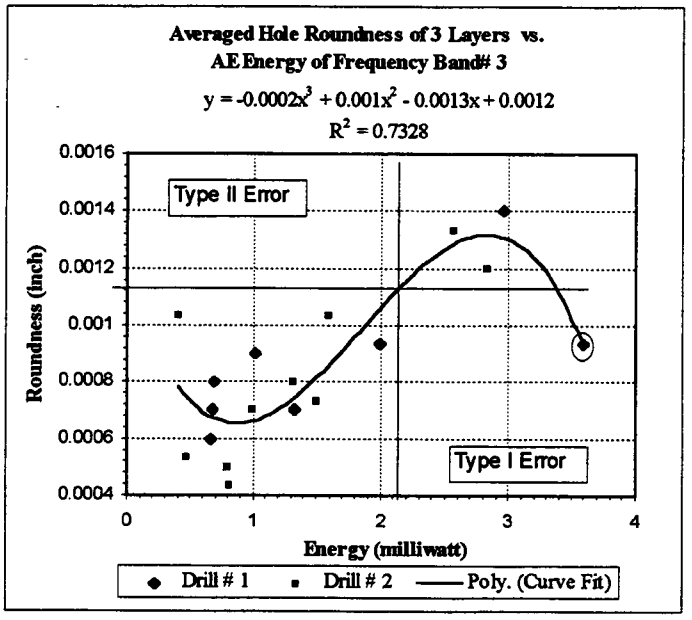

(d)

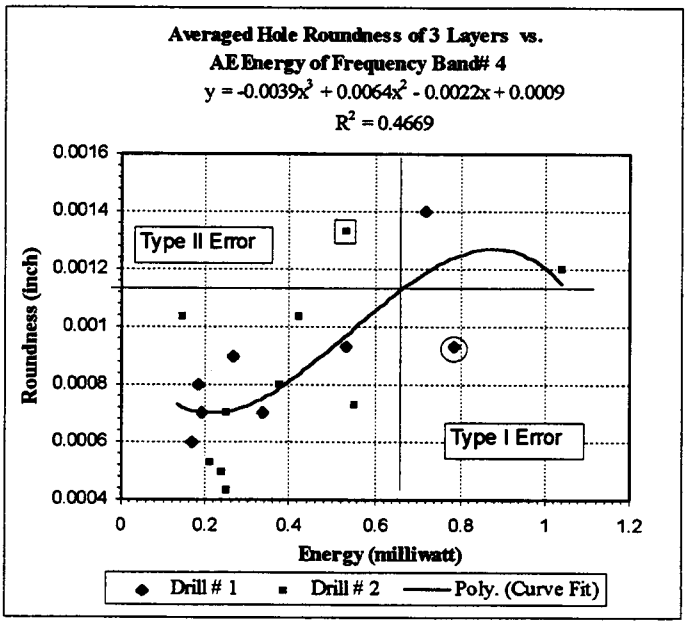

Figure 7.14 (Continued) (c) AE energy embedded in frequency band #3, (d) AE energy embedded in frequency band #4.

(e)

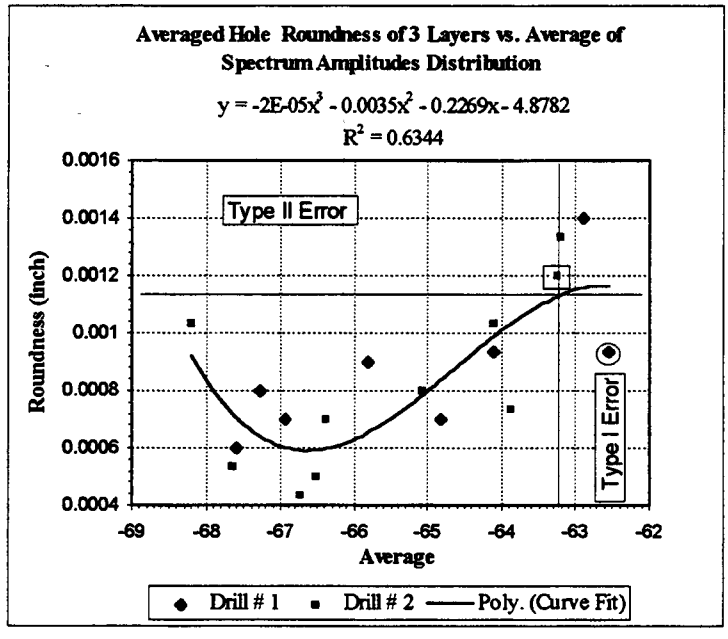

(f)

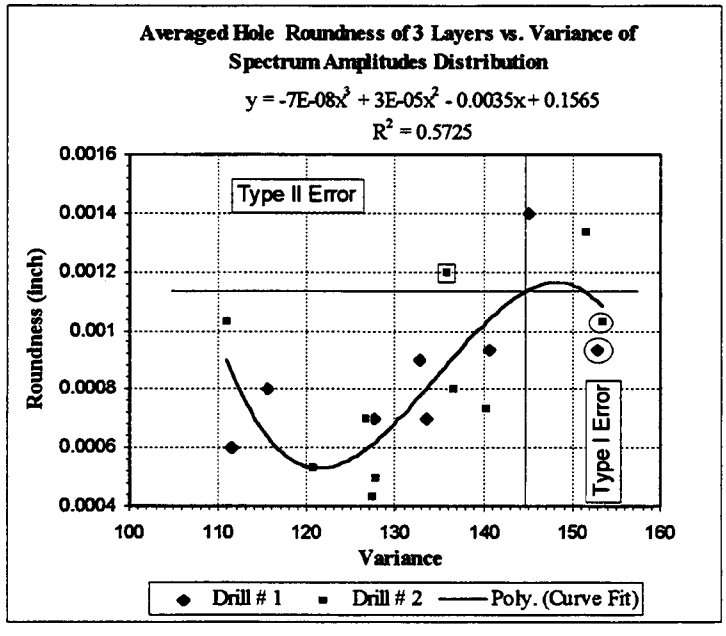

Figure 7.14 (Continued) (e) average of AE spectrum amplitudes for first-order moments, (f) variance among AE spectrum amplitudes for second-order moments.

(g)

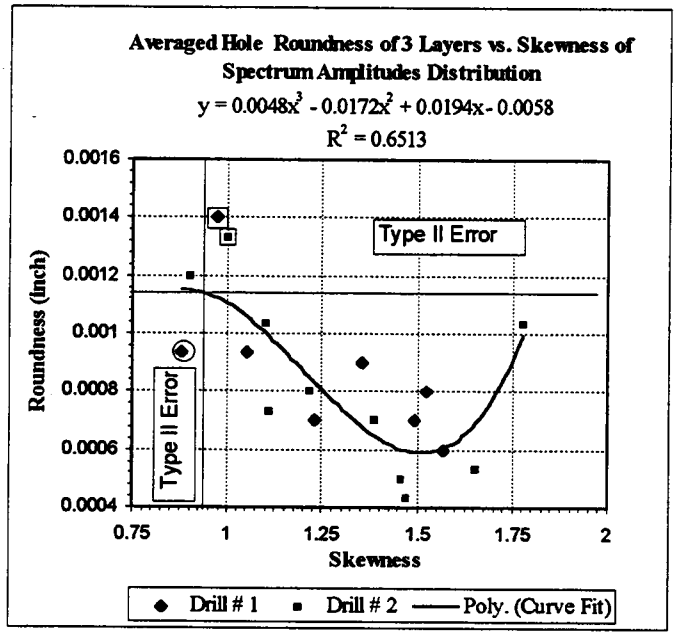

(h)

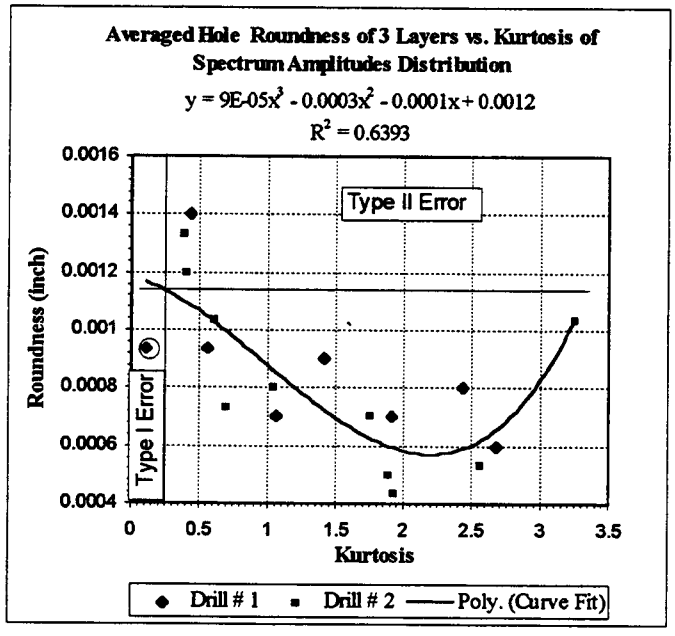

Figure 7.14 (Continued) (g) skewness of AE spectrum amplitudes for third-order moments, (h) kurtosis of AE spectrum amplitudes for fourth-order moments.

(a)

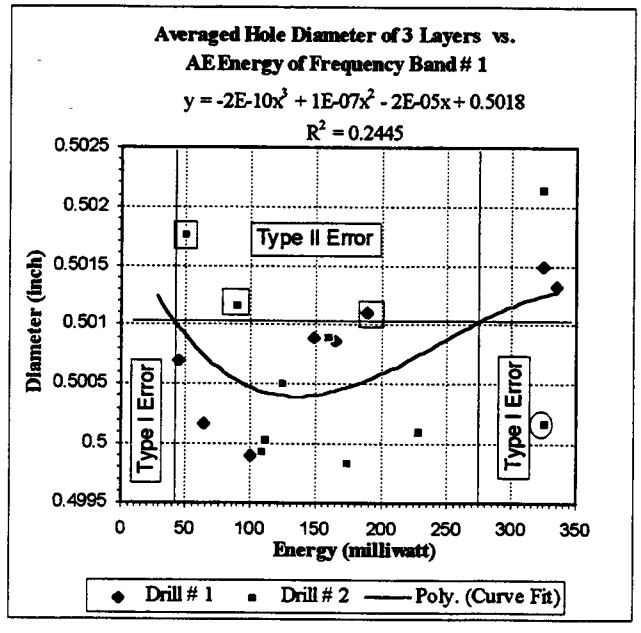

(b)

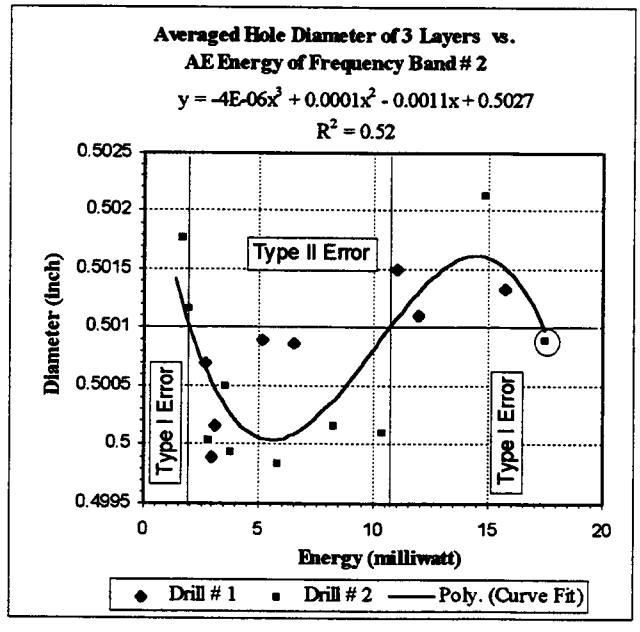

Figure 7.15 Schematic characterization of drilled-hole acceptable and unacceptable groups using different AE parameters to predict diameter measurements: (a) AE energy embedded in frequency band #1, (b) AE energy embedded in frequency band #2.

(c)

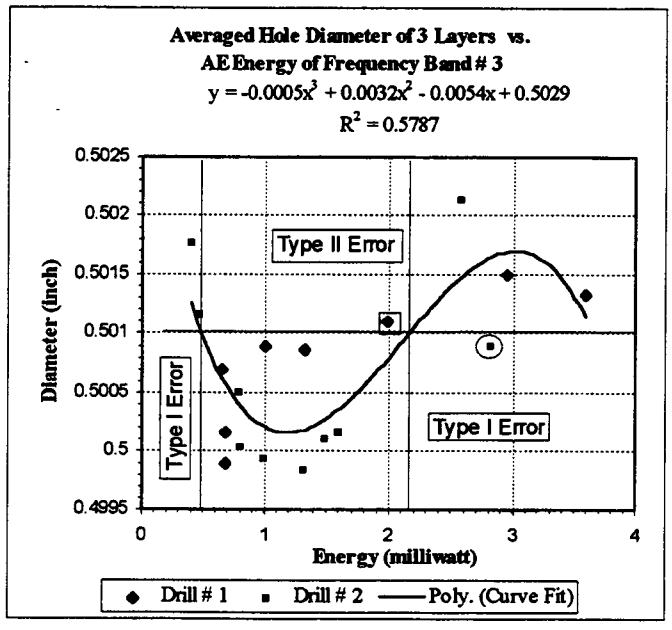

(d)

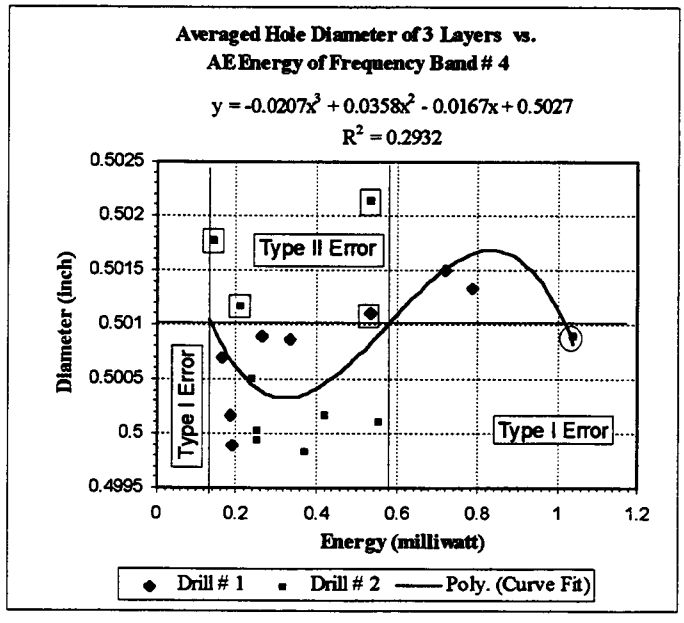

Figure 7.15 (Continued) (c) AE energy embedded in frequency band #3, (d) AE energy embedded in frequency band #4.

(e)

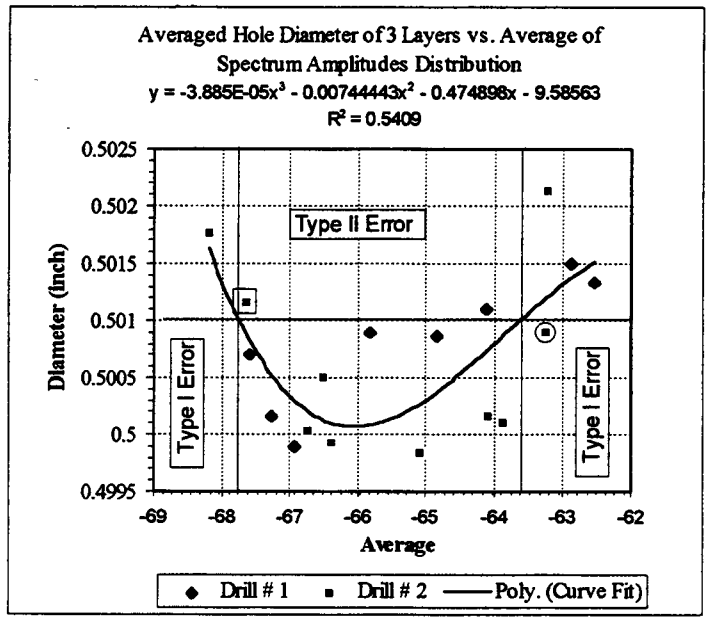

(f)

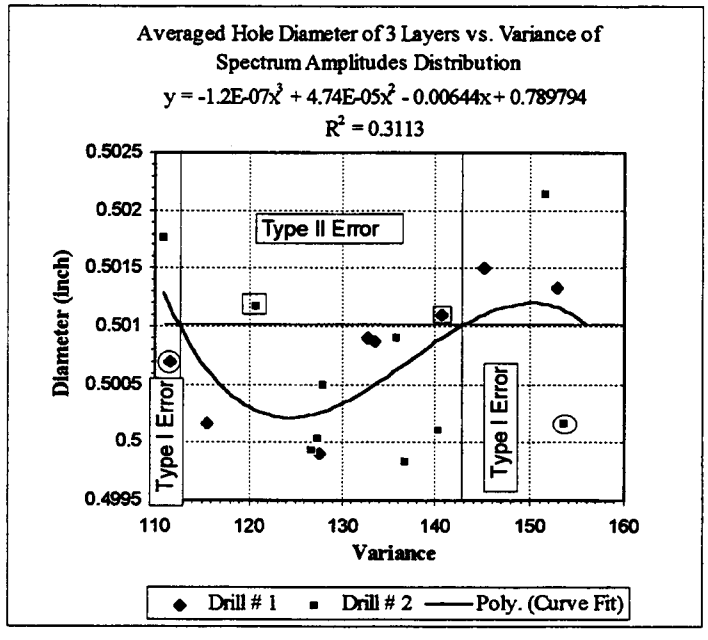

Figure 7.15 (Continued) (e) average of AE spectrum amplitudes for first-order moments, (f) variance among AE spectrum amplitudes for second-order moments.

(g)

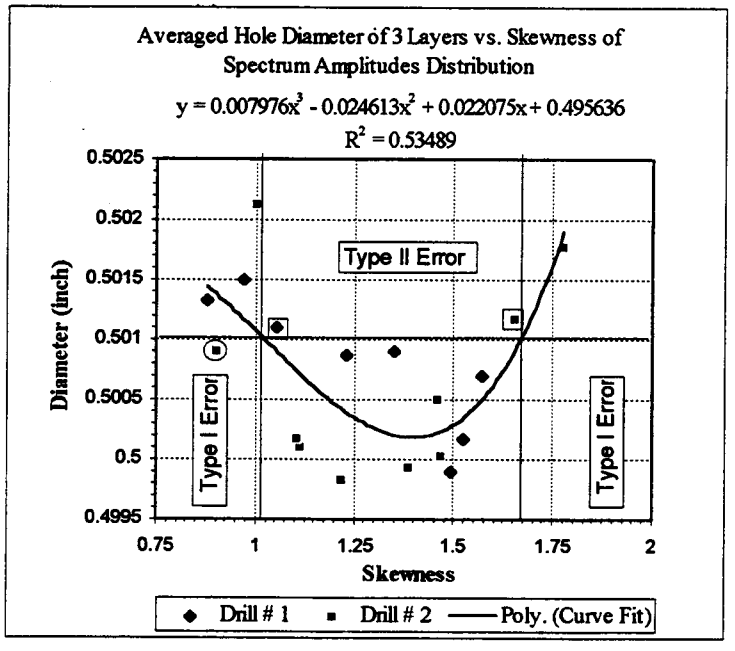

(h)

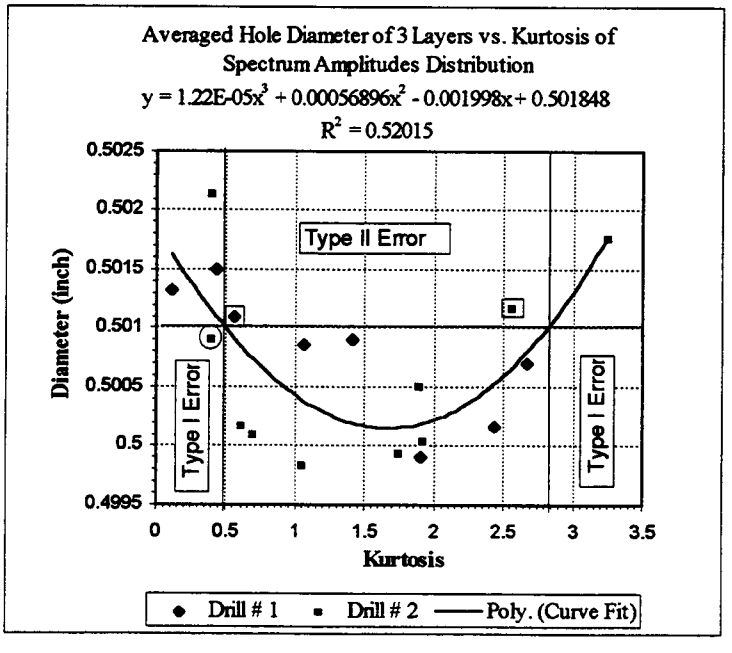

Figure 7.15 (Continued) (g) skewness of AE spectrum amplitudes for third-order moments, (h) kurtosis of AE spectrum amplitudes for fourth-order moments.

specific quality errors, the number of holes having been improperly predicted, and the types of errors occurring in the predictions are summarized below.

Examining the plots of perpendicularity error prediction in Figure 7.13, the plots in Figure 7.13a and 7.13f show that usage of AE parameters B1 and variance, V, may not be useful. In plots in Figure 7.13b-e,g-h, different boundary values are calculated for AE parameters, B2, B3, B4, A, S, and K for predicting group membership of a drilled hole according to perpendicularity error; these were 15.2, 2.9, 0.65, -63.1, 0.95, and 0.29 respectively. When the B2, B3, B4 and A of a drilled hole are larger than 15.5, 2.9, 0.65, and -63.1, respectively, the drilled hole is predicted to be unacceptable because the perpendicularity error is larger than 0.0067 inch. When the S and K of a drilled hole are smaller than 0.95 and 0.29, respectively, the drilled hole is predicted to be unacceptable, again because the perpendicularity error is larger than 0.0067 inch. By using these AE parameters to predict group membership of a drilled hole based on perpendicularity error, the numbers of type II prediction errors with respect to each AE parameter, B2, B3, B4, A, S, and K were 1, 1, 0, 1, 1, and 2. No type I error occurred in any prediction.

After examining the plots of the roundness error prediction in Figure 7.14, it was found that all the plots can be used to predict the group membership of a drilled hole according to roundness error. The boundary values calculated for AE parameters, B1, B2, B3, B4, A, V, S, and K for predicting group membership of a drilled hole were 271, 12.9, 2.17,0.67, -63.25, 144.5, 0.94 and 0.25, respectively. When the B1, B2, B3, B4, A and V of a drilled hole are larger than 271, 12.9, 2.17,0.67, -63.25 and 144.5, respectively, the drilled hole is predicted to be unacceptable

because the roundness error is larger than 0.00114 inch. When the S and K of a drilled hole are smaller than 0.94 and 0.25, respectively, the drilled hole is predicted to be unacceptable because the roundness error is larger than 0.00114 inch. By using these AE parameters to predict the group membership of a drilled hole according to roundness error, the number of type I prediction errors with respect to each AE parameter, B1, B2, B3, B4, A, V, S, and K were 2, 1, 1, 1, 1, 2, 1 and 1. Correspondingly, the number of type II prediction errors with respect to each AE parameter were 1, 1, 0, 1, 1, 1, 2 and 0.

Examining the plots of the diameter measurement prediction in Figure 7.15, all plots can be used to predict the group membership of a drilled hole according to diameter measurement. Neither larger nor smaller than a specific boundary value, two boundary values which formed an interval were used. For a drilled hole, when the value of the AE parameter was outside the interval, the hole was characterized as unacceptable according to diameter measurement, which means the hole diameter was larger than the desired value of 0.501 inch. The boundary intervals calculated for AE parameters, B1, B2, B3, B4, A, V, S, and K were [43, 275], [3.9, 10.9], [0.49, 2.18], [0.13, 0.58], [-67.8, -67.8], [112.5, 142.8], [1.01, 1.675] and [0.5, 2.85], respectively. By using these AE parameters to predict the group membership of a drilled hole according to the diameter measurement, the numbers of type I prediction error with respect to each AE parameter, B1, B2, B3, B4, A, V, S, and K were 1, 1, 1, 1, 1, 2, 1 and 1. Correspondingly, the numbers of type II prediction error which occurred with respect to each AE parameter were 3, 0, 1, 4, 1, 2, 2 and 2.

7.7 Discussion of Practical Tolerancing Application with Current Results

In this chapter, the cut-off values for different quality errors used to characterize drilled holes as acceptable or unacceptable were determined according to the results of statistical analysis. The cut-off values for straightness, perpendicularity, roundness and diameter were 0.002, 0.006, 0.001 and 0.501 inches, respectively. Based on these cut-off values, the prediction algorithms developed in the current study were able to predict the status of a drilled hole with some accuracy. However, in practical tolerancing application, the cut-off values may be decided by the designer instead of by statistical analysis. In such situations, if the cut-off values are not as the same as those used here, the designed cut-off value will be either higher or lower than the current cut-off value derived from statistical analysis.

If the cut-off values decided for these quality measures are higher than the current values (i.e., encompassing looser tolerance requirements), the current results cannot be adequate for use. More drilled hole samples and spectrums would have to be collected using drill bits more worn than those used in the current experiment. These additional samples and spectrums could be used to expand the prediction model for the wider prediction range. Similarly, if the cut-off values decided for these quality measures are lower than the current values (i.e., reflecting tightened tolerance requirements), the prediction algorithm developed here to characterize the drilled holes may not be adequate.

Since from the cluster analysis used in the current study, the characteristics of the holes in the "unacceptable" group were much different from the holes in the

acceptable group using discriminant function analysis, good classification results can be obtained based on the evident difference. When the cut-off values are lower than the current values, no apparent boundary can be found among these holes. For example, in Figure 7.9, the perpendicularity measures of three unacceptable holes were much larger than those of acceptable holes. It is easy to separate these unacceptable holes from all the samples. However, since there is no apparent difference among those acceptable holes which are in the lower perpendicularity range, good classification results based on discriminant function analysis cannot be expected if we further divide those acceptable holes into two groups. Although the discriminant function models are not able to provide categorical information about the quality status of a drilled hole, the regression models developed here can still be used to obtain predicted results on a numerical format. From the regression models, some information about quality status of a drilled hole can be provided.

Another consideration of tolerancing application is the interrelationship between the quality measures. The allowable tolerance assigned to one quality measure is usually dependent on the tolerance status of other quality measures. For example, in Figure 7.16, the effect of tolerance on perpendicularity as it deviates from exact perpendicularity is shown. The feature control symbol means that the hole must be perpendicular to the datum surface A within 0.001-inch tolerance zone at MMC (maximum material condition). When the hole is at MMC, the dimension is 0.500 inches. The table in Figure 7.16 shows the changes of the actual size (diameter) of the hole, from 0.500 to 0.503, allowing changes in perpendicularity tolerance from 0.001 to 0.004 without affecting functional assembly with the

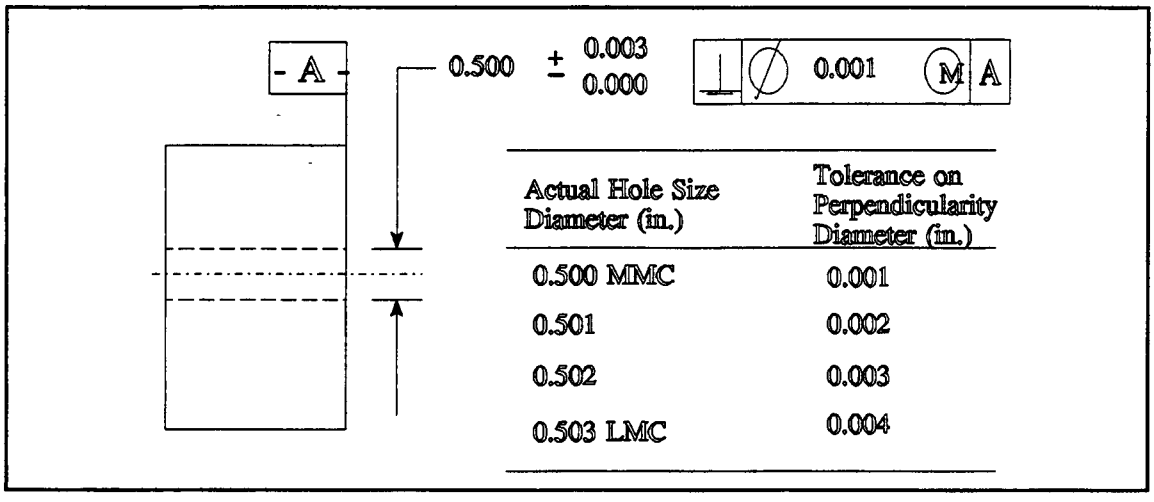

Figure 7.16 Interrelationship between tolerance zones for perpendicularity and hole feature size.

mating part [45,46]. Similarly, considering the straightness tolerance for the axis of a hole, the quality measures such as perpendicularity, roundness, and size, all contribute indirect control over the straightness of the axis of a hole.

Conclusively, the practical tolerance requirements for a drilled hole are important for the current results in practical tolerancing applications. However, when the tolerance requirements for a hole have been chosen, the results of the current study can provide some on-line information to the operator of a drilling operation. Although the current study is just a starting point in tolerancing application, it provides pilot information for the advanced development of tolerance control for automated machine tool systems. With on-line tool-status monitoring and a product-quality prediction system for tolerance control, fully automated machine tool systems which produce high quality products could be expected.

7.8 Summary

In this chapter, the relationships among drill wear, AE parameters, and different hole quality measurements were examined and demonstrated from the experimental results. This affirmation provides a foundation for investigating the possibility of using AE parameters to predict both drill wear and hole-quality variations. Three methods of statistical analysis, multiple regression analysis, cluster analysis, and discriminant function analysis, were used to develop the prediction algorithms for the status of both drill wear and hole quality variations. In addition, a schematic means and rules were proposed to predict the drilled holes as either "acceptable" or "unacceptable" in quality. Through these proposed prediction algorithms, either the numerical hole quality measurements or the categorical information of hole quality variations could be provided. The summary and conclusions of this research as well as recommendations for future work are discussed in next chapter.

CHAPTER 8. SUMMARY, CONCLUSIONS AND FUTURE RESEARCH

8.1 Summary

Hole quality and drill bit wear in the drilling process have been evaluated and found to be correlated with and represented by corresponding acoustic emission (AE) signals. Acoustic transducers were used because they are small, cheap, do not disturb the normal machining processes, and tend to isolate noise. Spectrum analyzers, being standardized and popular, were chosen to collect spectral information. The resulting AE spectral information has been utilized for on-line monitoring and evaluation of hole quality variations associated with drill wear.

Eight parameters were selected to provide relevant AE spectral information for this study. The parameters can be grouped into two categories: (1) energy embedded beneath four dominant peak frequencies and (2) distribution parameters of spectral amplitudes within the frequency range considered, 0 to 1 MHz. Four of the eight parameters represented the energy under the four peak frequencies which are calculated with selected frequency bandwidths (i.e., [74 200] kHz, [200 374] kHz, [376 550] kHz and [550 676] kHz, respectively). The other four parameters were obtained by computing the moments of the spectral amplitude distribution, including average, variance, skewness and kurtosis.

Under fixed drilling conditions, the AE information was analyzed via statistical techniques, including stepwise multiple regression, classification and grouping. Major concluding remarks are as follows.

8.2 Conclusions

Close relationships between hole quality variations and drill wear, drill wear and AE parameters were experimentally observed. The intent was thus to fully reflect the quality of drilled holes using AE parameters. Furthermore, the possibility of extending the results of the present study to advance the automation of the metal machining process was indicated. Experimental observations and associated conclusions concerning the relationships between hole quality variations and drill wear, drill wear and AE parameters, and hole quality variations and AE parameters are represented in separate sections as follows.

8.2.1 Relationship Between Hole Quality and Drill Wear

1. Straightness of drilled hole and drill wear status are correlated. Straightness increases as drill wear area increases.
2. It is indicated that the perpendicularity of a hole remains constant throughout drill life. The increase of drill wear area results in no significant changes in hole perpendicularity variation. It is believed that consistent perpendicularity measurements are established by the initial displacement of the spindle axis of a drilling machine.
3. There is apparent dependence of roundness measurements on drill wear areas. In general, roundness error increases as drill wear increases. However, much of the initial roundness error for the holes

drilled is present even when the drill bit is new or has been little used.

4. Despite the absence of a strong relationship between diameter and drill wear areas, diameters tend to be oversized for holes drilled at both the beginning and the end of drill life. This tendency is similar to that found for roundness measurements.

8.2.2 Relationship Between Drill Wear and AE Parameters

As a result of statistical analysis of the relationship between drill wear and data, based on AE energy embedded in individual frequency band and distribution parameters, conclusions were as follow.

1. Proposed AE spectral parameters regarding energy and amplitudes distribution parameters are found to be good indicators of drill wear areas.
2. With high R^2 values, coefficient of multiple determination, drill-wear areas are successfully related to each AE parameter via a third-order polynomial model. With the chosen models, drill wear can be predicted quantitatively.

8.2.3 Relationship Between Hole Quality and AE Parameters

As a result of the statistical analysis of quality measurements of drilled holes, and the data based on AE energy embedded in individual frequency bands and distribution parameters, conclusions are as follow.

1. Results of stepwise multiple regression analysis strongly indicate that the hole quality measurements of straightness, perpendicularity and roundness of drilled holes are statistically related to each AE parameter. With the regression models for different quality measurements, the AE parameters could be used to predict quantitatively the on-line straightness, perpendicularity, and roundness of drilled holes.
2. AE energy embedded in the second and third frequency bands are found to be closely related to diameter measurements.
3. In place of using quality measurements which are unmeasurable on-line, AE parameters are used to categorize drilled holes into two groups: "acceptable" and "unacceptable." Results indicate that as a linear combination of the AE parameters, the discriminant models demonstrate successful rates, from 83% to 100%, for separating acceptable from unacceptable drill holes.
4. A schematic means to use a single AE parameter to categorize drilled holes with a clear and simple classification algorithm has been developed. Based on the algorithm, rules were developed to predict the

status of hole quality and drill wear for drilling process evaluation and control.

8.3 Recommendations for Future Research

Despite some apparent instrumentational limitations, the current study provides a first attempt at correlating AE signals and drilled hole quality via quantitative analysis. The limitations include a limited supply of work-piece materials, the low accuracy and repeatability of machine vision system, and the low precision of the designed fixture. For advanced drill-wear monitoring and hole-quality prediction in drilling processes, several modifications need to be considered.

1. Improvement of accuracy, repeatability and lighting equipment for machine vision are needed to provide more accurate drill wear measurements.
2. For improved experimental control, information on the geometrical dimensions and material properties of drill bits needs to be collected. Through multivariate analysis of variance, the effects of these parameters can be examined and controlled.
3. To obtain more practical regression models, three modifications are recommended:
   (a) Drill additional holes at specific levels of drill wear to provide more degrees of freedom in the statistical analysis;

(b) Reduce intervals between holes to measure hole quality and drill wear more often and to obtain closer profiles of changes in quality measurements and drill wear;

(c) Use of wider ranges of drilling conditions in size of drill bits, cutting speed, feed rate to further confirm the relationships between acoustic emissions, drill wear, and hole quality measurements and to determine or clarify the effects of corresponding changes of drilling conditions.

4. As previously observed, for both roundness and diameter measurements, there exist larger diameter and roundness variations for holes drilled at both the very beginning and end of drill life. Moreover, to obtain a comparatively more normal and practical discriminant model to characterize drilled holes, additional drilling data in each group are necessary. Thus, more hole samples should be collected at the very beginning and end of drill life.

5. The classification rates of the discriminant models, based on existing data sets, may be overestimated. To ensure accuracy in estimation, more data sets are recommended for cross validations.

The AE parameters using the multiple regression model and the categorizing algorithm developed in the present study can be used to monitor on-line the drill wear and quality changes of drilled holes for only fixed drilling conditions and highly precise hole-drilling processes. Subject to these fixed and precise drilling conditions, drill wear is the only variable and the tolerance requirements are precise,

such as 0.002 inch for straightness, 0.0016 inch for roundness and 0.001 inch for diameter. However, with the AE transducer sensor, which does not interfere with normal drilling operations, the AE parameters and the general methodology should be applicable to a wide range of on-line drill-wear monitoring and quality prediction applications, as long as the AE parameter data are collected and analyzed under a wide range of drilling conditions.

This research project has advanced the state of the art in the area of developing fully automated machine tool systems which may be used to produce high-quality products by providing on-line tool-status monitoring and product-quality prediction systems.

REFERENCES

[1] Dornfeld, D. A., "The Role of Acoustic Emission in Manufacturing Process Monitoring", SME Manufacturing Engineering Trans. 13th NAMRC, 1985, pp. 69-74.

[2] Kahng, C. H. and Ham, I., "A Study on Sequential Quality Improvement in Hole-Making Processes", Annals of the CIRP, Vol. 24/1/1975, pp. 27-32.

[3] Jones, B. E., "Sensors in Industrial Metrology", Journal of Physics. E, Scientific Instruments, Vol. 20, 1987, pp. 1113-1126.

[4] Galloway, D. F., "Some Experiments on the Influence of Various Factors on Drill Performance," ASME Journal of Engineering for Industry, February, 1957, pp. 191-230.

[5] Fujii, H., Marui, E. and Ema, S., "Whirling Vibration in Drilling. Part 1: Cause of Vibration and Role of Chisel edge," ASME Journal of Engineering For Industry, Vol. 108, August, 1986 pp. 157-162.

[6] Fujii, H., Marui, E. and Ema, S., "Whirling Vibration in Drilling. Part 2: Influence of Drill Geometries, Particularly of the Drill Flank, on the Initiation of Vibration," ASME Journal of Engineering For Industry, Vol. 108, August, 1986 pp. 162-168.

[7] Ema, S., Fujii, H. and Marui, E.,"Whirling Vibration in Drilling. Part 3: Vibration Analysis in Drilling Workpiece with a Pilot Hole," ASME Journal of Engineering For Industry, Vol. 110, November, 1988 pp. 315-321.

[8] Ema, S., Fujii, H. and Marui, E., "Chatter Vibration in Drilling," ASME Journal of Engineering For Industry, Vol. 110, November, 1988 pp. 309-314.

[9] Lee, S. J., Eman, K. F. and Wu, S. M., "An Analysis of the Drill Wandering Motion,", ASME Journal of Engineering For Industry, Vol. 109, November, 1987 pp. 297-305.

[10] Lenz, E. and Mayer, J. E., "Investigation in Drilling," Annals of the CIRP, Vol. 27/1/1978, pp. 49-53.

[11] Yee, K.W. and Bloomquist, D.S.,"An on-line method of determining tool wear by time-domain analysis", SME paper No. MR82-901, 1982.

[12] Thangaraj A. and Wright, P. K., "Computer-Assisted Prediction of Drill-Failure Using In-Process Measurements of Thrust Force", ASME Journal of Engineering For Industry, Vol. 110, May 1988, pp. 192-200.

[13] Liu, T. I. and Wu, S. M., "On-Line Detection of Drill Wear", ASME Journal of Engineering For Industry, Vol. 112, August 1990, pp. 299-202.

[14] Dornfeld, D. A., "Neural Network Sensor Fusion for Tool Condition Monitoring," Annals of the CIRP, Vol. 39, 1990, pp. 101-105.

[15] Rangwala, S. and Dornfeld, D. A., "Sensor Integration Using Neural Networks for Intelligent Tool Condition Monitoring," ASME Journal of Engineering For Industry, Vol. 112, August 1990, pp. 219-228.

[16] Govekar E. and Grabec, I., "Self-Organizing Neural Network Application to Drill Wear Classification," ASME Journal of Engineering For Industry, Vol. 116, May 1994, pp. 233-238.

[17] Chandrashekhar, S., Osuri, R. H. and Chatterjee, S., "A Preliminary Investigation Into the Prediction of Drill Wear Using Acoustic Emission," In *Fundamental Issues In Machining*, PED Vol. 43 ASME, 1990, pp. 123-137.

[18] Kannatey-Asibu, E., Jr. and Dornfeld, D. A., "Quantitative Relationship for Acoustic Emission from Orthogonal Metal Cutting," ASME Journal of Engineering For Industry, Vol. 103, No.3 1981, pp. 330-340.

[19] Pal, A. K., Bhattacharyya, A. and Sen, G. C., "Investigation of the Torque in Drilling Ductile Materials," International Journal of Machine Tool Design and Research, Vol. 4, 1965, pp. 205-221.

[20] Williams, R. A., "A Study of the Basic mechanics of the Chisel Edge of a Twist Drill," International Journal of Production Research, Vol. 8, 1970, pp. 325-343.

[21] Williams, R. A., "A Study of the Drilling Process," ASME Journal of Engineering For Industry, November, 1974, pp. 1207-1215.

[22] Armarego, E. J. A. and Cheng, C. Y., "Drilling With Flat Rake Face and Conventional Twist Drills-I. Theoretical Investigation," International Journal of Machine Tool Design and Research, Vol. 12, 1972, pp. 17-35.

[23] Armarego, E. J. A. and Cheng, C. Y., "Drilling With Flat Rake Face and Conventional Twist Drills-I. Experimental Investigation," International Journal of Machine Tool Design and Research Vol. 12, 1972, pp. 37-54.

[24] Wiriyacosol, S., Armarego, E. J .A., "Thrust and Torque Prediction in Drilling From a Cutting Mechanics Approach," Annals of the CIRP, Vol. 28/1/1979, pp. 87-91.

[25] Lan, M. S. and Dornfeld, D. A., "Acoustic Emission ans Machining Process Analysis and Control, " An International Journal of Advanced Manufacturing Process, Vol. 1, (1), 1986, pp. 1-12.

[26] Radhakrishnan, T. and Wu, S. M., "On-line Hole Quality Evaluation for Drilling Composite Material using Dynamic Data," ASME Journal of Engineering For Industry, Vol. 103, February, 1981, pp. 119-125.

[27] Wu, S. M., "Dynamic Data System: A New Modeling Approach," ASME Journal of Engineering For Industry, Vol. 99, Series B, No. 3, August, 1977, pp. 708-714.

[28] Boothroyd, G. and Knight, W. A., "Mechanics of Metal Cutting." In *Fundamentals of Machining and Machine Tools*, G. Boothroyd (ed.), 2nd Edition, Marcel Dekker, Inc. 1989. pp. 73-108.

[29] Merchant, M. E., "Mechanics of Metal Cutting Process," Journal of Applied Physics, No. 16, 1945, pp. 267-284 and pp. 318-324.

[30] Armarego, E. J. A. and Brown, R. H., "Mechanics of Orthogonal Cutting," In *The Machining of Metals*, Prentice-Hall, Inc. 1969, pp. 36-72.

[31] Palmer, W.B. and Oxley, P.L. ,"Mechanic of Orthogonal Machining," Proceeding Institution Mechanical Engineers, No.24, 173, 1959. pp. 623-628.

[32] Oxley, P. L., *Mechanics of Machining; An Analytical Approach to Assessing Machinability*, Ellis Horwood Limited, Halsted Press Edition 1989, pp. 01-49.

[33] Iwata, K., "An Application of Acoustic Emission Measurement to In-Process Sensing of Tool Wear," Annals of the CIRP, Vol. 26, No. 1, 1977, pp. 21-26.

[34] Kannatey-Asibu, E., Jr. and Dornfeld, D. A., "A Study of Tool Wear Using Statistical Analysis of Metal-cutting Acoustic Emission," Wear, Vol. 76, 1982, pp. 247-261.

[35] Bandyopadhyay, P. and Wu, S. M. "Signature Analysis of Drilling Dynamics for On-Line Drill Life Monitoring", In *Sensors and Controls for Manufacturing*, PED-Vol. 18, ASME 17/11/1985, pp. 101-110.

[36] Zorev N. N., "Experimental Studies of Chip Formation and Contact Processes on the Tool Face at Low Cutting Speed," In *Metal Cutting Mechanics*, Pergamon Press Ltd., 1966, pp. 56-124.

[37] Kannatey-Asibu, E. Jr., "Investigation of the Metal Cutting Process Using Acoustic Emission Signal Analysis," University of California, Berkeley, Ph.D. Thesis 1980.

[38] Rubenstein C., " An Analysis of Tool Life Based on Flank-Face Wear, Part I: Theory," ASME Journal of Engineering For Industry, Vol. 98, February, 1976, pp. 221-226.

[39] Connolly, R. and Rubenstein C., "The Mechanics of Continuous Chip Formation in Orthogonal Cutting," International Journal of Machine Tool Design and Research, Vol. 8. 1968, pp. 159-187.

[40] Armarego, E. J. A. and Brown, R. H., "Mechanics of Oblique Cutting," *The Machining of Metals*, Prentice-Hall, Inc. Englewood Cliffs, New Jersey, 1969, pp. 74-95.

[41] Scruby, C. B. "Instrument Science and Technology; An Introduction to Acoustic Emission," Journal of Physics. E, Scientific Instruments, Vol. 20, 1987, pp. 946-953.

[42] Blum, T. and Inasaki, I. "A Study On Acoustic Emission from the Orthogonal Cutting Process," ASME Journal of Engineering for Industry, Vol. 112, August 1990, pp. 203-211.

[43] Noori, M. and Hakimmashhadi, H. "Vibration Analysis," *Signal Processing Handbook* (C. Chen, ed.), Marcel Dekker, New York, 1988

[44] Liang, S. Y. and Dornfeld, D. A., "Tool Wear Detection Using Time Series Analysis of Acoustic Emission," ASME Journal of Engineering for Industry, Vol. 111, August 1989, pp. 199-205.

[45] Krulikowski, A., *Geometric Dimensioning and Tolerancing, Self-Study Workbook*, Effective Training, Inc. Westland, MI, 1990.

[46] Tandler, B., *The Little Encyclopedia of ANSI Y 14.5M Tolerance Zone Shapes and Terminology*, Multi Metrics, Inc., Menlo Park, CA, January, 1994.

[47] Pollack, H. W., "Fixture Design," *Tool Design*, Prentice-Hall, Inc. 1988, pp. 252-277.

[48] Farkas, J., "Machine Vision Based Measurement System," Master's Project, Department of Mechanical Engineering, Oregon State University, 1994.

[49] Ramsey, F. and Schafer, D., "Regression with Many Possible Explanatory Variables Strategies for Variable Selection," *The Statistical Sleuth*, Statistics Department, Oregon State University, 1993, pp. 227-296.

[50] Ramsey, F. and Schafer, D., "Multiple Regression: Modeling the Means as a Function of Explanatory Variables," *The Statistical Sleuth*, Statistics Department, Oregon State University, 1993, pp. 183-208.

[51] Johnson, R. A. and Wichern, D. W., "Part IV Classification and Grouping Techniques, Chapter 10. Discrimination and Classification and Chapter 11 Clustering," In *Applied Multivariate Statistical Analysis*, Prentice-Hall, Inc., Englewood Cliffs, New Jersey, 1982, pp. 459-578.

[52] Ramsey F. and Schafer D., "Linear Combination Constructed from the Data," *The Statistical Sleuth*, Statistics Department, Oregon State University, 1993, pp. 365-388.